ISTANBUL TECHNICAL UNIVERSITY ★ GRADUATE SCHOOL OF SCIENCE
ENGINEERING AND TECHNOLOGY

ANALYSIS OF WAVE PROPAGATION CHARACTERISTICS AND DESIGN METHODS IN TWO DIMENSIONAL PHOTONIC BANDGAP STRUCTURES

Ph.D. THESIS

Onur ERKAN

Department of Electronics and Communication Engineering

Telecommunication Engineering Programme

AUGUST 2019

ISTANBUL TECHNICAL UNIVERSITY ★ GRADUATE SCHOOL OF SCIENCE
ENGINEERING AND TECHNOLOGY

ANALYSIS OF WAVE PROPAGATION CHARACTERISTICS AND DESIGN METHODS IN TWO DIMENSIONAL PHOTONIC BANDGAP STRUCTURES

Ph.D. THESIS

Onur ERKAN
(504132304)

Department of Electronics and Communication Engineering

Telecommunication Engineering Programme

Thesis Advisor: Associate Prof. Dr. Serkan ŞİMŞEK

AUGUST 2019

İSTANBUL TEKNİK ÜNİVERSİTESİ ★ FEN BİLİMLERİ ENSTİTÜSÜ

İKİ BOYUTLU FOTONİK BANT DURDURAN YAPILARDA DALGA ANALİZİ VE TASARIM YÖNTEMLERİ

DOKTORA TEZİ

Onur ERKAN
(504132304)

Elektronik ve Haberleşme Mühendisliği Anabilim Dalı

Telekomünikasyon Mühendisliği Programı

Tez Danışmanı: Doç. Dr. Serkan ŞİMŞEK

AĞUSTOS 2019

Onur ERKAN, a Ph.D. student of ITU Graduate School of Science Engineering and Technology 504132304 successfully defended the thesis entitled “ANALYSIS OF WAVE PROPAGATION CHARACTERISTICS AND DESIGN METHODS IN TWO DIMENSIONAL PHOTONIC BANDGAP STRUCTURES”, which he/she prepared after fulfilling the requirements specified in the associated legislations, before the jury whose signatures are below.

Thesis Advisor :	**Associate Prof. Dr. Serkan ŞİMŞEK** Istanbul Technical University	....
Jury Members :	**Prof. Dr. Cevdet IŞIK** Istanbul Technical University	....
	Prof. Dr. Hülya ŞAHİNTÜRK Yıldız Technical University	....
	Associate Prof. Dr. Mehmet ÇAYÖREN Istanbul Technical University	....
	Assistant Prof. Dr. Özlem Ünverdi Yıldız Technical University	....

Date of Submission : 14 June 2019
Date of Defense : 06 August 2019

FOREWORD

Foremost, I would like to express my sincere gratitude to my advisor Prof. Serkan Şimşek for having accepted to examine this work and for his valuable insights. His guidance helped me in all the time of research and writing of this thesis. Without his encouragement this dissertation would not have materialized. Besides my advisor, I would like to thank the Dr. Mehmet Nuri Akinci for his encouragement, insightful comments, and support. Also I thank my friend Agah Oktay Ertay who I received generous support.

My special thanks goes to my spouse for the continuous support of my Ph.D study and research, for her patience, motivation, enthusiasm, and immense knowledge. I am also grateful to my other family members and friends who have supported me along the way.

AUGUST 2019

Onur ERKAN
(Electronics and Communication Engineer, M.Sc.)

TABLE OF CONTENTS

Page

ABBREVIATIONS

GSM	: Generalized Scattering Matrix
AFGSM	: Auxiliary Functions of Generalized Scattering Matrix
HM	: Hybrid Method
EMT	: Effective Medium Theory
RCWA	: Rigorous Coupled Wave Analysis
PC	: Photonic Crystal
PBG	: Photonic Bandgap
EBG	: Electromagnetic Bandgap
TMM	: Transfer Matrix Method
PWE	: Plane Wave Expansion
FDTD	: Finite Difference Time Domain
FEM	: Finite Element Method
FPR	: Fabry Perot Resonator
OBG	: Omnidirectional Bandgap
ORB	: Omnidirectional Relative Bandwidth
GMR	: Gap-midgap ratio
TE	: Transverse Electric
TM	: Transverse Magnetic
FR	: Filling Ratio
LSM	: Laser Scanning Microscopy
SHG	: Second Harmonic Generation
NIR	: Near Infrared

SYMBOLS

$\mathbf{E}$	: Electric field (V/m)
$\mathbf{H}$	: Magnetic field (A/m)
$\mathbf{D}$	: Displacement vector (C/m^2)
$\mathbf{B}$	: Magnetic induction (T)
η_i	: Characteristic impedance of $i-th$ medium
k_i	: Wavenumber in $i-th$ medium
ε_0	: Dielectric permittivity of the vacuum (F/m)
μ_0	: Magnetic permeability of the vacuum (Tm/A)
ε_r	: Relative permittivity of the medium
μ_r	: Relative Permeability of the medium
β	: Propagation phase constant
α	: Attenuation constant
γ	: Propagation constant
Z	: Wave impedance
Γ	: Reflection coefficient
κ	: Bloch wave vector
ε_{eff}	: Effective permittivity
Λ	: Period of the structure (m)
θ_i	: Electrical length of layer
λ	: Eigenvalue of the periodic structure
$X_{\pm}$	: Auxiliary functions of AFGSM method
θ_{inc}	: Angle of incidence $(degree)$
$S^{Li}_{m,n}$	: Scattering matrix elements of layer i
$\mathbf{S_{m,n}}$	: Subblock matrix of Generalized scattering matrix (m,n: out, input ports)
$u(.)$	: Arbitrary wave function
$R(.)$	: Arbitrary periodic function

LIST OF TABLES

Page

LIST OF FIGURES

Page

ANALYSIS OF WAVE PROPAGATION CHARACTERISTICS AND DESIGN METHODS IN TWO DIMENSIONAL PHOTONIC BANDGAP STRUCTURES

SUMMARY

Over the last few decades, demand for higher data transmission rates increased drastically due to emergence of applications requiring higher bandwidth services. Recent advances in photonics and fabrication of nanometer scaled components enabled the high capacity data transmission in communication technologies. The research field of periodic structures which ranges from microwave to optical frequencies became attracting in the sense that their special electromagnetic waveguiding properties constitute the basis of many promising applications. Among various metallic and dielectric materials considered in the context of periodic structures, photonic crystals which are found to have unique propagation characteristics for a certain frequency range, are one of the most popular. Photonic crystals can be tailored to address desired bandgap characteristics. Particularly, two-dimensional photonic crystals are regarded as the essential elements that incorporate periodicity features and enable the development of new optical components such as filters, waveguides, cavities, splitters, couplers and reflectors.

Investigation of the photonic bandgaps (PBG) in a photonic crystal plays a fundamental role coincided in numerous engineering-science applications and design purposes. The method reported in the literature investigate the problem associated with the conventional approach of solving eigenvalue equation. This solution approach requires computationally large memory sources and becomes inefficient especially when large number of eigenmodes are required at the layer interfaces. The focus of this dissertation is to present accurate and numerically efficient alternative methods to analyze bandgap characteristics of two-dimensional PBGs. Full wave analysis of bandgap structures is addressed by calculating the supported Floquet modes of infinitely periodic structures, i.e. seeking for the permitted and forbidden band regions of the unit-cell. A novel approach based on auxiliary functions of generalized scattering matrix (AFGSM) method is introduced. The proposed technique provides estimations of the stopband or passband frequencies accurately supported by the single Floquet mode region simply by carrying through a basic root-search routine. For a lossless PBG structure real numbered roots correspond to propagating modes and complex-values roots correspond to non-propagating modes (stopband) respectively. Therefore, the aim of this thesis is to develop alternative techniques to determine bandgap characteristics of PBG structures based on AFGSM method.

First section of this dissertation includes a literature survey and introduction of the thesis scope. The second chapter gives a brief review of wave propagation in periodic structures and highlight the key theoretical concepts. The third chapter is concerned with the methodology employed for a fast and hybrid bandgap analysis of two-dimensional photonic crystals. First, effective medium theory (EMT) is employed to mitigate two-dimensional geometry (for a structure which has a period much

smaller than the wavelength) to one-dimensional multilayered equivalence in order to simplify the computation of the photonic bandedges. Then, bandedges of equivalent one-dimensional structure are examined using AFGSM method. Subsequently, in the fourth section, the analysis is extended to a comprehensive and full wave analysis of 2D PBG structures utilizing the rigorous coupled wave analysis (RCWA) to determine scattering parameters (S-parameters) of unit cell. Thereafter, AFGSM method is used to investigate bandedge frequencies of infinitely layered periodic media. In the fifth chapter, different types of filter applications operating in the optical wavelength region are designed using novel algorithm based on AFGSM method. The final chapter summarises the principal findings given in the thesis and identifies areas for further research.

İKİ BOYUTLU FOTONİK BANT DURDURAN YAPILARDA DALGA ANALİZİ VE TASARIM YÖNTEMLERİ

ÖZET

Son yıllarda gelişen kablolu ve kablosuz haberleşme teknolojileriyle birlikte yüksek bant genişliğine ihtiyaç duyan uygulamaların kullanımı artmış, bu da beraberinde veri kullanım oranının yükselmesine sebep olmuştur. Bu durum taşıyıcı ortamda bant genişliklerinin etkin kullanımı gereksinimini doğurmuştur. Genellikle GHz bölgesindeki frekanslarda veri iletiminde, sınırlanmış kesite sahip tek iletkenli veya dielektrik dolu yapılar kullanılarak elektromanyetik dalganın kılavuzlanması sağlanmaktadır. Benzer şekilde optik frekanslarda da iletken duvarı olmayan dielektrik tabaka ve çubuklar da temelde dielektrik ortama sınırlanmış veya kılavuzlanmış dalga modlarını destekleyebilmektedir. Böylece THz bölgesindeki frekanslarda malzemelerin dielektrik geçirgenliklerine göre mikrometre ve daha küçük boyutlarda optik dalga kılavuzları, kaviteler ve rezonatörler gibi uygulamalar tasarlanabilmektedir. Dalga kılavuzlarının bir alt araştırma konusu olan periyodik katmanlı yapılarda dalga propagasyonu uzun yıllardır bilim insanları ve mühendislerin ilgisini çekmiştir. Haberleşme teknolojilerinde ise periyodik yapılar, mikrodalgadan optik frekansa kadar değişen geniş bir frekans bölgesinde elektromanyetik dalganın iletimi, yansıması ve kılavuzlanması gibi temel mühendislik problemlerinde yer bulmuştur. Periyodik yapıların tasarımında kullanılan çeşitli metalik ve dielektrik malzemeler arasında fotonik kristaller, fabrikasyon sonucu her üç boyutta da periyodiklik özelliği kazandırılabilen yapılardır. Fotonik kristallerin teknolojik olarak çok sayıda uygulama alanı bulunması ile birlikte haberleşme, elektronik devreler ve tıp uygulamaları gibi alt başlıklarda yoğun olarak incelenmektedir. Değişen dielektrik özellikleri ile periyodik olarak dizilimleri sonucu belirli frekans bölgesinde sergiledikleri iletim/durdurma karakteristikleri (fotonik bant aralığı, PBG) sebebiyle THz bölgesindeki uygulamalarda popüler olarak tercih edilen malzemeler arasındadır. Fotonik kristaller istenen bant aralığı özelliklerini sergilemek üzere uyarlanabilmektedir. Bir boyutlu (1D), iki boyutlu (2D) ve üç boyutlu (3D) fotonik kristallerin periyodik, yarı-periyodik, kare, üçgen vb. örgü yapılarında dizilimleri sonucu ortaya çıkan bant yapılarının belirlenmesi, iletim-yansıma katsayılarının hesaplanması ve analizi üzerine kayda değer sayıda çalışmalar yapılmıştır. En basit haliyle farklı kırılma indisine sahip dielektrik malzemelerin farklı dizilimlerde uygun şekilde tasarımı ile ışığın istenen doğrultu ve belirli frekans bölgesinde ilerleyebilmesini/sınırlandırılmasını sağlayan yapıların analizi, gerçekleme ve simülasyon çalışmaları bu alandaki en önemli araştırma konuları haline gelmiştir. Günümüzde nanometre boyutlarında malzemelerin fabrikasyonunda elde edilen iyileştirmeler sayesinde düşük güçle çalışan ve optik spektrumun verimli kullanılmasını sağlayacak fotonik kristal temelli optik filtreler, dalga kılavuzları, elektro-optik modülatörler, güç bölücüler, kutuplayıcılar, algılayıcılar gibi bileşenlerin tasarlanması mümkün olmuştur.

Fotonik kristallerin bant yapısının belirlenmesi birçok mühendislik uygulamasında ve tasarım probleminde önemli rol oynamaktadır. Hassas fabrikasyon süreci öncesinde tasarım aşamasında gerek duyulan sayısız modelleme işlemine hızlı tepki verecek etkin bir matematiksel model arayışı literatürde bulunan çalışmalarda farklı bakış açıları ile incelenmeye devam etmektedir. Periyodik yapıların dalga propagasyonu problemini çözmek için sonlu sayıda birim hücre içeren sonlu periyodik yapılar ve sonsuz sayıda kaskat bağlı birim hücreden oluştuğu varsayılan yapılar referans alınmaktadır. Sonlu periyodik yapıda (yarı-periyodik) birim hücre yaklaşımı, yapının dispersiyon karakteristiği için yaklaşık bir çözüm sağlamakta olup bu yaklaşımın doğruluğu da kullanılan birim hücre sayısı artırılarak yükseltilebilmektedir. Fakat birim hücre sayısının artması cevabın doğruluğunu artırırken, hesaplama yükündeki artışı da beraberinde getirmektedir. Literatürde yer alan geleneksel yaklaşımlar özdeğer denkleminin çözümüne dayanan yöntemlerdir. Bu yaklaşım özellikle katman arayüz geçişlerinde çok sayıda özdeğer denkleminin hesaplanmasını gerektirdiğinden verimsiz hale gelmekte ve hesap uzayında büyük bellek kaynakları gerektirmektedir. Bu sebeple tez çalışmasında, fotonik bant aralığı karakteristiklerini belirlemeyi sağlayacak alternatif yöntemler araştırılmış ve geliştirilmiştir. Bu bağlamda mikrodalga tekniği çerçevesinde daha önce geliştirilen genelleştirilmiş saçılma matrisi kullanılarak iletim/durdurma bant bölgelerinin kestirimi yöntemi optik THz bölgesine uygulanarak iki boyutlu periyodik yapının bant aralığı analizine genişletilmiş ve bu bölgedeki tasarım çalışmalarına entegre edilmiştir. Fotonik bant aralığı yapısının tam dalga analizi sonsuz periyodik yapıda desteklenen Floquet modları hesaplanarak, başka bir deyişle sonsuz periyodiklikte olduğu varsayılan birim hücre için izin verilen veya sınırlanan bant kenar frekansları bulunarak ele alınır. Böylece sonsuz periyodik birim hücreden oluşan yapının iletim/durdurma bant bölgelerinin belirlenmesi Floquet koşulu altında birim hücrenin özdeğer denkleminin çözümüne indirgenmektedir. Çalışmada, önerilen teknik, problemi basit bir kök bulma algoritmasına indirgeyerek, tek Floquet modlu bölgede bulunan iletim/durdurma band geçiş frekansları için doğru kestirimler elde edilmiştir. Genelleştirilmiş Saçılma Matrisi Yardımcı Fonksiyonları (AFGSM: Auxiliary Functions of Generalized Scattering Matrix) yöntemi olarak literatüre giren yaklaşım ile periyodik yapının dispersiyon karakteristiğinin elde edilmesi işleminde geleneksel yöntemlere göre sayısal iş yükünün azaltıldığı gösterilmiştir. Önerilen yöntemin fotonik bant aralığı analizinin yanı sıra tasarım amacıyla ters problem çözümü şeklinde birim hücre parametrelerinin belirlenmesinde etkili olarak kullanılabilineceği tez çalışmasında elde edilen sonuçlarla ortaya konulmuştur.

Fotonik kristallerin belirli bir frekans bandında geliş açısından ve polarizasyondan bağımsız olarak tam yansıtıcılık gösterdiği frekans bandı tümyönlü yansıtıcı bant aralığı (OBG: omnidirectional bandgap) olarak adlandırılmaktadır. Tez kapsamında yapılan konferans bildirileri ve ulusal dergilerde yayınlanmış çalışmalarda önerilen yöntem kullanılarak geniş bantlı tümyönlü yanısıtıcı tasarımı yapılmış elde edilen sonuçlar düzlem dalga açılım yöntemi (PWE: Plane Wave Expansion) ile doğrulanmıştır. Bu özellik sayesinde fotonik kristaller dağılmış geri-beslemeli lazerler, dielektrik Fabry-Perot filtreler, ayarlanabilir polarizörler, dar-bandlı filtreler ve dielektrik yansıtıcılar gibi çok sayıda önemli uygulamada yoğun olarak kullanılmaktadır. Günümüzde mobil ve sabit haberleşme şebekelerinin temel altyapısını oluşturan fiber optik haberleşme sistemlerinde uzak mesafelere yüksek kapasiteli veri aktarımı yeterince yüksek bant genişlikleri ile mümkün olmaktadır. Yüksek band genişliği ise kısıtlı frekans spektrumunun etkin bir şekilde kullanılabilemesi için sık ve dar bandlı filtrelerin uygulanmasını gerektirir. Tümyönlü yansıtıclara ek olarak tez çalışmaları kapsamında telekomünikasyon sistemlerinde Yoğun Dalgaboyu Bölmeli Çoğullama (DWDM) birleştirici ve çoğullayıcı (MUX DEMUX) olarak kullanılan fotonik kristalli dört kanallı optik filtrelerin tasarımı yapılmıştır. Elde edilen sonuçlar ulusal konferaslarda sunulmuştur.

Tezi oluşturan bölümler kısaca şu şekilde özetlenebilir: Tezin ilk bölümü kapsamlı bir literatür taraması ve tez amacını vermektedir. İkinci bölüm, periyodik yapılarda dalga yayılımını özetleyerek periyodik yapılarda dalga propagasyonuna ilişkin temel teorik kavramları hatırlatmaktadır. Üçüncü bölümde iki boyutlu problem geometrisinin bant aralığı analizi yapılmıştır. Önerilen yöntemde öncelikle efektif ortam teorisi (EMT: Effective Medium Theory) ile problem bir boyutlu eşleniğine uygun olarak indirgenmiş, bir boyuta indirgenen problem geometrisi için ise iletim-durdurma bant kenar frekanslarının tespitinde AFGSM yöntemi etkili ve hızlı bir şekilde uygulanmıştır. Elde edilen sonuçlar CST benzetim programının çıktıları ve literatürde yer alan benzer problem sonuçlarıyla doğrulanmıştır. Bu yaklaşım, iki boyutlu geometrilerin bant karakteristiğinin çözümünde kullanılmak üzere literatüre Hibrid Yöntem (HM) ismiyle önerilmiştir. Tezin dördüncü bölümünde ise, iki boyutta sonlu periyodik yapının tam dalga analizi için Kesin Kuple Dalga Analizi (RCWA: Rigorous Coupled Wave Analysis) ve Genelleştirilmiş Saçılma Matrisi (GSM) yöntemleri birleştirilerek 2D yarı periyodik yapının birim hücre saçılma matrisi hesaplanmıştır. Sonsuz periyodik yapının iletim-durdurma band kenar frekansları ise AFGSM yöntemi kullanılarak tespit edilmiş ve böylece çalışma iki boyutlu fotonik bant aralığı yapısının kapsamlı ve tam dalga analizine genişletilmiştir. İki boyutlu dikdörtgen ve üçgen dizilimli, kare ve dairesel dielektrik sütun kesitine sahip problem geometrileri modellenmiş ve önerilen yöntemin uygulanabilirliği test edilmiştir. Dispersiyon diyagramı üzerinde iletim-durdurma bantlarını veren sonuçlar literatürde yeralan benzer çalışmalar ve HFSS benzetim programından elde edilen sonuçlarla karşılaştırılmıştır, oldukça tutarlı sonuçların elde edildiği görülmüştür. Beşinci bölümde ise yöntemin ultraviyole, görünür bölge ve kızılötesi bölgesinde geçerliliğinin irdelenmesi amacıyla Lazer Taramalı Mikroskobi (LSM) uygulamalarında kullanılan band geçiren, band durduran, dikroik ve çentik filtre bileşenleri AFGSM yöntemine dayanan yeni algoritmalar kullanılarak tasarlanmıştır. Tasarlanan filtre karakteristikleri endüstride ticari olarak kullanılan filtre parametreleri ile kıyaslanmıştır.

Tez çalışması kapsamında genel anlamda periyodik yapıların iletim durdurma band bölgelerinin tespiti özelde ise farklı dizilim ve kesit alanına sahip dielektrik sütunlardan oluşan iki boyutlu fotonik bant ileten/durduran yapıların bant aralığı karakteristiklerini ortaya koyan bant kenar frekanslarının kestirimi için kapsamlı ve özgün yöntemler literatüre kazandırılmıştır. Sonuç olarak yapılan analizler ve tasarımlar literatürdeki farklı sonuçlar ile karşılaştırılmış ve hesaplama süresi açısından doktora tezinde önerilen yöntemlerin benzetim simülasyonlarına ve bilinen diğer sayısal yöntemlere göre oldukça hızlı olduğu gösterilmiştir.

1. INTRODUCTION

Periodic structures are constituted the basis of many promising applications in the microwave to optical wave region. For several decades subject of electromagnetic field interaction with periodic structures such as wave scattering and wave guiding has attracted a lot of researches. Latest advancements in material science and modeling processes revealed the existence of bandgaps in periodic structures. So far, many studies have been carried out to show that the light propagation in an artificially designed periodic structure could be prohibited or assisted for a specified frequency range. In the case of a wave incident to a periodic structure within a certain frequency range it appears to be reflected completely. This forbidden band in the frequency spectrum is cited to as electromagnetic bandgap (EBG) or photonic band gap (PBG) and this phenomenon is mostly realized with periodic dielectric structures known as photonic crystals (PCs) [1]. In the recent years, many optical devices constructed by photonic crystals received great attention because of their potential applicability in the field of optical communication networks and photonic integrated circuits. These features of photonic crystals have certain advantages not only in wired telecommunication applications but also in some specific industrial applications. Some of the most promising applications of band gap technology include antennas, antenna feeds, high precision GPS, mobile telephony, wearable antennas, duplexing antennas, filters, phase shifters, slow-wave structures, travelling-wave tubes, planar wave applications such as frequency selective surfaces (FSS) and phased array antennas. Additionally, photonic crystals are used as a dielectric mirror in optical applications due to the very high reflectivity for all incident angles and all polarization states within a specified frequency range [2].

Recent improvements in high resolution lithography and etching processes made the optoelectronic device applications advantageous with the lower power consumption, scalable size for device dimension and reliable high performance features required in optical integrated circuits. These characteristics allows designing important practical components in optoelectronic and microwave engineering fields e.g. thin-film filters, channel drop filters, optical delay lines [3–6], optical isolators [7], resonance filters [8], photonic nanocavities, photonic crystal mirrors [9, 10], polarization splitters, optical interleavers [11, 12], photonic crystal tapers, splitters and combiners [13, 14], planar reflectors, waveguide bends [15]. Various new reports examining the manipulation of light confinement with PCs have been evaluated i.e., 2D defect included magneto-photonic crystal structures for circulator design [16], experimental studies of cross-shaped PC waveguide with wide bandwidth configuration [17] and reconfigurable PBG structures by modification of the permittivity of materials using an explicit parameters e.g. temperature [18, 19], electric field [20, 21] and magnetic field [22], and so on.

Similar to the principle of electron-wave propagation in semiconductors, PCs can be used to create either allowed or forbidden photonic bands with respect to their permittivity in the periodicity direction. The pioneering work of E. Yablonovitch in 1987, as it is underlying this phenomena, remains crucial as revealed a three dimensional periodic structure that could have the capability to completely inhibit spontaneous emission within its band gap. Following to this work, S. John's study is of great significance as it marks the possibility of light localization by scattering in periodic structures. Above mentioned works focused on designing the proper materials at microwave and millimeter-wave frequencies to control electromagnetic modes where operating wavelength is proportional to the lattice constant. However fabricating nanometer-scale structures was a challenge due to the difficulties in manufacturing techniques. Subsequent advances in Nano-scale silicon processing technologies extended band gap device developments into infrared and terahertz regimes with the strong reduction of device sizes. The first demonstration of a photonic crystal at optical wavelengths was made by Thomas Krauss in 1996. Artificially designing the material properties allows different frequency ranges to be covered to utilize target applications.

Depending on the geometry and periodicity direction, PCs are categorized as one-dimensional (1D), two-dimensional (2D) and three-dimensional (3D) structures. The conventional well-known configuration of a 1D-PC is composed of periodically arranged layers which have alternating refractive index variation along the periodicity axis. The theory relies on the reflections at the boundaries of those alternating materials of different refractive index (n_1, n_2) yielding a phase difference where light cannot propagate through the structure at certain frequency bands and specific incident angles [1]. This feature can be explained by wave-energy interaction in different frequencies defined as; the energy of lower frequency modes is concentrated within the higher refractive index regions whereas oppositely, the energy of higher frequency modes is concentrated within the lower refractive index regions. Transmission and reflection properties of periodic structure can be selectively designed by increasing the index contrast between the alternating layers for desired wavelength region. Besides the permittivity difference, implementing a variation of thicknesses (p_1, p_2) between the connected sections of PCs yields the widening of photonic bandgaps (PBGs). Theoretically, photonic band structure is analyzed by the variation between the wavelength (λ) (or frequency) of the light and wave vector ($\mathbf{k}$) which is represented in dispersion diagram (dispersion curve). The field inside a periodic structure governed by Maxwell's wave equations incorporated with Floquet theorem which is the superposition of the Floquet modes or Bloch waves. The electric field vector of a normal mode of propagation in a periodic medium is given by multiplication of a periodic function with period $p = p_1 + p_2$ and wave vector of propagation. The wavevector which indicates the energy concentration in forbidden bands is known as Bloch wavevector. For an infinite periodic structure bandgaps are represented in dispersion curves where Bloch modes are used to identify the properties of structure.

One dimensional photonic crystals are the simplest form of periodic structures that can be constructed by cascading the dielectric layers periodically in the direction of propagation. However, restricting the periodicity in a single direction limits the accessibility to wide application areas of photonic crystals. Therefore, broad omnidirectional bandgaps or complete bandgaps in any direction with the different geometric configurations of 2D and 3D photonic crystal structures are exploited in many real-world problems. A typical 2D PC is comprised of infinitely long rods or air holes arranged in an array formation. Furthermore, such a structure can be designed to guide the light in a certain band range by applying a point defect or a line defect. Introducing the appropriate defects into the structure breaks its characteristic periodicity in PBG region and generates resonance (defect) modes. Particularly, lattice defect prevents the reflection of the light and ensures that the light is confined. Designing these devices requires numerous numerical modeling attempts to determine the near-ideal design (complete physical insight) just before going through the fabrication process. Therefore, fast and accurate numerical modeling of desired structure is very significant. As the complexity of the structure increased intricate formulations required to solve the problem. To date, many analytical or numerical techniques such as plane wave expansion method and transfer matrix method provide appropriate solutions to band structure computation, most of these approaches are inefficient and suffer from the high computational burden. Traditional methods for determination of band diagrams and radiation modes in literature rely on solving eigenvalue equation. Hence, the algorithms used to analyze band structure require very long computer time and excessive memory. Hence, in this thesis we intend to develop a customized method, and investigate the 2D problem. Particularly, a general framework for the analysis and design of 1.5D and 2D photonic crystals presented and simulation validations which will contribute to the development of microwave bandpass/stopband filter applications are exploited.

1.1 Purpose of Thesis

As mentioned beforehand, this research examines the emerging role of photonic crystals in the practical applications and focuses on the theoretical and numerical alternate methods of photonic band-gap structure determination techniques. In the first part of this thesis, a hybrid technique incorporates the effective medium theory (EMT) and 1D auxiliary functions of generalized scattering matrix (AFGSM) method is developed to investigate photonic bandgaps of two-dimensional (2D) photonic crystals. In the developed method, identification of the UC parameters simply allows to evaluate bandgap edges of photonic bandgap structure. In order to reduce dimensional complexity of the problem EMT is used to reduce parameters of 2D geometry to 1D equivalent. AFGSM is then employed to determine bandedge frequencies of 1D infinite (ideal) structure. Our results show that computation time is remarkably reduced. Findings of this study are key contribution to literature for the research of PBGs in 2D design subjects.

In the second part of this thesis, we mainly focused on an efficient and accurate method for determining the characterization of 2D photonic crystal is performed under oblique plane wave excitation for both TE and TM polarizations. Considered 2D PCs are stack of unit cells which are 1D gratings with a periodicity in the transverse propagation direction whereas identical unitcells are periodic in longitudinal direction. Rigorous Coupled Wave Analysis (RCWA) method is implemented to consider higher order mode interactions in modal expansion analysis of unitcell. Transmission and reflection spectra of finitely periodic stack are calculated by means of GSM method. Finite number of periodic cascade connection does not provide full-wave analysis of such a media. In the proposed technique, instead, 2D photonic crystal is assumed to be an infinite periodic structure that ideally provides band-edge frequencies of supported Floquet modes. Moreover finite periodic scattering matrix cascading algorithm is inherently time consuming due to the existence of two matrix inversions. Therefore, efficient and less time-consuming proposed technique can be implemented for modeling of finitely periodic practical applications.

In the third part of this thesis, to reveal the capability of the proposed method on filter applications we developed a novel and robust filter design algorithm. Presented filters are hybrid type of structure comprising periodic and degenerated multilayered dielectrics. One of the key features of the proposed approach is flexibility in designing desired transmission band while offering widened stop-bands. The transmission and stopband characteristics are attained using Auxiliary Functions of Generalized Scattering Matrix Method (AFGSM) which has computationally better performance. In order to demonstrate the suitability of the proposed design strategy, we have investigated and designed four different types of filters including a laser line filter at 800 nm wavelength for reflectance confocal microscopy, a band-pass filter at 400 nm wavelength for second harmonic generation microscopy, a laser block filter at 800 nm wavelength and a dichroic filter blocking 350-400 nm while transmitting higher wavelengths for multiphoton microscopy.

Consequently, in this thesis, a novel method has been proposed based on the generalized scattering matrix representation of a unit cell pattern to determine the bandgap characteristics of specified PC structure. Since the proposed method does not require the solution of the eigenvalue equation unlike the other conventional methods reported in the literature, it yields solutions with higher accuracy and much lower complexity.

1.2 Literature Review

Controlling the wave propagation in periodic structure has led to developments in engineering of artificial crystals which can be used to employ bandgap properties. Most of the promising applications were found in the microwave and optical engineering fields. In particular, microwave field contains frequency-selective structures, leaky-wave antennas, phase-array antennas, slow-wave structures, travelling wave tubes applications; whereas optical field includes grating couplers and splitters, leaky-wave structures, diffraction gratings for beam splitting, dielectric gratings, waveguides, microcavities, resonator applications. Many of the aforementioned devices require complex production mechanisms as long as the scale mitigated to nanometer dimensions. Indeed, before stepping into the fabrication process, necessary measurements need to be executed in order to deal with design changes. However, surveying in every step of design is not feasible in terms of cost and speed. Therefore, between the design and fabrication process a mathematical method (computational modeling) should be implemented to predict electromagnetic wave behavior in the designed structure. In this regard, simulation tools have attained more importance to illustrate results numerically.

Several mathematical approaches are developed to analyze propagation characteristics of periodic structures. Conventionally, periodic boundary conditions are incorporated into Maxwell's equations which results in a characteristic equation consisting of necessary dispersion properties. The eigenvalues (roots) of the dispersion equation corresponds to propagation constants. Dispersion curves enable one to identify transmission and reflection properties of the infinitely periodic photonic crystal structure [23]. The Plane Wave Expansion (PWE) method is the most common technique used to calculate band structure of an infinite photonic crystal based on the unit cell approach [24–26]. However, in case of considering large dielectric contrast between layers and analysis of complex PC structures, method requires excessive number of plane waves which results in a poor performance in terms of the convergence. Also mathematical description of lattice structure and eigenfunctions requires set of equations to be solved by converting them into a Hermitian eigenvalue problem. In [27] the convergence problems with the plane-wave method in photonic crystals have been proposed. The convergence of the method can be improved in case of using alternate basis system functions i.e. spherical waves may be used instead of plane waves as a fundament set whenever the 3D photonic crystal is combined from spherical or cylindrical parts. This technique is known as the spherical-wave expansion method or vectorial KRR (Koringa Kohn Rostker) method [28]. The Transfer Matrix Method (TMM) is another essential technique to analyze the bandgap of photonic crystals. In this method, layers of structure assumed to be invariant along the direction of propagation and the field transferred from each layer is calculated with Maxwell's equations incorporated with boundary conditions. Total transfer matrix is used to represent the band diagram of the PC and it can be calculated as a product of each layer's transfer matrices [23, 29, 30]. Finite difference time domain (FDTD) method is mathematically derived by differential equations with derivatives of the field components in a finite computational domain. Conventionally a Cartesian grid is used to discretize the set of points called mesh. Discretization of each mesh element is often set to a proper value (e.g. $\lambda/20$) where sensitive to field variations accurately. Differential form of Maxwell's equations is solved with finite difference solver considering the related boundary conditions for each material interface. In order to ensure the stability of the method for different geometries the mesh grid size and time steps must be selected appropriately. However, discretization of the problem mesh limits the computational efficiency of the method adversely [31–33]. Finite element method (FEM) is another widely used technique in computational electromagnetics in addition to solid modeling of mechanical engineering problems. In this method, partial differential equations (PDE) incorporated with related boundary conditions are used to find approximate solutions. Similar to FDTD in FEM computational domain is divided to sub mesh domains (finite elements) in order to solve simple functions for each element instead of entire structure. Moreover, in FEM mesh elements can be selected from various small shapes such as triangular or tetrahedral elements and allows modifying the element size unequally depending on irregularity of the structure. Both FDTD and FEM approaches are limited by mesh definition of computational domain and results in an eigenvalue equation to be solved numerically [34, 35]. Certainly specified geometry of a PC constitutes particular bandgap properties valid for a specified frequency region, incidence angle and polarization. In case of varying these parameters might fade the photonic bandgap away. Hence, a frequency region which is insensitive to incidence angle and polarization setting, called omnidirectional bandgap (OBG), appears as a requirement for relevant applications. Many researches published related to OBG structures in literature [36, 37].

Numerous applications acquired by employing 1D PC in the designed structures can be found in the literature such as distributed feedback lasers (DFB) [23], dielectric Fabry-Perot filters [38], reconfigurable polarizers [39], narrow-band filters [40], dielectric reflectors [41, 42]. On the other hands, some dielectric mirrors and optical filter applications driven by introducing the defect formations through the structure where localized modes of light appears [43].

2D PCs are classified depending on lattice types (periodicity formation) of the structure such as square lattice, circular lattice, hexagonal lattice etc. Photonic bandgaps in 2D arrays of PCs can be designed by varying the lattice form comprised of air or dielectric columns immersed in the structure with a definite refractive index contrast [44–47]. In the study of Kee, for a 2D PC in the form of square lattice, PBG responses are compared for dielectric columns and air columns cases. His study revealed that a 2D PC having dielectric columns immersed in an air medium configuration constitutes a wider PBG in comparison to opposite case [48]. Haas and Hwang are investigated the OBG responses for 2D PCs in their studies [49, 50]. Chen proposed OBG reflectors in 2D PCs for the design purposes of waveguides [51, 52]. Furthermore, some heuristic approaches to design wide photonic OBG responses have been proposed to literature [53, 54].

Employing the PBG structures in antenna applications improves the antenna directivity and supports to suppress surface waves which intensify the directivity of antenna [55, 56]. Developing narrowband channelized devices is another requirement in telecommunication systems due to the excessive rates of data. Sharp and narrow band filter devices can be designed using the PC integrated structures in order to use frequency spectrum efficiently without interfering the adjacent channels. Some optical filter application examples can be found in the references [57, 58].

Most of the abovementioned applications and numerical approaches in these studies eventually require solving eigenvalue equation. However, an alternative method can be maintained to investigate and design PBG structures which can provide highly accurate results and does not require excessive computation resources. Previously, similar to PBG structures, passband stopband regions of periodically dielectric loaded rectangular waveguides have been determined using an alternative method based on Generalized Scattering Matrix (GSM) approach [59]. This thesis intends to extend proposed approach to solve 2D PC problems without need to solve common eigenvalue equation. This method is called Auxiliary Functions of Generalized Scattering Matrix (AFGSM) method and has been published in literature recently [60].

1.3 Hypothesis

In this thesis, a new method is proposed which can be used to design an optical component consisting of PBG structures such as omnidirectional reflector, cavity, and dual-polarized waveguide for different frequency regions. The contributions of the proposed method in this thesis covers following remarks; 1) the transmission stop bands of the photonic crystals will be calculated more efficiently and faster than the methods in the literature, 2) to develop an approach that will give fast and accurate results in determining the electrical and geometrical parameters of the structure to work in a given frequency domain for the inverse problem (design), 3) to enable the design of optical components to work independently of variables such as polarization and incidence angle, 4) Due to the difficulty of fabrication of photonic crystals (especially 2D PCs) in nanoscale, modeling with a fast response approach dielectric lattice and defect forms will be suitable for scaling of lithography. The theory relies on the concatenation of scattering parameters (S-parameters) of a single unit cell providing a generalized scattering matrix of the global structure. Floquet theory is incorporated to constitute periodicity through the layers of 2D PC where frequency responses and modal properties of entire structure can be obtained to characterize bandgap properties.

2. WAVE PROPAGATION IN PERIODIC STRUCTURES

2.1 Transmission Line Theory

Electromagnetic wave propagation through a periodic structure is addressed with the solutions of wave equations where Floquet's (Bloch) theorem is incorporated into the Maxwell's equations. The solutions (propagating modes or evanescent modes) of the wave equation supported by a periodic medium are called Floquet modes (Bloch waves). In the problem statement periodic structures are considered as two-port networks or transmission lines which have identical layers (unit cells) cascaded through the boundaries (ports). Fields at the input and output ports of the unit cell can be decomposed into the modes supported by transmission line/network. Each explored Floquet mode corresponds to a Bloch wave vector (propagation constant). Hence, propagation characteristics of a wave guided by a periodic structure can be analyzed via Floquet's theorem [61].

In the following part a brief summary of Floquet's theorem is introduced with brief overview on transmission line theory. We start by deriving basic proof of the Floquet's theorem for a periodic transmission line below. In this case periodic transmission line consist of two sections with different parameters repeated in z direction. In Figure 2.1, the corresponding parameters of each section are defined as follows: l_1 and l_2 are lengths, η_1 and η_2 are characteristic impedances, k_1 and k_2 are wavenumbers of first and second sections of transmission line respectively.

One period of periodic transmission line is denoted by $L = l_1 + l_2$ as given in Figure 2.1. Since the structure is infinitely periodic, there should be no difference between the fields at z and at $z+L$ except for the constant attenuation and phase shift. In other words, the fields at a point z in an infinite periodic structure differ from the fields one period L away by a complex constant. Let $u(z)$ represent a wave (either voltage or current value). Then, a wave $u(z)$ at z and a wave $u(z+L)$ at $z+L$ are related as defined in Floquet's theorem definition. For each intersection of the transmission line can be written as follows

$$\frac{u(z+L)}{u(z)} = \frac{u(z+2L)}{u(z+L)} = ... = \frac{u(z+mL)}{u[z+(m-1)L]} = C \tag{2.1}$$

where C is a constant value.

After applying some basic mathematic steps on equation (2.1) we obtain

$$\frac{u(z+L)}{u(z)} = \frac{u(z+2L)}{u(z+L)} = ... = \frac{u(z+mL)}{u[z+(m-1)L]} = C \rightarrow u(z+mL) = C^m u(z) \tag{2.2}$$

In equation (2.2) the constant C is generally complex and can be represented by $C = e^{-jkL}$ where k is the complex wave number.

Consider function $R(z)$

$$R(z) = e^{jkz}u(z) \tag{2.3}$$

and adding one period of phase shift gives,

$$R(z+L) = e^{jk(z+L)}u(z+L) \text{ or } R(z+L) = e^{jkz}e^{jkL}u(z+L) \tag{2.4}$$

Then, if we substitute $u(z)e^{-jkL}$ by $u(z+L)$ we get

$$R(z+L) = e^{jkz}e^{jkL}e^{-jkL}u(z) = R(z) \tag{2.5}$$

Therefore, $R(z)$ is a periodic function of z with period L and it can be represented in a Fourier series given by

$$R(z) = \sum_{n=-\infty}^{+\infty} A_n e^{-j(2n\pi/L)z} \tag{2.6}$$

if we equate (2.3) to (2.6) we get

$$R(z) = e^{jkz}u(z) = \sum_{n=-\infty}^{+\infty} A_n e^{-j(2n\pi/L)z} \rightarrow u(z) = \sum_{n=-\infty}^{+\infty} A_n e^{-j(k+2n\pi/L)z} \tag{2.7}$$

Another representation of (2.7) is

$$u(z) = \sum_{n=-\infty}^{+\infty} A_n e^{-j(k_n)z}, \quad k_n = k \pm \frac{2n\pi}{L} \tag{2.8}$$

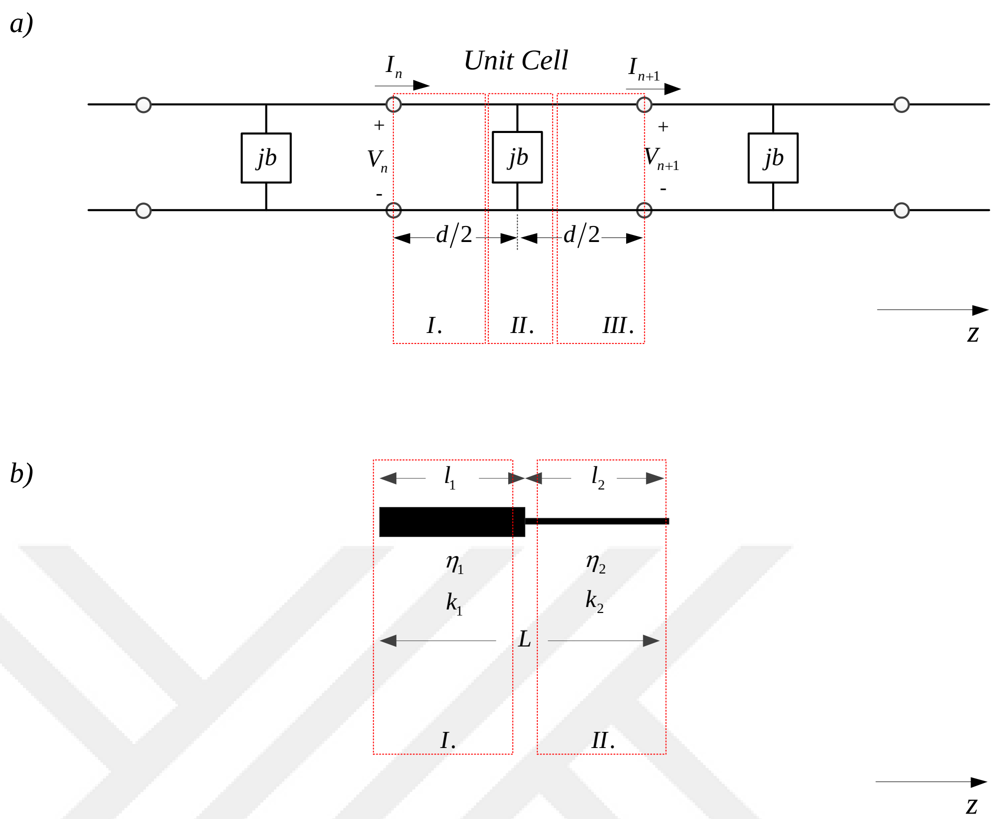

Figure 2.1 : a) Periodically loaded transmission line model, b) two-section line model.

The nth term of the the equation (2.8) is called Floquet's mode or Bloch wave. Floquet's theorem states that a wave guided by a periodic structure contains infinite number of space harmonics [61]. Figure 2.1(a) represents the infinitely long periodic transmission line model and unit cell that comprised of three sections [62]. Each section of unit cell can be represented by a transmission line section of length $d/2$ and a shunt susceptance of b. The unloaded transmission line (TL) has a characteristic impedance Z_0 and a propagation constant k. Infinitely periodic TL can be considered as being composed of two-port identical networks including the voltages and currents on either side of the nth unit cell which can be related as:

$$\begin{bmatrix} V_n \\ I_n \end{bmatrix} = \begin{bmatrix} A & B \\ C & D \end{bmatrix} \begin{bmatrix} V_{n+1} \\ I_{n+1} \end{bmatrix} \tag{2.9}$$

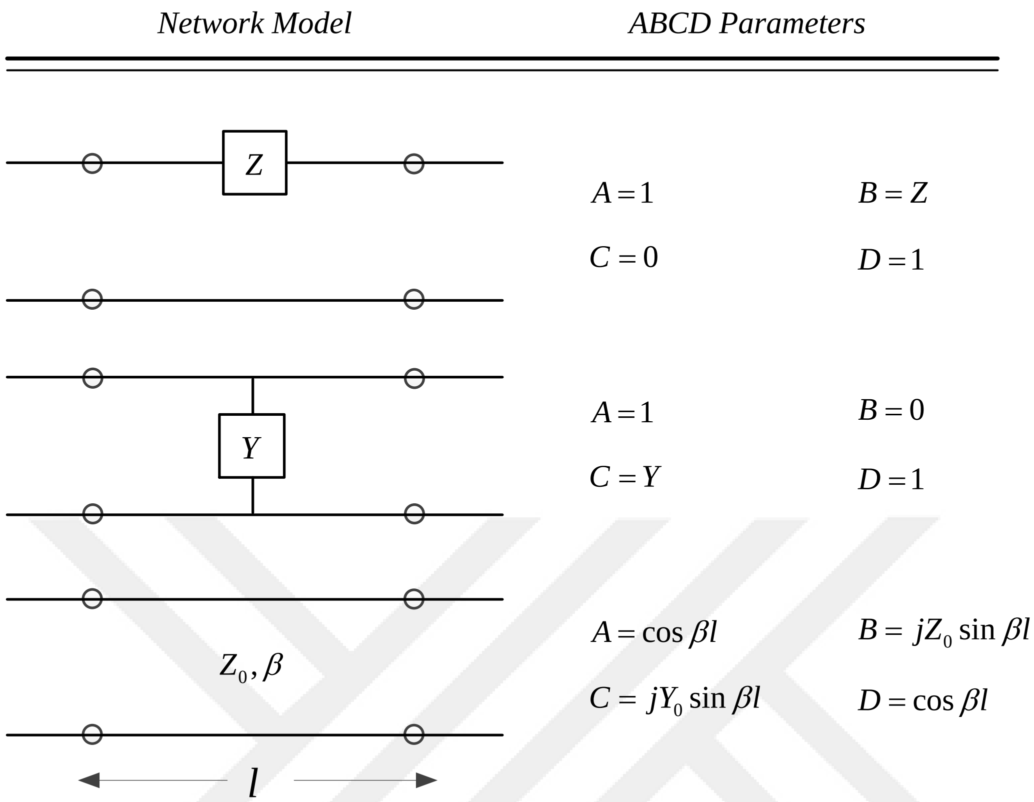

Figure 2.2 : ABCD Parameters of Transmission Line Network Model.

Therefore, each section of unit cell in Figure 2.1(a) can be expressed in ABCD matrix as given in Figure 2.2 [62]. The first and third sections in Figure 2.1(a) corresponds to third type of network model in Figure 2.2 and middle section can be represented by second type of microwave network model in Figure 2.2. Using the related ABCD matrix equivalents the cascade connection of each section can be easily found by multiplying the ABCD matrices of each individual section (equation 2.10).

$$\begin{aligned}\begin{bmatrix} A & B \\ C & D \end{bmatrix} &= \begin{bmatrix} \cos\frac{\theta}{2} & j\sin\frac{\theta}{2} \\ j\sin\frac{\theta}{2} & \cos\frac{\theta}{2} \end{bmatrix} \begin{bmatrix} 1 & 0 \\ jb & 1 \end{bmatrix} \begin{bmatrix} \cos\frac{\theta}{2} & j\sin\frac{\theta}{2} \\ j\sin\frac{\theta}{2} & \cos\frac{\theta}{2} \end{bmatrix} \\ &= \begin{bmatrix} (\cos\frac{\theta}{2} - \frac{b}{2}\sin\theta) & j(\sin\theta + \frac{b}{2}\cos\theta - \frac{b}{2}) \\ j(\sin\theta + \frac{b}{2}\cos\theta - \frac{b}{2}) & (\cos\frac{\theta}{2} - \frac{b}{2}\sin\theta) \end{bmatrix}\end{aligned} \tag{2.10}$$

where $\theta = kd$ and k is the propagation constant. Due to considered network is reciprocal $AD - BC = 1$. Wave analysis of the network can be done assuming a propagating wave in the $+z$ direction. Applying Floquet's theorem to the infinitely long structure provides that the voltage and current at the n-th terminal can differ from the that of at $(n+1)$th terminals only by a propagating factor $e^{\gamma d}$ given by

$$
\begin{aligned}
V_{n+1} &= V_n e^{-\gamma d} \\
I_{n+1} &= I_n e^{-\gamma d}
\end{aligned}
\tag{2.11}
$$

If we substitute equation (2.11) into (2.9) we get

$$
\begin{bmatrix} A - e^{\gamma d} & B \\ C & D - e^{\gamma d} \end{bmatrix} \begin{bmatrix} V_{n+1} \\ I_{n+1} \end{bmatrix} = 0 \tag{2.12}
$$

For a nontrivial solution, determinant of the matrix must be equal to zero:

$$
AD + e^{2\gamma d} - (A+D)e^{\gamma d} - BC = 0, \quad \text{and } AD - BC = 1 \tag{2.13}
$$

$$
1 + e^{2\gamma d} - (A+D)e^{\gamma d} = 0 \tag{2.14}
$$

$$
e^{-\gamma d} + e^{\gamma d} = A + D \tag{2.15}
$$

Using trigonometric identities we obtain

$$
\frac{A+D}{2} = cos\gamma d = cos\theta - \frac{b}{2} sin\theta \tag{2.16}
$$

Propagation constant can be represented as $\gamma = \alpha + j\beta$ and since the right hand-side in equations in (2.16) is purely real, $\alpha = 0$ or $\beta = 0$ is possible. In this case there are two physical results:

If $\alpha = 0, \beta \neq 0$. Then, $\cos(\beta d) = \cos\theta - \frac{b}{2} sin\theta$ which corresponds to a propagating wave with no attenuation which identifies the passband of the periodic structure,

If $\alpha \neq 0, \beta = 0$ or π. Then, $\cos(\alpha d) = |\cos\theta - \frac{b}{2} sin\theta| \geq 1$ which corresponds to a none-propagating wave and attenuates which is the stopband of the periodic structure.

Physically, $\alpha > 0$ states only one solution for positively traveling waves whereas $\alpha < 0$ states only one solution for negatively traveling waves. As a result periodic transmission line can be considered as a filter depending on the exhibition of passband and stopband with related frequency and susceptance values.

Alternatively, unit cell of a TL can be considered as being composed of two different transmission-line sections repeated alternately as given in Figure 2.1(b). In this case two cascaded transmission line will be considered without a section consisting a shunt susceptance and characteristic impedance values "η_i" are used, where i denotes section number. Thus, cascade ABCD matrix is given as

$$\begin{bmatrix} A & B \\ C & D \end{bmatrix} = \begin{bmatrix} \cos\theta_1 & j\eta_1 \sin\theta_1 \\ j\frac{1}{\eta_1}\sin\theta_1 & \cos\theta_1 \end{bmatrix} \begin{bmatrix} \cos\theta_2 & j\eta_2 \sin\theta_2 \\ j\frac{1}{\eta_2}\sin\theta_2 & \cos\theta_2 \end{bmatrix}$$
$$= \begin{bmatrix} \cos\theta_1\cos\theta_2 - \frac{\eta_1}{\eta_2}\sin\theta_1\sin\theta_2 & \\ & -\frac{\eta_2}{\eta_1}\sin\theta_1\sin\theta_2 + \cos\theta_1\cos\theta_2 \end{bmatrix} \tag{2.17}$$

where $\theta_i = k_i l_i = \omega\sqrt{\mu_i \varepsilon_i l_i}$ and $i = 1,2$.

As a result dispersion relation can be expressed as

$$\cos(kL) = \frac{A+D}{2} = \cos k_1 l_1 \cos k_1 l_1 - \frac{1}{2}(\frac{\eta_2}{\eta_1} + \frac{\eta_1}{\eta_2}) \sin k_1 l_1 \sin k_1 l_1 \tag{2.18}$$

Consequently, equations (2.16) and (2.18) are the dispersion equations of periodic transmission line and multilayered structures respectively. Thus, based on the frequency and normalized susceptance values, the periodically loaded TL can be used to exhibit either passbands or stopbands which can be considered as a type of filter. Generally, when investigating the passband or stopband characteristic of a periodic structure, variation of propagation constant β versus the frequency ω is plotted to illustrate wave propagation. This representation is called dispersion diagram (or sometimes called $k-\beta$ or *Brillouin* diagram). Thus far, microwave TL approach is used to derive dispersion relations in periodic structures. In the following section same dispersion equation (eigenvalue equation) will be examined in terms of wave analysis using the conventional ABCD matrix representation [62].

2.2 Conventional ABCD Matrix Method

In this section we have examined "Conventional ABCD Matrix Representation" to understand the relations between the selected geometry and corresponding reflectance spectrum. One-dimensional layered periodic medium is considered to derive dispersion relations. Considered geometry is assumed to be isotropic and nonmagnetic made of different refractive indexed materials where an incident wave propagating in the direction of periodicity z as shown in Figure 2.3.

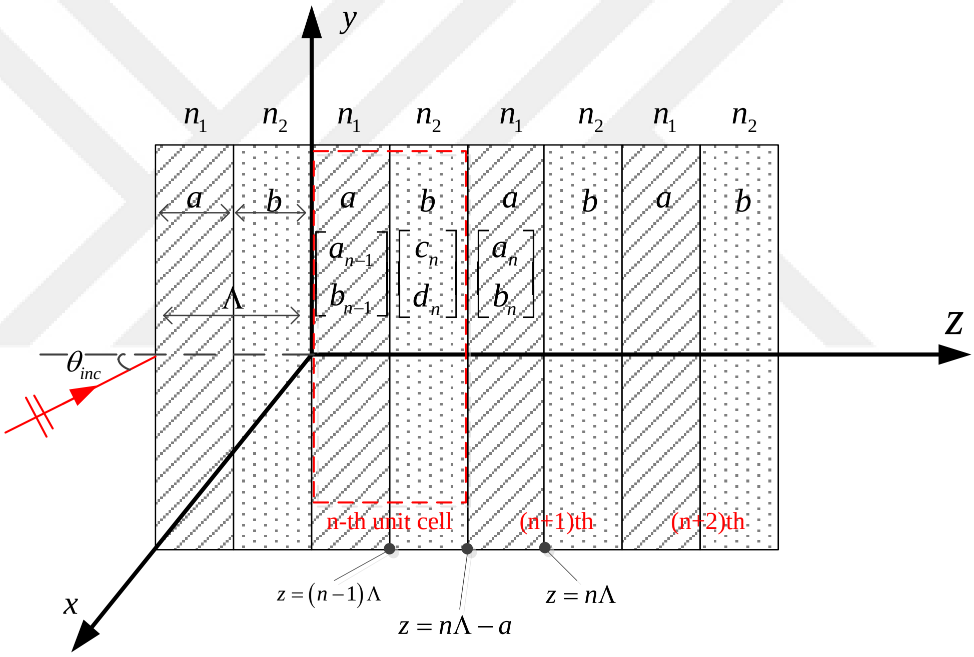

Figure 2.3 : Schematic drawing of a periodic layered medium consisting of alternating layers of two different transparent materials with refractive indices n_1 and n_2 and thicknesses a and b, respectively.

Due to periodicity dielectric constant of the considered geometry is a periodic function of position i.e. $\varepsilon(z) = \varepsilon(z+\Lambda)$ where Λ, namely, the arbitrary lattice constant or spatial period of structure. Here, we derive reflection and transmission spectrum of a periodic medium particularly a 1D PC whose bandgaps can be determined by solving the wave equation.

Therefore, starting with Maxwell's equations for lossless source free region; (time dependency is taken as $e^{j\omega t}$)

Maxwell's equations:

$$\nabla \times \vec{E} = -\frac{\partial \vec{B}}{\partial t}, \tag{2.19a}$$

$$\nabla \times \vec{H} = +\frac{\partial \vec{D}}{\partial t}, \tag{2.19b}$$

$$\nabla \cdot \vec{E} = 0, \tag{2.19c}$$

$$\nabla \cdot \vec{B} = 0 \tag{2.19d}$$

Using the constitutive relations $\vec{D} = \varepsilon_0 \varepsilon_r \vec{E}$ and $\vec{B} = \mu_0 \mu_r \vec{H}$ for simple medium right-hand side of equation (2.19) will take the form

$$\nabla \times \vec{H} = j\omega\varepsilon\vec{E}, \tag{2.20a}$$

$$\nabla \times \vec{E} = -j\omega\mu\vec{H} \tag{2.20b}$$

In order to use periodicity properties fields can be expressed with periodic functions $E_K(z)$ and $H_K(z)$ using the Floquet's (Bloch) theorem given in section 2.2 such that;

$$\vec{E} = E_K(z)e^{-jKz} \tag{2.21}$$

$$\vec{H} = H_K(z)e^{-jKz} \tag{2.22}$$

where

$$E_K(z) = E_K(z+\Lambda) \tag{2.23}$$

$$H_K(z) = H_K(z+\Lambda) \tag{2.24}$$

where K indicates Bloch wave vector (wave number) which functions E_K and H_K depend on. Using the matrix method exact solution of wave equations for periodic layered PC can be obtained as follows;

Assume that an isotropic and nonmagnetic ($\mu = \mu_0$ throughout the periodic structure) periodic layered media consists of two different materials with different refractive indices described as given below:

$$n(z) = \begin{cases} n_2, & 0 < z < b \\ n_1, & b < z < \Lambda \end{cases} \tag{2.25}$$

where b is the thickness of layer with refractive index n_2, the layer with the refractive index n_1 has a thickness of $a = \Lambda - b$.

Periodicity of refractive index in the direction of wave propagation is $n(z) = n(z+\Lambda)$ or $\varepsilon(z) = \varepsilon(z+\Lambda)$ where Λ is the period shown in Figure 2.3 .

Assuming the incident plane wave in the zy-direction and medium is homogeneous in the y-direction thus a general solution for the wave equation can be written as

$$\vec{E}(y,z,t) = E(z)e^{j\omega t}e^{-jk_y y} \tag{2.26}$$

where k_y is the y-component of the wave vector of propagation, constant throughout the medium. Electric field in each layer can be expressed in terms of the travelling waves propagating in the +/- direction of propagation:

$$E(z) = \begin{cases} a_n e^{-jk_1^z(z-n\Lambda)} + b_n e^{jk_1^z(z-n\Lambda)} & n\Lambda - a < z < n\Lambda \\ c_n e^{-jk_2^z(z-n\Lambda+a)} + d_n e^{jk_2^z(z-n\Lambda+a)} & (n-1)\Lambda < z < n\Lambda - a \end{cases} \tag{2.27}$$

where

$$k_1^z = \sqrt{\left(\frac{\omega n_1}{c}\right)^2 - {k_y}^2}$$

$$k_2^z = \sqrt{\left(\frac{\omega n_2}{c}\right)^2 - {k_y}^2}$$

where n denotes n-th unit cell. While the wave propagates along the structure continuity of the tangential electric and magnetic fields at boundary of layers must be satisfied (see Figure 2.4). Then, unknown coefficients a_n, b_n, c_n, d_n can be determined.

Since there is no material change in x-direction $\frac{\partial}{\partial x} \equiv 0$ (yz plane of propagation).

For the TE-polarized modes there is no electric field in the direction of propagation (yz) whereas magnetic field has components in propagation direction

$$\begin{gathered} E_x \neq 0, E_y = 0, E_z = 0 \\ H_x = 0, H_y \neq 0, H_z \neq 0 \end{gathered} \tag{2.28}$$

$$\nabla \times \vec{E} = -j\omega\mu\vec{H} \tag{2.29}$$

$$\begin{bmatrix} \vec{u}_x & \vec{u}_y & \vec{u}_z \\ \frac{\partial}{\partial x} & \frac{\partial}{\partial y} & \frac{\partial}{\partial z} \\ E_x & E_y & E_z \end{bmatrix} = -j\omega\mu\vec{H} = -j\omega\mu \begin{bmatrix} H_x \\ H_y \\ H_z \end{bmatrix} = \vec{u}_y \frac{\partial E_x}{\partial z} - \vec{u}_z \frac{\partial E_x}{\partial y} \tag{2.30}$$

$$\frac{\partial E_x}{\partial z} = -j\omega\mu H_y, \frac{\partial E_x}{\partial y} = j\omega\mu H_z \tag{2.31}$$

Following wave continuity of E_x and H_y at the interfaces $z = (n-1)\Lambda$, $z = n\Lambda - a$ will be considered.

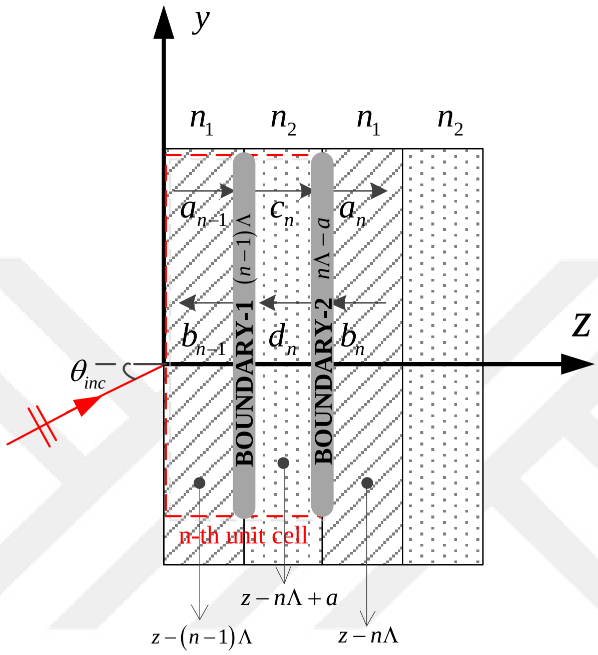

Figure 2.4 : Continuity of the tangential electric and magnetic fields at boundaries.

- Boundary 1: $(n-1)\Lambda$

Electric field, E_x

$a_{n-1}e^{-jk_1^z(z-(n-1)\Lambda)} + b_{n-1}e^{jk_1^z(z-(n-1)\Lambda)}$

$c_n e^{-jk_2^z(z-n\Lambda+a)} + d_n e^{jk_2^z(z-n\Lambda+a)}$

at $z = (n-1)\Lambda$ interface with $\Lambda = a+b$

$(n-1)\Lambda - (n-1)\Lambda = 0$

$(n-1)\Lambda - n\Lambda + a = n\Lambda - \Lambda - n\Lambda + a = a - \Lambda = -b$

Magnetic field, we take derivative of above equations $\frac{\partial E_x}{\partial z} = -j\omega\mu H_y$,

$-jk_1^z a_{n-1}e^{-jk_1^z(z-(n-1)\Lambda)} + jk_1^z b_{n-1}e^{+jk_1^z(z-(n-1)\Lambda)}$

$-jk_2^z c_n e^{-jk_2^z(z-n\Lambda+a)} + jk_2^z d_n e^{+jk_2^z(z-n\Lambda+a)}$

at $z = (n-1)\Lambda$ interface with $\Lambda = a + b$ gives

$$jk_1^z(a_{n-1} - b_{n-1}) = jk_2^z(c_n e^{+jk_2^z b} - d_n e^{-jk_2^z b}) \tag{2.32}$$

- Boundary 2: $n\Lambda - a$

  Electric field E_x

  $a_n e^{-jk_1^z(z-n\Lambda)} + b_n e^{+jk_1^z(z-n\Lambda)}$

  $c_n e^{-jk_2^z(z-n\Lambda+a)} + d_n e^{+jk_2^z(z-n\Lambda+a)}$

  at $z = n\Lambda - a$ interface

$$c_n + d_n = a_n e^{jk_1^z a} + b_n e^{-jk_1^z a} \tag{2.33}$$

  Magnetic field, we take derivative of above equations $\frac{\partial E_x}{\partial z} = -j\omega\mu H_y$,

  $-jk_1^z a_n e^{-jk_1^z(z-n\Lambda)} + jk_1^z b_n e^{+jk_1^z(z-n\Lambda)}$

  $-jk_2^z c_n e^{-jk_2^z(z-n\Lambda+a)} + jk_2^z d_n e^{+jk_2^z(z-n\Lambda+a)}$

  at $z = n\Lambda - a$ interface

$$jk_2^z(c_n - d_n) = jk_1^z(a_n e^{jk_1^z a} - b_n e^{-jk_1^z a}) \tag{2.34}$$

As a summary continuity equations can be written as

$$a_{n-1} + b_{n-1} = c_n e^{jk_2^z b} + d_n e^{-jk_2^z b} \tag{2.35a}$$

$$jk_1^z(a_{n-1} - b_{n-1}) = jk_2^z(c_n e^{+jk_2^z b} + d_n e^{-jk_2^z b}) \tag{2.35b}$$

$$c_n + d_n = a_n e^{jk_1^z a} + b_n e^{-jk_1^z a} \tag{2.35c}$$

$$jk_2^z(c_n - d_n) = jk_1^z(a_n e^{jk_1^z a} - b_n e^{-jk_1^z a}) \tag{2.35d}$$

Eqs. 2.35 can also be written in matrix form:

$$\begin{bmatrix} 1 & 1 \\ jk_1^z & -jk_1^z \end{bmatrix} \begin{bmatrix} a_{n-1} \\ b_{n-1} \end{bmatrix} = \begin{bmatrix} e^{jk_2^z b} & e^{-jk_2^z b} \\ jk_2^z e^{jk_2^z b} & -jk_2^z e^{-jk_2^z b} \end{bmatrix} \begin{bmatrix} c_n \\ d_n \end{bmatrix} \tag{2.36}$$

and

$$\begin{bmatrix} 1 & 1 \\ jk_2^z & -jk_2^z \end{bmatrix} \begin{bmatrix} c_n \\ d_n \end{bmatrix} = \begin{bmatrix} e^{jk_1^z a} & e^{-jk_1^z a} \\ jk_1^z e^{jk_1^z a} & -jk_1^z e^{-jk_1^z a} \end{bmatrix} \begin{bmatrix} a_n \\ b_n \end{bmatrix} \tag{2.37}$$

In order to solve matrix equation column vector $\begin{bmatrix} c_n \\ d_n \end{bmatrix}$ in equation (2.37) is eliminated, and using the unit-cell translation matrix $\begin{bmatrix} a_{n-1} \\ b_{n-1} \end{bmatrix} = \begin{bmatrix} A & B \\ C & D \end{bmatrix} \begin{bmatrix} a_n \\ b_n \end{bmatrix}$ which relates the amplitudes of the plane waves in first layer of n-th unit cell and first layer of $(n+1)$-th unit cell.

Since $\begin{bmatrix} A & B \\ C & D \end{bmatrix}$ matrix relates amplitudes of two equivalent layers with same refractive index, it's unimodular. Therefore $\begin{bmatrix} A & B \\ C & D \end{bmatrix} = AD - BC = 1$.

According to Bloch theorem , the electric field vector of a normal mode of propagation in a periodic medium is of the form

$$\vec{E}(y,z,t) = E(z)e^{j\omega t}e^{-jk_y y} \tag{2.38a}$$

and

$$\vec{E} = E_K(z)e^{-jKz} \tag{2.38b}$$

$$\vec{E} = E_K(z)e^{-jKz}e^{j(\omega t - k_y y)} \tag{2.38c}$$

where $E_K(z)$ is a periodic function with period Λ, $E_K(z) = E_K(z+\Lambda)$

Using the periodicity, Bloch wave can be expressed as

$$\begin{bmatrix} a_n \\ b_n \end{bmatrix} = e^{-iK\Lambda} \begin{bmatrix} a_{n-1} \\ b_{n-1} \end{bmatrix} \tag{2.39}$$

and substituting the unit-cell translation matrix into this equation gives;

$$\begin{bmatrix} a_n \\ b_n \end{bmatrix} = e^{-iK\Lambda} \begin{bmatrix} A & B \\ C & D \end{bmatrix} \begin{bmatrix} a_n \\ b_n \end{bmatrix} \longrightarrow \begin{bmatrix} a_n \\ b_n \end{bmatrix} e^{iK\Lambda} = \begin{bmatrix} A & B \\ C & D \end{bmatrix} \begin{bmatrix} a_n \\ b_n \end{bmatrix} \tag{2.40}$$

Final representation in equation (2.40) is an ordinary linear eigensystem problem in the form of $Ax = \lambda x$. The propagating modes are the solutions of the eigenvalue equation and $e^{iK\Lambda}$ is the eigenvalue of the unit-cell translation matrix $\begin{bmatrix} A & B \\ C & D \end{bmatrix}$.

$$\begin{bmatrix} a_n \\ b_n \end{bmatrix} e^{iK\Lambda} = \begin{bmatrix} A & B \\ C & D \end{bmatrix} \begin{bmatrix} a_n \\ b_n \end{bmatrix} \longrightarrow \begin{bmatrix} A & B \\ C & D \end{bmatrix} \begin{bmatrix} a_n \\ b_n \end{bmatrix} - e^{iK\Lambda} \begin{bmatrix} a_n \\ b_n \end{bmatrix} = 0$$

$$\left(\begin{bmatrix} A & B \\ C & D \end{bmatrix} - \mathbf{I}e^{iK\Lambda}\right)\begin{bmatrix} a_n \\ b_n \end{bmatrix} = 0$$

where $\mathbf{I}$ is the identity matrix and $e^{iK\Lambda}$ can be represented as a diagonal matrix such that
$\begin{bmatrix} e^{iK\Lambda} & 0 \\ 0 & e^{iK\Lambda} \end{bmatrix} \longrightarrow \begin{bmatrix} A - e^{iK\Lambda} & 0 \\ 0 & D - e^{iK\Lambda} \end{bmatrix}\begin{bmatrix} a_n \\ b_n \end{bmatrix} = 0.$
For a nontrivial solution, determinant of the matrix must be equal to zero:

$$AD - (A+D)e^{iK\Lambda} + e^{2iK\Lambda} - BC = 0, AD - BC = 1 \tag{2.41a}$$

$$1 + e^{2iK\Lambda} - (A+D)e^{iK\Lambda} = 0 \tag{2.41b}$$

$$e^{-iK\Lambda} + e^{iK\Lambda} = A + D \tag{2.41c}$$

Using the Euler identities:

$$e^{iK\Lambda} = \cos(K\Lambda) + i\sin(K\Lambda)$$

$$e^{-iK\Lambda} = \cos(K\Lambda) - i\sin(K\Lambda)$$

Thus

$$e^{iK\Lambda} + e^{-iK\Lambda} = 2\cos(K\Lambda) = A + D$$

Thus, $\cos(K\Lambda) = \frac{A+D}{2}$ or

$$e^{iK\Lambda} = \frac{1}{2}(A+D) \pm \sqrt{\frac{1}{4}(A+D)^2 - 1} \tag{2.42}$$

Matrix elements of TE wave and TM wave are

$$A_{TE} = e^{jk_1^z a}\left[\cos(k_2^z b) + \frac{j}{2}\left(\frac{k_2^z}{k_1^z} + \frac{k_1^z}{k_2^z}\right)\sin(k_2^z b)\right] \tag{2.43a}$$

$$B_{TE} = e^{-jk_1^z a}\left[\frac{j}{2}\left(\frac{k_2^z}{k_1^z} - \frac{k_1^z}{k_2^z}\right)\sin(k_2^z b)\right] \tag{2.43b}$$

$$C_{TE} = e^{jk_1^z a}\left[-\frac{j}{2}\left(\frac{k_2^z}{k_1^z} - \frac{k_1^z}{k_2^z}\right)\sin(k_2^z b)\right] \tag{2.43c}$$

$$D_{TE} = e^{-jk_1^z a}\left[\cos(k_2^z b) - \frac{j}{2}\left(\frac{k_2^z}{k_1^z} + \frac{k_1^z}{k_2^z}\right)\sin(k_2^z b)\right] \tag{2.43d}$$

$$A_{TM} = e^{jk_1^z a}\left[\cos(k_2^z b) + \frac{j}{2}\left(\frac{n_2^2 k_1^z}{n_1^2 k_2^z} + \frac{n_1^2 k_2^z}{n_2^2 k_1^z}\right)\sin(k_2^z b)\right] \tag{2.44a}$$

$$B_{TM} = e^{-jk_1^z a}\left[\frac{j}{2}\left(\frac{n_2^2 k_1^z}{n_1^2 k_2^z} - \frac{n_1^2 k_2^z}{n_2^2 k_1^z}\right)\sin(k_2^z b)\right] \tag{2.44b}$$

$$C_{TM} = e^{jk_1^z a}\left[-\frac{j}{2}\left(\frac{n_2^2 k_1^z}{n_1^2 k_2^z} - \frac{n_1^2 k_2^z}{n_2^2 k_1^z}\right)\sin(k_2^z b)\right] \tag{2.44c}$$

$$D_{TM} = e^{-jk_1^z a}\left[\cos(k_2^z b) - \frac{j}{2}\left(\frac{n_2^2 k_1^z}{n_1^2 k_2^z} + \frac{n_1^2 k_2^z}{n_2^2 k_1^z}\right)\sin(k_2^z b)\right] \tag{2.44d}$$

Therefore eigenvalue equation for TE and TM cases can be expressed as

$$\cos(K\Lambda) = \cos(k_1^z a)\cos(k_2^z b) - M\sin(k_1^z a)\sin(k_1^z b) \tag{2.45}$$

where

$$M = \begin{cases} \frac{1}{2}\left(\frac{k_2^z}{k_1^z} + \frac{k_1^z}{k_2^z}\right) & TE \\ \frac{1}{2}\left(\frac{n_1^2 k_2^z}{n_2^2 k_1^z} + \frac{n_2^2 k_1^z}{n_1^2 k_2^z}\right) & TM \end{cases} \tag{2.46}$$

and

$$k_i^z = \sqrt{\left(\frac{\omega n_i}{c}\right)^2 - (k^y)^2}, \qquad i = 1,2 \tag{2.47}$$

As a result following three important definitions can be stated as (see [23]):

1. If $\left|\frac{(A+D)}{2}\right| < 1 \longrightarrow K$ is real and corresponds to propagating Bloch waves,
2. If $\left|\frac{(A+D)}{2}\right| > 1 \longrightarrow K$ has real and imaginary parts. This type of waves are called Evanescent Bloch waves and correspond to "photonic bandgaps" of periodic medium,
3. If $\left|\frac{(A+D)}{2}\right| = 1 \longrightarrow$ corresponds to "photonic band edges"

2.3 Auxiliary Functions of Generalized Scattering Matrix (AFGSM) Method

In this section, bandgap characteristics of periodic structures are analyzed considering a two-port microwave circuit unit cell model. S-parameters of unit cell is determined with given corresponding voltage and current representations (see Figure 2.5).

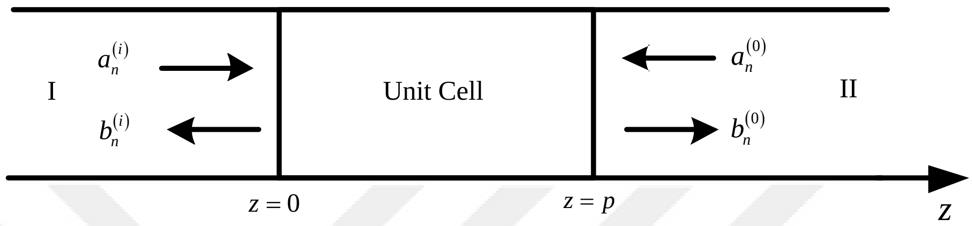

Figure 2.5 : Unit cell of periodic structure 2-port network.

$$a_i = \frac{V_i^+}{\sqrt{Z_{0i}}} = I_i^+ \sqrt{Z_{0i}} \tag{2.48a}$$

$$b_i = \frac{V_i^-}{\sqrt{Z_{0i}}} = I_i^- \sqrt{Z_{0i}} \tag{2.48b}$$

where a_i and b_i denote incident and reflected waves, V_i^+ and V_i^- denote incident and reflected voltages, I_i^+ and I_i^- denote incident and reflected currents respectively [62].

Using above relations S-matrix of the unit cell can be given as

$$\begin{bmatrix} b_1 \\ b_2 \end{bmatrix} = \begin{bmatrix} S_{11} & S_{12} \\ S_{21} & S_{22} \end{bmatrix} \begin{bmatrix} a_1 \\ a_2 \end{bmatrix} \tag{2.49}$$

with

$$S_{11} = \frac{b_1}{a_1}\bigg|_{a_2=0}, \quad S_{21} = \frac{b_2}{a_1}\bigg|_{a_2=0}, \quad S_{12} = \frac{b_1}{a_2}\bigg|_{a_1=0}, \quad S_{22} = \frac{b_2}{a_2}\bigg|_{a_1=0} \tag{2.50}$$

Electric and magnetic fields for a homogeneously periodic structured waveguide are given as

$$E_y^{(I)} = \sum_{n=1}^{N} a_n^{(i)} \sqrt{Z_n^{(i)}} f_n^{(i)} e^{-\alpha_n^{(i)} z} + \sum_{n=1}^{N} b_n^{(i)} \sqrt{Z_n^{(i)}} f_n^{(i)} e^{\alpha_n^{(i)} z} \tag{2.51a}$$

$$H_x^{(I)} = \sum_{n=1}^{N} -a_n^{(i)} \sqrt{Y_n^{(i)}} f_n^{(i)} e^{-\alpha_n^{(i)} z} + \sum_{n=1}^{N} b_n^{(i)} \sqrt{Y_n^{(i)}} f_n^{(i)} e^{\alpha_n^{(i)} z} \tag{2.51b}$$

$$E_y^{(II)} = \sum_{n=1}^{N} b_n^{(0)} \sqrt{Z_n^{(0)}} f_n^{(0)} e^{-\alpha_n^{(0)}(z-p)} + \sum_{n=1}^{N} a_n^{(0)} \sqrt{Z_n^{(0)}} f_n^{(0)} e^{\alpha_n^{(0)}(z-p)} \tag{2.51c}$$

$$H_x^{(II)} = -\sum_{n=1}^{N} b_n^{(0)} \sqrt{Y_n^{(0)}} f_n^{(0)} e^{-\alpha_n^{(0)}(z-p)} + \sum_{n=1}^{N} a_n^{(0)} \sqrt{Y_n^{(0)}} f_n^{(0)} e^{\alpha_n^{(0)}(z-p)} \tag{2.51d}$$

where Z is impedance, Y is admittance, f_n is used for wave expansion coefficients and they are symmetric such as $f_n^{(i)} = f_n^{(0)}$, $Z_n^{(i)} = Z_n^{(0)}$, $Y_n^{(i)} = Y_n^{(0)}$.

Using the boundary conditions i.e. for incident waves at $z = 0$ and for reflected waves at $z = p$

$$E_y^{(i)} = E_y^{(I)}\Big|_{z=0} \qquad E_y^{(0)} = E_y^{(II)}\Big|_{z=p} \tag{2.52a}$$

$$H_x^{(i)} = H_x^{(I)}\Big|_{z=0} \qquad H_x^{(0)} = H_x^{(II)}\Big|_{z=p} \tag{2.52b}$$

Applying Floquet condition with λ, eigenvalue of the periodic structure, which means reflected waves can differ from incident waves only by the λ as explained in the previous sections.

$$E_y^{(0)} = \lambda E_y^{(i)} \tag{2.53a}$$

$$H_x^{(0)} = \lambda H_x^{(i)} \tag{2.53b}$$

As a result field equations are simplified to

$$\sum_{n=1}^{N} (a_n^{(0)} + b_n^{(0)}) \sqrt{Z_n^{(0)}} f_n^{(0)} = \lambda \sum_{n=1}^{N} (a_n^{(i)} + b_n^{(i)}) \sqrt{Z_n^{(i)}} f_n^{(i)} \tag{2.54a}$$

$$\sum_{n=1}^{N} -(b_n^{(0)} - a_n^{(0)}) \sqrt{Y_n^{(0)}} f_n^{(0)} = -\lambda \sum_{n=1}^{N} (a_n^{(i)} - b_n^{(i)}) \sqrt{Y_n^{(i)}} f_n^{(i)} \tag{2.54b}$$

Due to symmetry condition $f_n^{(i)} = f_n^{(0)}$, $Z_n^{(i)} = Z_n^{(0)}$, $Y_n^{(i)} = Y_n^{(0)}$ equation (2.54a) simplifies to

$$\sum_{n=1}^{N} (a_n^{(0)} + b_n^{(0)}) = \sum_{n=1}^{N} \lambda (a_n^{(i)} + b_n^{(i)}) \tag{2.55a}$$

$$\sum_{n=1}^{N} (b_n^{(0)} - a_n^{(0)}) = \sum_{n=1}^{N} \lambda (a_n^{(i)} - b_n^{(i)}) \tag{2.55b}$$

Equations 2.55a(a-b) can be simplified and represented in a matrix form

$$\left.\begin{array}{l} (a^{(0)} + b^{(0)}) = \lambda (a^{(i)} + b^{(i)}) \\ (b^{(0)} - a^{(0)}) = \lambda (a^{(i)} - b^{(i)}) \end{array}\right\} \begin{array}{l} b^{(0)} = \lambda a^{(i)} \\ a^{(0)} = \lambda b^{(i)} \end{array} \tag{2.56}$$

by representing in the form of equation (2.49) we get

$$\begin{bmatrix} b^{(i)} \\ b^{(0)} \end{bmatrix} = \begin{bmatrix} S_{11} & S_{12} \\ S_{21} & S_{22} \end{bmatrix} \begin{bmatrix} a^{(i)} \\ a^{(0)} \end{bmatrix} \tag{2.57}$$

by replacing the zero-th incident and reflected waves with *i*-th elements using the equation (2.56)

$$\begin{bmatrix} b^{(i)} \\ \lambda a^{(i)} \end{bmatrix} = \begin{bmatrix} S_{11} & S_{12} \\ S_{21} & S_{22} \end{bmatrix} \begin{bmatrix} a^{(i)} \\ \lambda b^{(i)} \end{bmatrix} \tag{2.58}$$

we can represent equation (2.58) in the form of eigenvalue equation

$$\begin{bmatrix} 1 & -S_{11} \\ 0 & -S_{21} \end{bmatrix} \begin{bmatrix} b^{(i)} \\ a^{(i)} \end{bmatrix} = \lambda \begin{bmatrix} -S_{12} & 0 \\ -S_{22} & 1 \end{bmatrix} \begin{bmatrix} b^{(i)} \\ a^{(i)} \end{bmatrix} \tag{2.59}$$

Final equation 2.59 is the eigenvalue equation of the unit cell. Solution to this equation gives information of eigenstates which is the passband information of the system and it can be expresses as $S_{11} = S_{22}, S_{21} = S_{12}$,

$$\lambda^2 + \lambda \left(\frac{S_{11}^2 - S_{21}^2 - 1}{S_{21}} \right) + 1 = 0 \tag{2.60}$$

The roots of the equation (2.60)

$$\left.\begin{aligned}\lambda_1 &= \left(\frac{-S_{11}^2-S_{21}^2-1}{S_{21}}\right)+\sqrt{\Delta}\\ \lambda_2 &= \left(\frac{-S_{11}^2-S_{21}^2-1}{S_{21}}\right)-\sqrt{\Delta}\end{aligned}\right\} \lambda_1+\lambda_2 = \frac{-S_{11}^2-S_{21}^2-1}{S_{21}} \tag{2.61}$$

which corresponds to

$$\left.\begin{aligned}\lambda_1 &= e^{-j\theta}\\ \lambda_2 &= e^{+j\theta}\end{aligned}\right\} \lambda_1+\lambda_2 = 2\cos\theta \quad \text{thus,} \quad \cos\theta = \frac{1-S_{11}^2+S_{21}^2}{2S_{21}} \tag{2.62}$$

For the structures propagating single mode, stop bands and bandedges can be identified. At the stopbands λ and θ parameters take the following values

$\lambda_1 = \lambda_2 = 1$ while $\theta = 0$, $\lambda_1 = \lambda_2 = -1$ while $\theta = \pm\pi$, In the passband region $|\lambda_1| = |\lambda_2| = 1$.

Another possible formulation is stated which gets rid of the effort to solve eigen-equation, instead scattering-matrix of symmetric UC is used to interpretation as given in the RHS of equation (2.62). Generalized scattering matrix (GSM) of cascaded networks is well analyzed in the literature. Straightforward cascading of two scattering matrices solves the electromagnetic problem of junction scattering to avoid the often occurring large transmission matrix elements that lead to computational difficulties. After calculating the final scattering parameters of N cascaded unit cells, auxiliary functions X_+ and X_- are used to determine photonic edge frequencies by observing the zero transitions of the imaginary part of $(S_{11}\pm S_{21})$ given by;

$$X_\pm = Im\{S_{11} \pm S_{21}\} \tag{2.63}$$

It should be noted that some arbitrary roots might appear while searching the zero transitions of the auxiliary functions. In such a case, we discard the roots which correspond to bandedge frequencies located out of the interested waveband region which includes the photonic bandgap. The proposed technique effectively returns precise estimations for the calculation of bandedge frequencies supported by Floquet modes just by performing a straightforward root-determination algorithm based on auxiliary functions, namely Auxiliary Functions of Generalized Scattering Matrix (AFGSM). Convergency success of the integrated computational routine enables one to perform comprehensive studies in order to find PBG characteristics of stacked periodic mediums while maintaining the higher order Floquet modes.

2.4 Numerical Results

In this subsection, we considered two numerical examples in order to show applicability of proposed method to different applications. In the first problem a wideband omnidirectional bandgap (OBG) reflector design study is presented using photonic crystal structures (Te, Ta_2O_5, TiO_2) satisfying the periodicity condition and related simulation results were given. The designed final reflector provides an omnidirectional photonic stop band with a value of 56.63% omnidirectional relative bandwidth (ORB) in the range of 924 nm to 1654 nm of optical wavelength region.

In Figure 2.6 dashed lines represent the photonic crystal couple-1 (PC1) which consist of Tellurium ($n_1 = 4.6$) and Ta_2O_5 ($n_2 = 2.1$) and dashed-dot lines represent photonic crystal couple-2 (PC2) which consist of Tellurium ($n_1 = 4.6$) and TiO_2 ($n_2 = 2.45$), respectively. Incidence medium is assumed to be air ($n_0 = 1$).

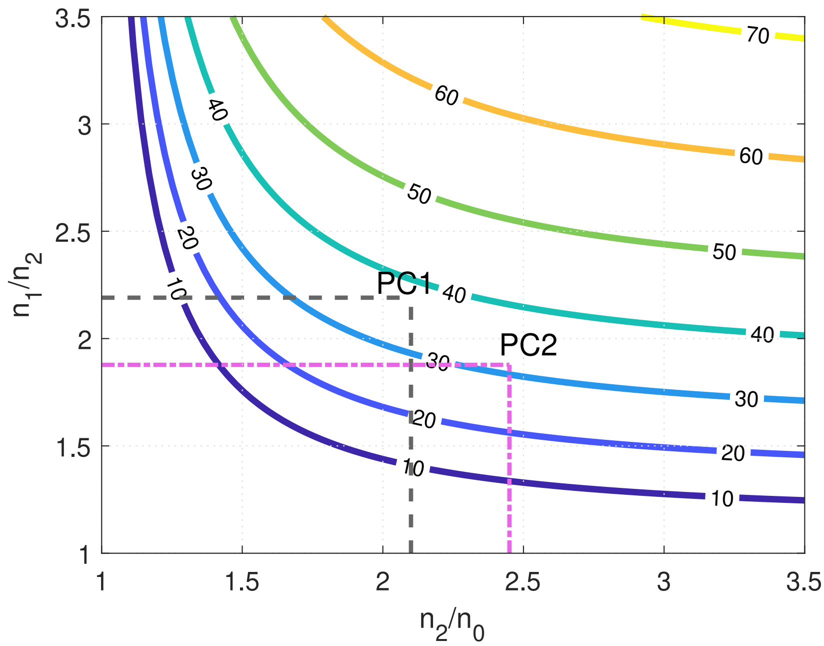

Figure 2.6 : Omnidirectional reflection contour plot as a function of n_1/n_2 and n_2/n_0.

Band edge frequencies of designed omnidirectional reflector can be calculated by utilizing AFGSM method on particular incidence angle and polarizations (TM-0^0 and TM-90^0). In Figure 2.7 and Figure 2.8 dashed blue lines represent X_+ curve and solid red lines represent X_- curve of AFGSM method in which zero transitions of the curves corresponds to bandedge frequencies of the bandgaps for PC1 and PC2, respectively. Obtained bandedge frequencies and ORB values are summarized in table 2.1. PC1 (Tellurium, Ta_2O_5) pair provides an ORB with 416 nm bandwidth and PC2 (Tellurium, TiO_2) pair provides an ORB value of 321 nm.

Table 2.1 : Summary of selected material properties and related bandgap responses.

PC pair	p_1(nm)	p_2(nm)	TM 0^0 (nm)	TM 89^0 (nm)	OBG (nm)	OBG (%)
PC1	112.8	96.8	1238.2 - 1821	1205.2 - 1654.9	416	28.76
PC2	48.8	132	924.6 - 1357	879.6 - 1245.6	321	29.58

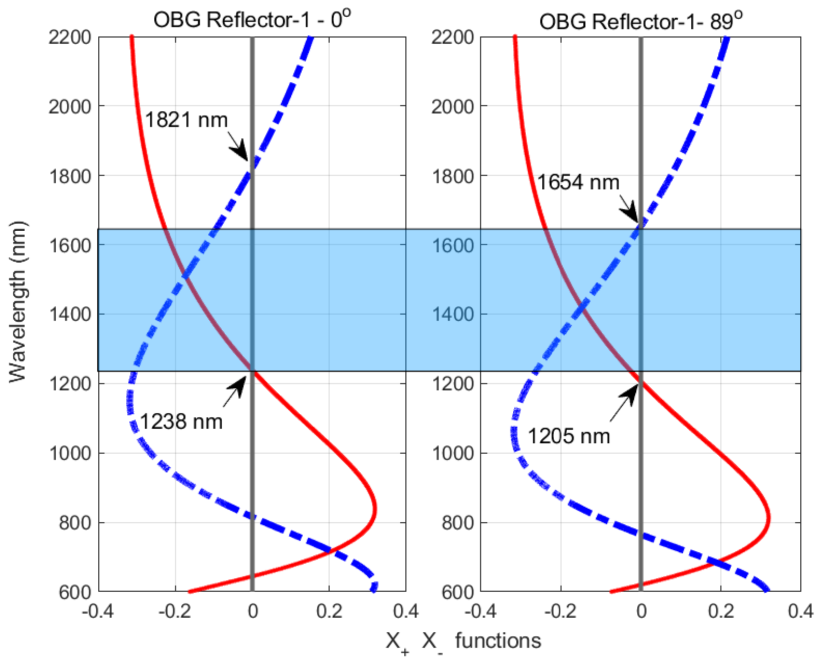

Figure 2.7 : Estimating bandedge frequencies of OBG reflectors using AFGSM method for PC1 pair.

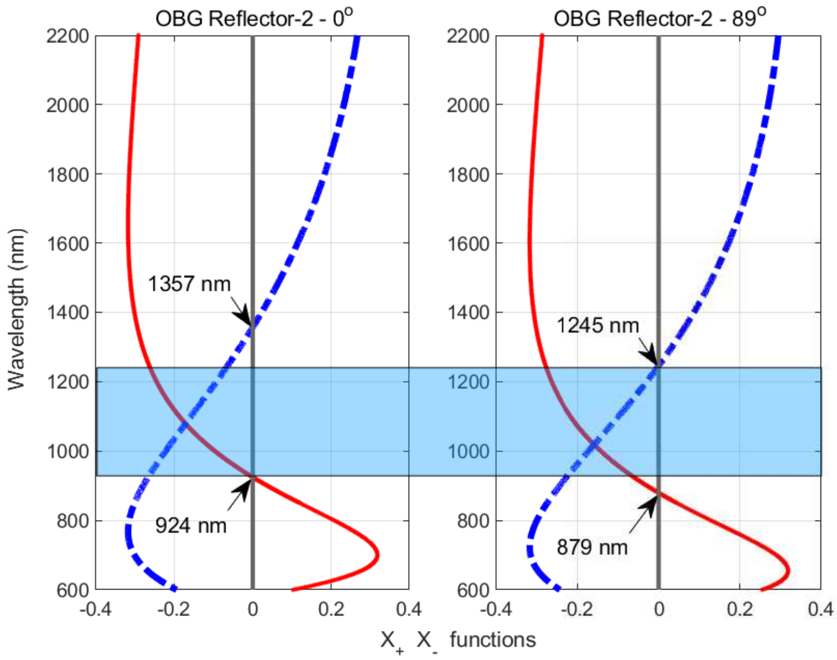

Figure 2.8 : Estimating bandedge frequencies of OBG reflectors using AFGSM method for PC2 pair.

Finally coupling of two PC pairs results in a wideband OBG reflector. Designed reflector has a stopband of 737 nm and ORB value of 56.63% (see Figure 2.9). Moreover, computational response is 10^3 times faster than commercial simulators (HFSS, CST).

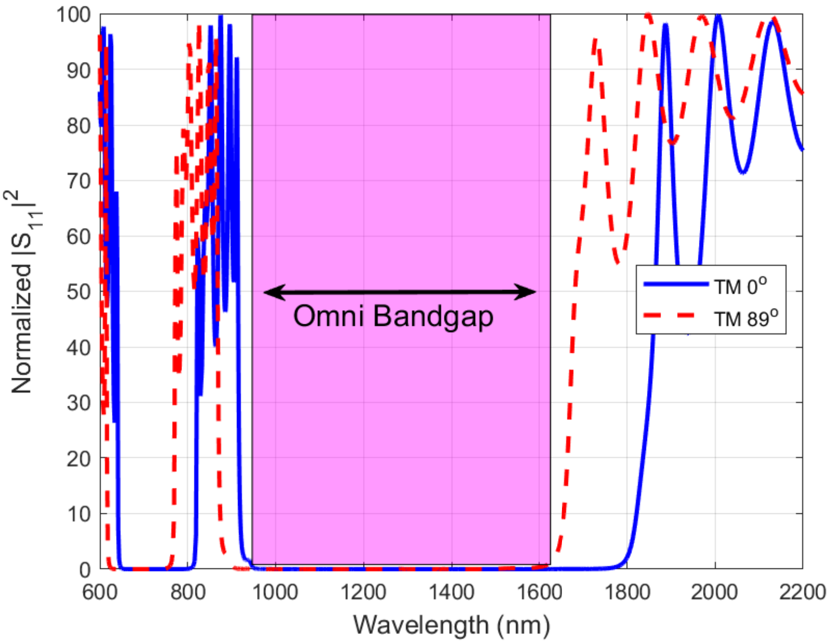

Figure 2.9 : OBG band region of wideband reflector.

In the second numerical example, 4-channel optical filter design is presented. Design algorithm comprised of two steps. In the first step, required layer thicknesses are determined using the AFGSM method for the desired bandgap. In the second step, transmission bands maintained by utilizing defect modes correspond to filter's center frequencies. Obtained results verified with transfer matrix method and CST electromagnetic simulation software.

For the design purposes Ta_2O_5, MgF_2 materials are selected with the refractive indices 2.11 and 1.38 respectively. Layer thicknesses are sweeped with AFGSM method widest stopband is obtained between 167.5 THz (1791 nm) and 219.2 THz (1368 nm) range with a layer thickness values of $p_1 = 183$ nm and $p_2 = 280$ nm, respectively. Zero transitions of auxiliary functions are illustrated in Figure 2.10.

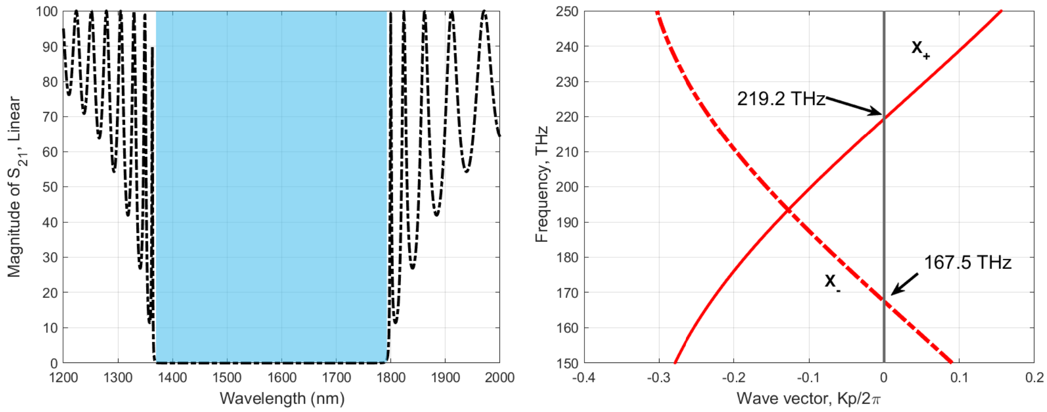

Figure 2.10 : Wide bandgap reflector design.

In table 2.2 desired filter channel center wavelengths and related defect layer thicknesses are given. Hence, 4-channel narrowband transmission channel responses can be designed in the 1550 nm region.

Table 2.2 : Designed filter parameters.

Optical channel no	Transmission band wavelengths	Defect layer thickness
λ_1	1496 nm	$0.8l_d$
λ_2	1523 nm	$0.9l_d$
λ_3	1550 nm	l_d
λ_4	1577 nm	$1.1l_d$

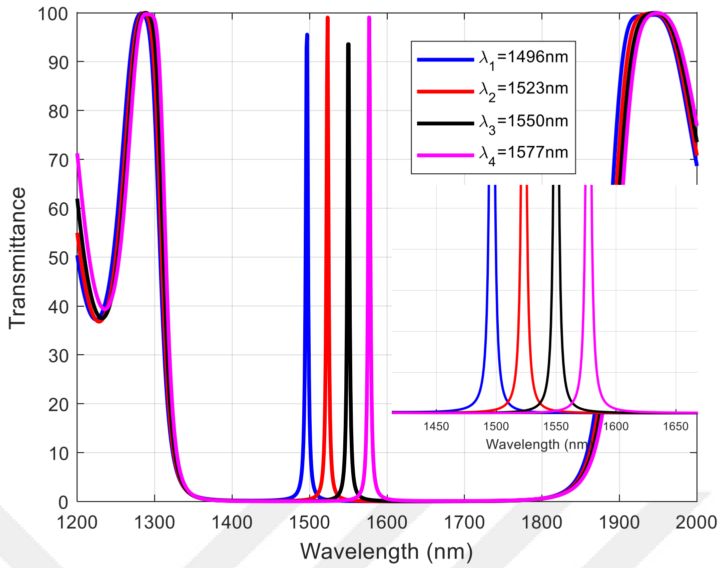

Figure 2.11 : 4 channel optical filter transmission bands.

As shown in numerical examples AFGSM method can be efficiently used for design of different photonic crystal based components in THz spectrum. Inverse problem which seek for proper physical parameters for desired objective is another area that the proposed method being employed. Preliminary simulation results showed that AFGSM method provides a computational advantage over CST more than 100 times (for a stack of 20 unit cells) whereas providing 1000 times faster response than HFSS does for a problem including 106 calculation steps. Therefore, AFGSM method can be used properly used in precisely modeling of photonic crystal based optical components.

3. A FAST HYBRID METHOD FOR THE BANDGAP ANALYSIS OF 2D PHOTONIC CRYSTALS BASED ON EMT AND AFGSM METHODS [1]

3.1 Introduction

For many years, phenomenal relation between the EM fields and periodic materials particularly scattering and confining effects of wave propagation, has attracted attention of many researchers [63, 64]. Numerous practical applications developed related to high refractive index contrast between concurrent layers and its effect on signal intensity yielding photonic bandgap (PBG) characteristics. Among available dielectric substrates photonic crystals (PCs) are the most popular ones used to achieve aforementioned refractive index contrast. Besides the contrast in refractive indices, implementing a modulation to thickness and formation allows to existance of PBGs. Hence, useful optical and photonic components can be modeled e.g. thin-film filters, channel drop filters, optical delay lines [3, 6, 65, 66], optical-isolators [7], resonance-filters [8], photonic-nanocavities, photonic-crystal mirrors [9, 10], polarization splitters, optical interleavers [11, 12], photonic-crystal tapers, splitters and combiners [13, 14], planar reflectors, waveguide bends and mirrors [15]. Various new surveys examining the modification of light confinement in PCs have been reported e.g. 2D magnetic photonic crystal defect structures for circulator design [16], cross-shaped PC waveguide with wide bandwidth configuration [17] and tunable PBG structures by modificating the permittivities of materials using an external parameter such as temperature [18, 67], electric field [20, 68] and magnetic field [22], etc.

Commonly, the wave propagation in 2D periodic structures is analyzed using the dispersion relation governed by Bloch waves which is initially derived from solutions of Maxwell's equations. A lot of mathematical techniques have been formulated to specify the photonic band structure of PCs. Typically employed techniques include Transfer Matrix Method (TMM), Finite-Difference Time-Domain (FDTD) method,

[1] This chapter is based on the paper "Erkan, O., Akıncı, M. N., Şimşek, S., 2018. A fast hybrid method for the bandgap analysis of 2D photonic crystals based on EMT and AFGSM methods, AEU-International Journal of Electronics and Communications, 87, 107-112."

Multiple Scattering (MST) method, Plane-Wave Expansion (PWE) method,and Finite Element Method (FEM) [1, 2, 69–73]. Nevertheless, effectiveness and precision of abovementioned techniques are still important parameters to be concerned. Even transmission matrices are generally applied, it may cause numerically unstability because of the exponential functions including positive and negative arguments in essence. In contrast to the TMM, the direct association of generalized scattering matrices yields exponential functions with only negative arguments. Hence, GSM remaines numerically stable [74]. Since PCs exhibit symmetry properties in the direction of periodicity, electromagnetic modes of the structure decouples into transverse magnetic (TM) and transverse electric (TE) modes for corresponding symmetry planes [24]. Results are presented for both TE and TM polarizations showing the magnitude of scattering parameter (S_{11}) as a function of frequency.

So far, we represented hybrid method (HM) to specify 2D PBGs which provides faster response in simulations and requires less computational resources. Described process involves two steps. In the first one, rather than executing an analysis in two dimensions, problem is considered for mitigated geometry of 1D equivalent films in which transformed refractive indices are calculated via EMT. Subsequently, photonic bandgap of 1D homogenised structure is found by employing AFGSM approach [59, 75–77]. In the method given in [76], roots of two analytic auxiliary functions are used to estimate band edges effectively. Here, calculation of the auxiliary functions does not necessitate the eigensystem of the GSM [76]. Thus the presented approach provides a significant reduction for the analysis of 2D problems.

Theoretically EMT produces better results when the selected wavelength is much larger than the period of the structure. Thus, performance of HM is only limited by the operating spectrum of the EMT. Yet, by comparing the numerical results with simulation results gathered from CST (Computer Simulation Technology), it is revealed that the our method yields accurate results with realistic wavelength-to-period ratios.

3.2 Analyzing Method

A periodic square array of 2D PC which includes dielectric squares having width of p_1, relative permittivity of ε_1, embedded in background material which has relative permittivity of ε_2 and period p is depicted in Figure 3.1. Geometry and parameters of 2D PC given in this paper is based on Lalanne's work in [78] for verification.

For the analysis of the original problem simulated in CST (see Figure 3.2), periodic boundary condition is applied in two dimensions (dielectric properties of media are invariant in the transverse (x, y) plane). In the z-direction, six layers of unit cell is periodically arranged and TE/TM plane wave is incident with θ_{inc} angle with respect to surface normal (Floquet boundary condition is applied). Corresponding unit cell model of 2D square lattice PC is given at right side of Figure 3.2.

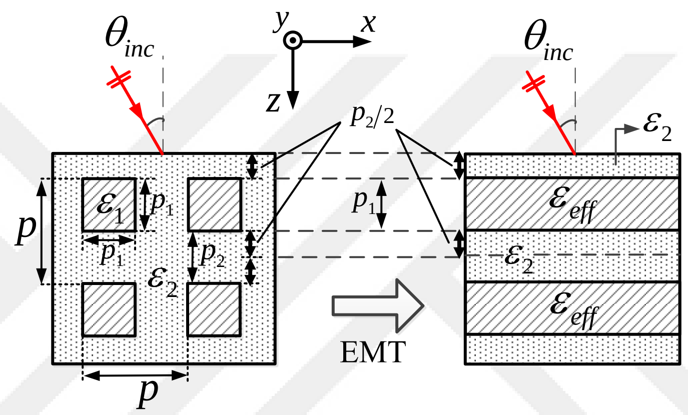

Figure 3.1 : Representation of EMT transformation
(a) 2D square lattice periodic structure consists of square shaped dielectrics with relative permittivity of ε_1 immersed in background material with relative permittivity of ε_2
(b) 1D equivalent thin films (effective indices calculated by EMT).

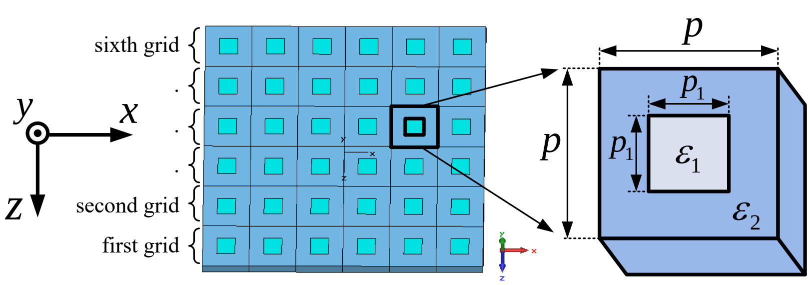

Figure 3.2 : 2D Photonic crystal square array composed of dielectric square rods and corresponding unit cell design ($\varepsilon_1 = 4$, $\varepsilon_2 = 1$, $\lambda = 1310$ nm (operating wavelength), $p_1 = 209$ nm, $p = 537$ nm).

In order to simplify the computations of 2D PC geometry is reduced to 1D periodic media using EMT. Effective permittivity of the homogenized 1D geometry can be

Table 3.1 : Calculated parameters of 1D PC for different polarization, incidence angle and wavelength.

$\lambda(nm)$	TE/TM, $\theta_{inc}(deg)$	ε_{eff}	p_1 (nm)	p_2 (nm)
1310 nm	TE-wave, 0^0	2.4524	209	328
700 nm	TE-wave, 30^0	2.4524	112	175
900 nm	TM-wave, 15^0	2.7384	175	225

calculated by expanding period-to-wavelength ratio (α) to power series as follows: for TE polarization;

$$\varepsilon_{eff} = \varepsilon_{avg} + \frac{\pi^2}{3}[f(1-f)(\varepsilon_2 - \varepsilon_1)]^2\alpha^2 \tag{3.1}$$

for TM polarization;

$$\varepsilon_{eff} = \frac{1}{\varepsilon_{inv}} + \frac{\pi^2}{3}\left[\frac{f(1-f)(\varepsilon_2 - \varepsilon_1)}{\varepsilon_2\varepsilon_1}\right]^2 \frac{\varepsilon_{avg}}{\varepsilon_{inv}{}^3}\alpha^2 \tag{3.2}$$

where $\varepsilon_{avg} = \varepsilon_2 f + \varepsilon_1(1-f)$ is the average relative permittivity and $\varepsilon_{inv} = f/\varepsilon_2 + (1-f)/\varepsilon_1$ is the arithmetic average of the inverse relative permittivity, $f = p_1/p$ is the fill factor (duty cycle), $p_1 = fp$, $p_2 = (1-f)p$ and α is as used in [78].

Simulation parameters (for the selected geometry depicted in Figure 3.2) f, α and ε_{eff} are derived using equations (3.1) and (3.2) as follows (see Table 3.1):

$$f_{TE} = 0.390, \quad \alpha_{TE} = 0.410, \quad \varepsilon_{eff-TE} = 2.4524$$

$$f_{TM} = 0.437, \quad \alpha_{TM} = 0.444, \quad \varepsilon_{eff-TM} = 1.6564$$

It is important to note that when EMT is applied considering arbitrary angle of incidence, second-order effective index formulation has to be used given in [79]. The high order EMT closed form expressions as given in [79] as a function of x-component ($\beta = n_1\sin(\theta)$), covers the effective dielectric constants up to 2nd order for TM polarization and up to 4th order for TE polarization. Consequently, zeroth order EMT considers only zeroth transmitted and reflected orders of propagating light. In order to provide a complete model one must take into account evanescent modes that are covered in high-order EMT expressions.

Propagation constants of plane waves are the solutions of dispersion equation. In the classical approach these solutions are obtained by solving the roots of eigenvalue equation of the form [23]

$$\cos(Kp) = \cos(k_1^z p_1)\cos(k_2^z p_2) - M\sin(k_1^z p_1)\sin(k_2^z p_2) \tag{3.3}$$

where

$$M = \begin{cases} \frac{1}{2}\left(\frac{k_2^z}{k_1^z} + \frac{k_1^z}{k_2^z}\right) & TE \\ \frac{1}{2}\left(\frac{n_1^2 k_2^z}{n_2^2 k_1^z} + \frac{n_2^2 k_1^z}{n_1^2 k_2^z}\right) & TM \end{cases} \tag{3.4}$$

By assuming the unit cell (UC) as a two-port network photonic bandgap characteristics of periodic structure can be determined in terms of scattering parameters. After applying the boundary conditions and Floquet periodicity condition eigenvalue equation of the symmetric UC can be expressed in the following alternative form

$$\cos(Kp) = \frac{1 - {S_{11}}^2 + {S_{21}}^2}{2S_{21}} \tag{3.5}$$

Our procedure is a clear improvement on traditional bandgap investigations that are considerably time-consuming. Following the application of EMT the scattering parameters of the 1D UC is calculated using GSM method. Accordingly, edge of the photonic bandgaps are determined by calculating roots of two analytic auxiliary functions

$$X_{\pm} = Im\{S_{11} \pm S_{21}\} \tag{3.6}$$

where $Im\{.\}$ denotes the imaginary part operator and S_{11} and S_{21} are the scattering parameters of the UC, respectively [76].

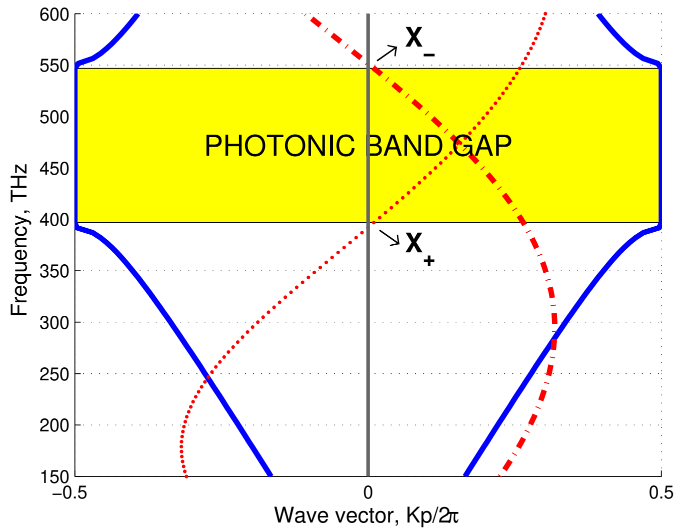

Figure 3.4 : Photonic band structure of 1D equivalent PCs (solid-blue) and variation of X_+ and X_- functions (dashed-red) (700 nm (470.968 THz), $\theta_{inc} = 30^0$, TE-polarization).

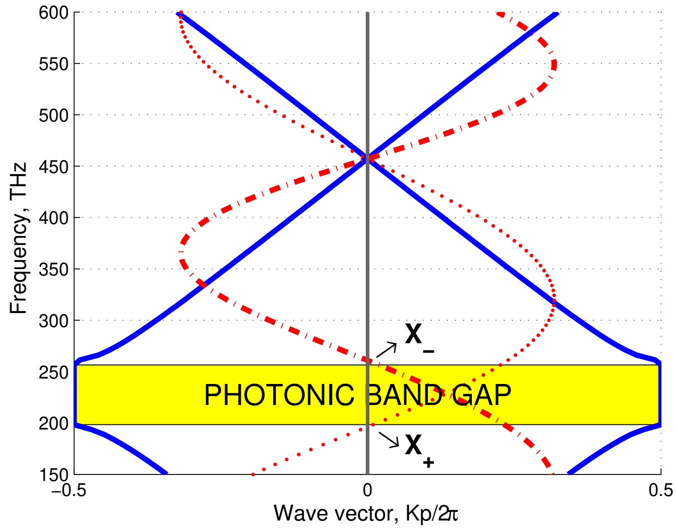

Figure 3.3 : Photonic band structure of 1D equivalent PCs (solid-blue) and variation of X_+ and X_- functions (dashed-red) (1310 nm (227.419 THz), $\theta_{inc} = 0^0$, TE-polarization).

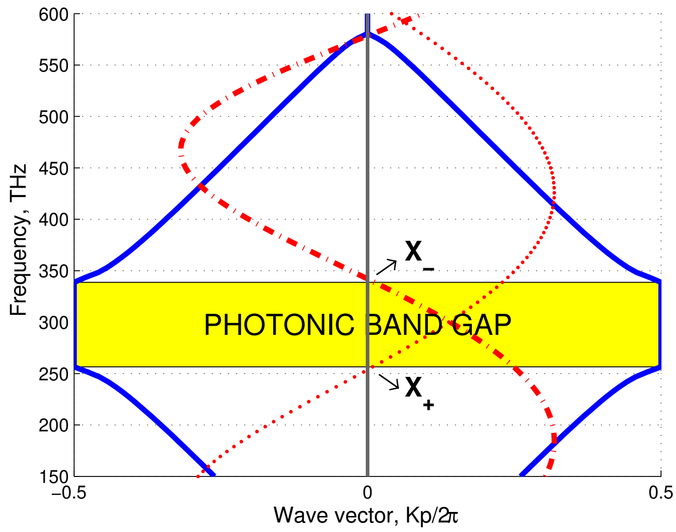

Figure 3.5 : Photonic band structure of 1D equivalent PCs (solid-blue) and variation of X_+ and X_- functions (dashed-red) (900 nm (297.581 THz), $\theta_{inc} = 15^0$, TM-polarization).

In Figures 3.3, 3.4, 3.5, solid blue line represents the photonic band structure (dispersion diagram) of 1D PC, dashed lines represent the variation of X_+ and X_- functions and shaded region represents photonic bandgap of the periodic structure. It can be seen that, zero transitions of X_+ and X_- functions perfectly match with bandgap edge frequencies of dispersion diagram.

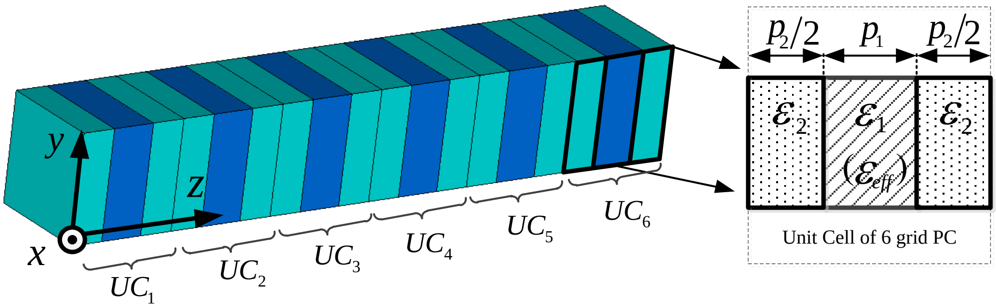

Figure 3.6 : Geometry of cascaded 6 unit-cells of 1D PC and unit cell design ($\varepsilon_1 = 2.4524$, $\varepsilon_2 = 1$, $p_1 = 209$ nm, $p_2 = 328$ nm, $\theta_{inc} = 0^0$).

Figure 3.6 represents the effective 1D PC model simulated in CST design environment. Periodic array of 1D PC is assumed to be finite (periodically arranged 6 layers) along z-direction and infinite in other directions as shown in Figure 3.6. Corresponding unit cell model of 1D PC is given at the right side of Figure 3.6.

For designing purposes of optical components geometry of interest can be simulated with a mesh close to its exact shape. Proper discretization of the object often requires a great amount of computation. The objective of EMT is to reduce the computation time by replacing the periodic structure with a more simple homogenized layer. Generally use of EMT yields a good approximation if the wavelength is sufficiently large compared to period of the structure which is summarized as $\alpha = p/\lambda_0 << 1$ with λ_0 is being the incident wavelength. The range of validity that the condition is satisfied is called as long-wavelength limit (or static limit). As a characteristic behaviour of EMT, approximation cannot predict accurate effective index results for large α values. Hence, EMT yields valid results around the region of long-wavelength limit [80–82].

Although the AFGSM method does not have any limitation itself in case of symmetric UC, application of EMT makes an overall limitation for HM. This limitation means that study findings need to be interpreted in the sense of EMT boundaries.

In order to provide these findings an illustrative example is provided in Figure 3.7 with given initial values of structure same as in Figure 3.2 ($\lambda_0 = 1310nm, p = 537nm, \alpha = 0.41, f = 0.39, \varepsilon_{eff} = 2.452$)

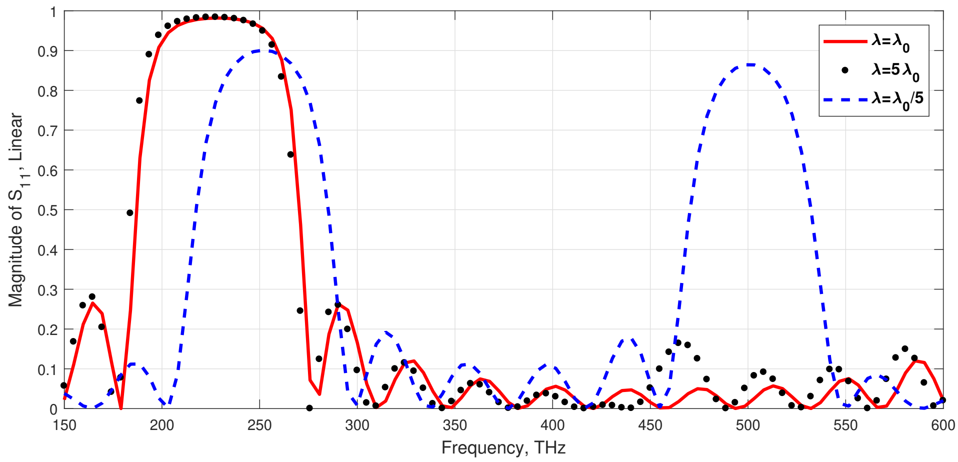

Figure 3.7 : Validity of EMT for varying operating wavelength (λ_0). Solid-red line represents $\lambda = \lambda_0$, black-dots represent $\lambda = 5\lambda_0$ with $\alpha = 0.082, f = 0.402, \varepsilon_{eff} = 2.506$ and blue-dashed line represents $\lambda = \lambda_0/5$ with $\alpha = 2.049, f = 0.277, \varepsilon_{eff} = 1.974$
.

In Figure 3.7 period of the structure is taken as constant and the operating wavelength is changed to higher and lower values of $5\lambda_0$ and $\lambda_0/5$ respectively. The dashed line in Figure 3.7 clearly shows that EMT is not valid for analyzing the structures with large α values, whereas dots show very good agreement with the results of $\lambda = \lambda_0$.

To examine the effects of different shapes of cross sections, circular rod shaped square lattice PC is demonstrated in Figure 3.8. Simulation results reported by Frezza *et al.* and experimental data given in [83] are compared with results obtained with HM plotted in Figure 3.8. The results are consistent with data obtained in [83] and [84]. Moreover, when 2D PC structure is considered with hexagonal (or honeycomb) lattice, EMT cannot resolve spatial arrangement of hexagonal symmetry. In that case, due to the directional dependency of structure 2D homogenization needs to be applied. Some different approaches such as multiple-scattering technique (MST), tight-binding method, coherent potential approximation (CPA) method and Mie scattering theory exist in the literature [85–88]. However in this context, the proposed HM cannot be directly applied to the Honeycomb lattice.

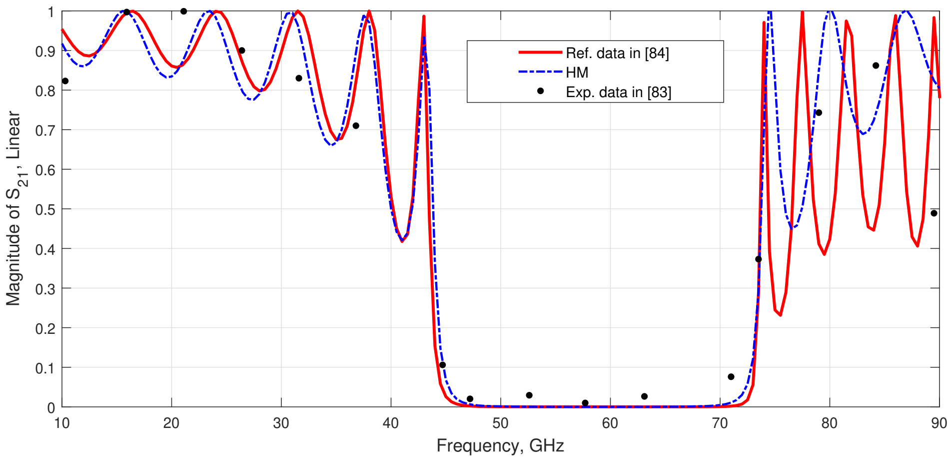

Figure 3.8 : Transmittance of dielectric circular rods immersed in air. $n_1 = 1, n_2 = 2.98, radius = 0.37mm, p = 1.87mm$ and 7 cascaded layers. Solid-red line shows simulation results given in Frezza et al., 2003, blue-dashed line represents HM results, block-dots show experimental data given in Robertson et al., 1992

.

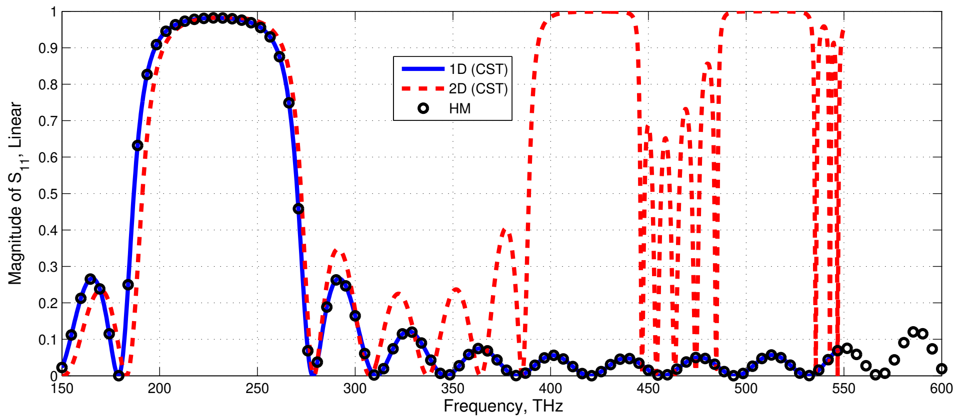

Figure 3.9 : Magnitude response of S_{11} for 6 period of PC. Solid blue line represents 1D PC-CST, dashed red line represents 2D PC-CST and circle black line represents HM results respectively. (1310 nm (227.419 THz), $\theta_{inc} = 0^0$, TE-polarization).

In order to verify validity of the HM for finite periodicity, problem geometries of 2D and 1D PC lattices (Figure 3.2 and Figure 3.6) are modelled in CST design environment and obtained simulation results are presented in Figures 3.9 to 3.11. Moreover, calculated GSM-Matlab results of 1D PC comprised of 6 unit cells are shown in Figures 3.9 to 3.11 marked as circles. The comparison of the numerical and simulation results reveals that HM produces consistent results even in the case of different wavelengths, incidence angles and polarization (see Figures 3.3 to 3.5 and see

Figures 3.9 to 3.11). In Figure 3.10, the stop band is centered on a certain wavelength such that the bandgap is shifted towards larger frequencies [78].

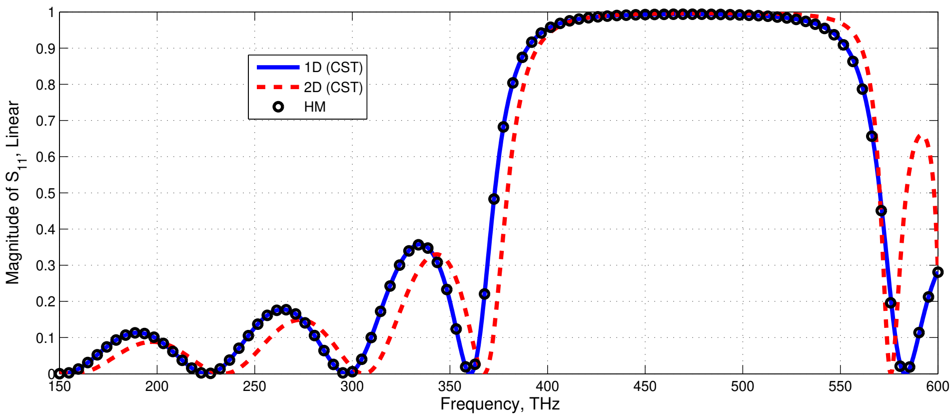

Figure 3.10 : Magnitude response of S_{11} for 6 period of PC. Solid blue line represents 1D PC-CST, dashed red line represents 2D PC-CST and circle black line represents HM results respectively. (700 nm (470.968 THz), $\theta_{inc} = 30^0$, TE-polarization).

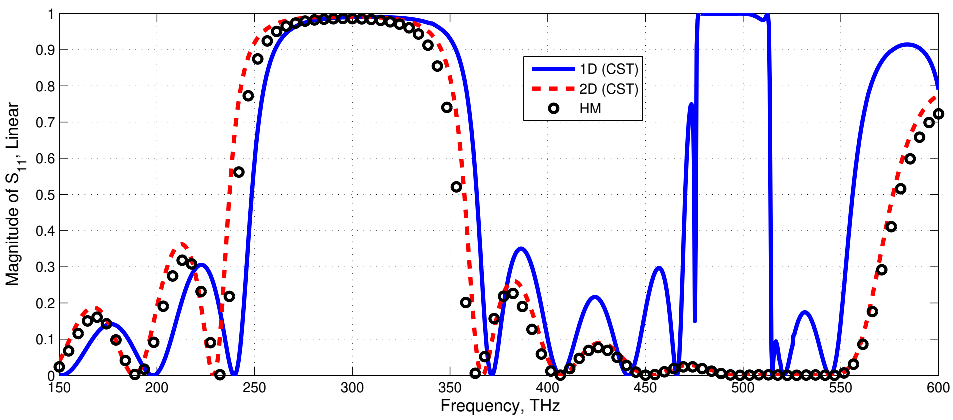

Figure 3.11 : Magnitude response of S_{11} for 6 period of PC. Solid blue line represents 1D PC-CST, dashed red line represents 2D PC-CST and circle black line represents HM results respectively. (900 nm (297.581 THz), $\theta_{inc} = 15^0$, TM-polarization).

In identification of photonic bandgaps, use of X_+ and X_- is computationally more efficient than the conventional solution of eigenvalue equation by a factor of more than 10 [76]. Furthermore, the HM has a substantial advantage over the numerical computation tools in terms of computation time (see Table 3.2). It also has to be noted that band edge frequencies obtained from CST simulation are in perfect agreement with those obtained by HM. When 2D PC problem is reduced to effective dielectric

Table 3.2 : Comparison of computation time for different methods.

$\lambda(nm)$	TE/TM, $\theta_{inc}(deg)$	$2D\ CST$	$1D\ CST$	HM	Units
1310 nm	TE-wave, 0^0	890	125	0.596	(sec.)
700 nm	TE-wave, 30^0	137	20	0.525	(sec.)
900 nm	TM-wave, 15^0	626	113	0.482	(sec.)

layers, AFGSM method can be used to calculate band edges of UC without being need to cascading procedure that gives opportunity to design wide range of applications such as filters, cavity resonators, power splitters and PC waveguides constructed by just applying defect layers in 2D PCs. Numerical computations are obtained on a modest PC which has Intel i7 @2.60 GHz Processor and 12 GB RAM.

3.3 Conclusion

In this research a unique approach is presented to identify photonic bandgaps of 2D periodic structures rapidly. Successful execution of HM shows that band structure computation for the 1D equivalence mitigates the calculation time considerably. It is also noticed that when period-to-wavelength ratio approaches to zero, results become consistently good in quality and performance. Likewise, recommended HM is not only limited to square cross sectional shapes exercised in this paper but also it can address arbitrary profiles even with different angle of incidence and polarization states. Thus, we believe that our approach will be useful in further design stages for 2D PC structures.

4. BANDGAP ANALYSIS OF 2D PHOTONIC CRYSTALS WITH AUXILIARY FUNCTIONS OF GENERALIZED SCATTERING MATRIX (AFGSM) METHOD [2]

4.1 Introduction

Photonic crystals (PCs) are a substantial class of periodic structures because of unique features used to control the light propagation particularly to restrict or allow inside the material. PCs are the made out of dielectric materials having periodicity in cross section and being composed of elements bearing symmetry properties with intermittent index of refraction. When a light penetrates in a dielectric structure physical phenomenon appears by adjustment of the electrical and dimensional attributes of PC. Equivalent to idea of implementing waveguiding structures and resonant-cavities to forbid or permit EM wave flow in a certain direction and spectral region, simply by varying the electrical and physical attributes of a PC can also lead to obtain desired propagation properties. Employing the modification in material properties could results in appearance of photonic bandgap (PBGs) which are effective in a particular wavelength range and disallows wave propagation regardless from the direction [1,89].

When concerning the two dimensional geometries the most popular and common forms of the structure comprises of dielectric columns placed in air or air columns embedded in a material which has a higher index of refraction contrast arrayed in distinct alignment patterns e.g. square grid, triangular grid, and hexagonal grid [90–92]. In addition, defect implementation in photonic crystals might grow because of manufacturing faults or might be applied advisedly to mold its transmittivity features. Particular defect shapes can be inserted into a 2D PC with the method of dropping some columns or by utilizing asymmetric dimensional parameters which leads to asymmetric placement pattern [93–97].

[2] This chapter is based on the paper "Erkan, O., Akıncı, M. N., Şimşek, S., 2018. Bandgap analysis of 2D photonic crystals with Auxiliary Functions of Generalized Scattering Matrix (AFGSM) method, AEU-International Journal of Electronics and Communications, 95, 287-296."

Propagation characteristics of 2D PCs constitute significant importance encountered in several applied science applications especially in designing numerous components in optical and microwave region e.g. polarization-splitters, optical bandpass-filters, resonance filters, photonic crystal waveguides, tapers, thin-film lasers, optical switches and resonators, dielectric mirrors, and patch and microstrip antennas [8,11,13,98–106]. A lot of mathematical techniques have been formulated to specify the photonic band structure of PCs. Typically employed techniques include Transfer Matrix Method (TMM), Finite-Difference Time-Domain (FDTD) method, Multiple Scattering (MST) method, Plane-Wave Expansion (PWE) method,and Finite Element Method (FEM) [69, 70, 73, 107–109]. Besides these frequently used investigation routines, Fourier Modal Method (FMM) is one of the significant methods used in similar studies [84]. Considerable quantity of the studies available in the literature is concerning the evaluation of the eigenvalue relations obtained by expanding the considered structure's dielectric function into series of modes. Generally, considered models are not advantageous enough to estimate results precisely because of lacking applicable constraints conceived during modeling process. Nevertheless, comprehensive EM survey of a periodically patterned medium can be ascertained by examining the dispersion plot of the Floquet modes assisted by an infinite periodic structure, that is to say by discovering the permitted and confined wavebands [110].

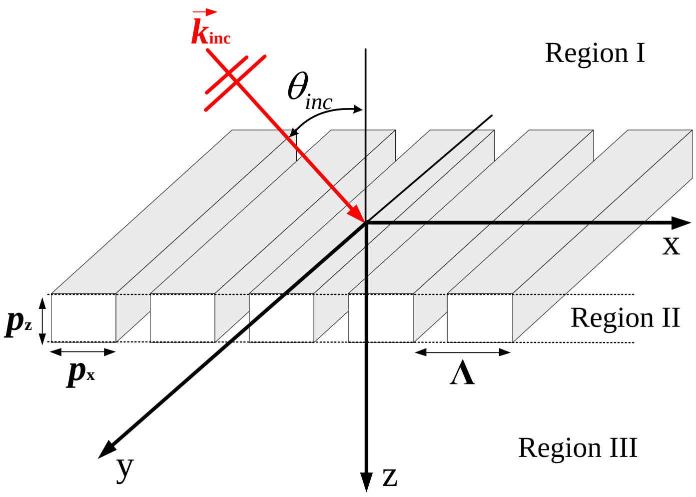

Figure 4.1 : Considered 2D rectangular grating structure.

In this chapter of the thesis, we investigate the photonic bandgap characteristics of 2D photonic crystals using auxiliary functions based on generalized scattering matrix representation, which preliminary findings of that presented in [59,76]. The alternative technique introduced recently in [59, 76] is called Auxiliary Functions of Generalized Scattering Matrix (AFGSM) method. As we already concerned in [59, 76, 111], utilizing AFGSM method provides an effective subroutine as it is examined for the dielectric loaded periodic waveguides and 1D PCs. This technique does not necessitate satisfying Floquet-condition and maintaining the solution of eigenvalue relation. Hence, it is quite practicable and viable in comparison to computational performance of available techniques in the papers. Thus, AFGSM method outputs precise approximations for the stopband/passband passage wavelengths supported by Floquet modes.

In this research, considered 2D PCs assumed to composed of cascaded 1D gratings which constitute the unit cell (UC) of the total geometry (see Figure 4.1). Scattering-parameters of the UC is determined by employing the Rigorous Coupled Wave Analysis (RCWA) which is regarded as a subblock of the technique given in this context [112]. Subsequently, AFGSM method is incorporated to specify PBG edges of infinitely periodic structure. The objective of this study is to evaluate the findings for different types of grid patterns formed by rectangular or circular dielectric columns and compare them with the results given in technical papers. In particular, triangular lattice form is maintained by shifting the middle row of the UC in lateral properties whereas defect pattern is provided by eliminating that row of columns. PBG spectral response is quantified in case of a variation in the essential configuration parameters such as polarization, duty cycle, angle of incidence. Convergency of the integrated computational routine is assessed when the number of diffraction orders raised and precisely discretized mesh. Furthermore, numerical results attested with High Frequency Structure Simulator (HFSS).

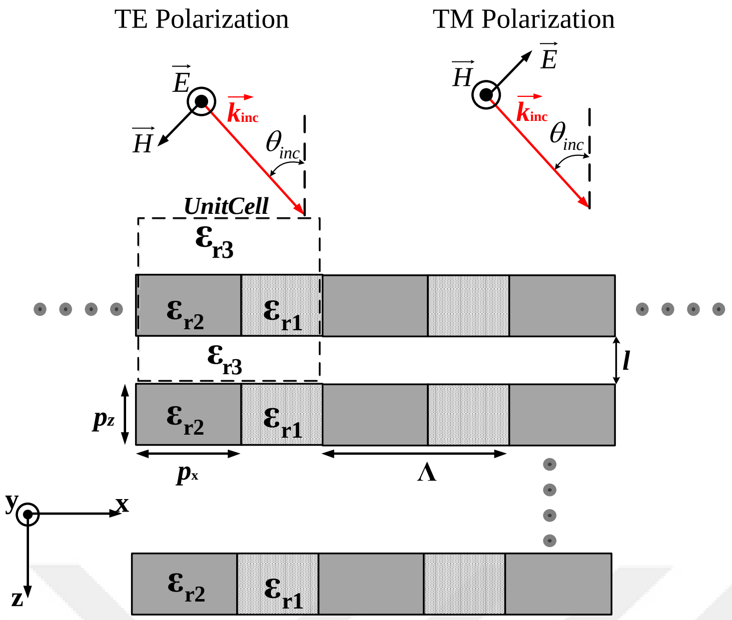

Figure 4.2 : TE and TM polarization for a wave incident on two-dimensional rectangular stacked PC.

4.2 Theory

4.2.1 Problem statement

Basic geometry of the problem comprises of three domains: Region I, II and III where Region I and III are designated as uniform, homogenous mediums while Region II consists of rectangular grating pattern periodically arranged along the x axis. As shown in Figure 4.1 rectangular columns of Region II has dimensional parameters of p_x and p_z and Λ denotes the period which includes grooves and ridges. Refractive index of uniform mediums, Region I and III are stationary and denoted by $n_I = n_{III} = \sqrt{\varepsilon_{r3}}$ whereas dielectric constant in Region II is a periodic function of x and refractive indices of the dielectric columns in that grating region denoted by $n_1 = \sqrt{\varepsilon_{r1}}$ and $n_2 = \sqrt{\varepsilon_{r2}}$ respectively (see Figure 4.2) . It should be noted that, for the entire geometry dielectric properties are invariant in y-direction and throughout the paper we assumed that $n_{III} = n_1\sqrt{\varepsilon_{r1}}$, where ε_{ri}, $i = 1,2,3$ represents the relative permittivity of considered region. 2D finitely periodic structure constituted by cascading UC in z-direction. In the full-wave analysis a plane wave is considered to be incident through the geometry from Region I having a wave number k_{inc} in x-z plane, applied angle of incidence θ_{inc} defined as the angle between propagation vector and surface normal. Only planar diffraction is investigated satisfying the Transverse Electric (TE) polarization in which $\mathbf{E} = (0, E_y, 0)$ (electric field vector) is perpendicular to the plane of incidence (x-z plane) and $\mathbf{H}$ (magnetic field vector) is parallel to the x-z plane whereas for the Transverse Magnetic (TM) polarization in which $\mathbf{H} = (0, H_y, 0)$ is perpendicular to x-z plane and E is parallel to the x-z plane as shown in Figure 4.1.

4.2.2 Analyzing method

This study concerns with photonic bandgap characterization of 2D photonic crystals having different lattice forms and cross sections. In order to examine PBGs we first calculate scattering parameters of 1D grating structure using RCWA as a subblock. Subsequently, obtained s-parameters cascaded in z-direction via generalized scattering matrix (GSM). Final output provides scattering parameters of finitely periodic 2D structure. Results compared with that of obtained in HFSS simulations. Thus far, attested results show the accuracy of RCWA subblock. However, instead of computational costly calculations in finite system we can estimate band information only by calculating first Floquet modes of infinitely periodic structure. Theoretically, a comprehensive wave study including Floquet modes of infinitely periodic structure provides the band information of the finite system. In other words, evanescent waves of first Floquet modes in infinite periodic structure corresponds to stopbands of zero order Floquet modes in finite periodic system. Hence, AFGSM can be applied in order to determine bandedges of infinitely periodic structure properly. The proposed technique effectively returns precise estimations for the calculation of bandedge frequencies supported by Floquet modes just by performing a straightforward root-determination algorithm. In the following section, we have emphasised a concise introduction of applying RCWA to 1D periodic grating structure as a subroutine for investigating scattering parameters. We intended to unveil the performance benefits of employing AFGSM in comparison to traditional band exploring approaches. The incident electric field, which is normal to the plane of incidence with TE polarization, is formulated by

$$E_y^{inc} = e^{jk_I n_I (x \sin\theta + z \cos\theta)} \tag{4.1}$$

where $k_I = k_0 = 2\pi/\lambda_0$ and λ_0 denotes the wavelength of free space and n_I is the index of refraction in Region I. The wave numbers of the structure defined as $k_I = k_{III} = k_0$ where k_I and k_{III} denote that of the Regions I and III respectively. The electric field in homogenous regions (Region I and Region III) satisfies form of Floquet condition

$$E_y(x,z) = \sum_m E_m e^{j(k_{xm}x + k_{zm}z)}; \quad (m = 0, \pm 1, \pm 2 ...) \tag{4.2}$$

where $k_{xm} = k_I \sin\theta + \left(\frac{2\pi}{\Lambda}\right), \quad m = 0, \pm 1, \pm 2...$ E_m in (4.2) represents the magnitudes of the fields in the summation and could be obtained by ensuring the boundary conditions at for each layer. In the uniform host regions $E_y(x,z)$ must fulfil the Helmholtz wave equation

$$\nabla^2 E_y + k_H^2 E_y = 0 \tag{4.3}$$

where $k_H = k_I = k_{III}$ and every partial wave satisfies the dispersion equation provided by $k_{zm} = \pm\sqrt{k_I^2 - k_{xm}^2}$. In order to identify the exact fields propagated in the total structure, allowed waves in Region II must be determined. Commonly, wave vector $k(x)$ in Region II is presented by Fourier series

$$k^2(x) = k_0^2 \sum_n k_n e^{j\left(\frac{2\pi n}{\Lambda}\right)x} \tag{4.4}$$

where k_n denotes the Fourier coefficients. Then, electric field in grating region can be derived as

$$E_y(x,z) = \sum_{m=-\infty}^{+\infty} \phi_m(z) e^{jk_{xm}x} \tag{4.5}$$

where $\phi_m(z)$ is a periodic function which associates the Floquet theory with the electric field in periodic medium. Replacing equalities (4.4) and (4.5) into Helmholtz equation (4.3) after utilizing some mathematical initiatives we obtain uncoupled second order differential equations for unknown coefficients $\phi_m(z)$,

$$\left(\frac{d^2}{d_z^2} + \tilde{L}\right)\tilde{\phi} = 0 \tag{4.6}$$

where $\tilde{\phi}$ is a column vector which has elements $\tilde{\phi}_m(z)$, $\tilde{L}$ is a full matrix which has elements in diagonal $k_{nn} - \left(k_I \sin\theta + (\frac{2\pi}{\Lambda})m\right)^2, \quad n : -N \le n \le N$ and N is the order of diffraction for related modes. Solution to equation (4.6) can be derived as

$$\tilde{\phi} = \tilde{C} e^{jkz} \tag{4.7}$$

where $\tilde{C}$ is a constant vector and κ is the propagation constant in z-direction. Along with the equation (4.6) we gather linear homogeneous equation in the form of

$$\tilde{L} \cdot \tilde{C} = \kappa^2 \cdot \tilde{C} \tag{4.8}$$

κ^2 in equation (4.8) denotes the eigenvalues of matrix $\tilde{L}$ that can be found as the solution of characteristic equation such as

$$\det\left[\tilde{L} - \kappa^2 I\right] = 0 \tag{4.9}$$

Assuming that κ_p is the eigenvalue of characteristic relation and C_p is the corresponding eigenvector. Accordingly, solutions of eigenfunctions can be calculated as

$$\tilde{\phi}_m^+(z) = \tilde{C}_p e^{-j\kappa_m z} \tag{4.10a}$$

$$\tilde{\phi}_m^-(z) = \tilde{C}_p e^{+j\kappa_m z} \tag{4.10b}$$

In equation 4.9 the sign of $\tilde{\phi}_m^+$ stands for waves that travel in the forward and backward directions through the z-axis respectively. Components of eigenvector $\tilde{C}_p$ are the modal solutions of the field in the periodic region that includes an infinite set of space harmonics with an amplitude C_{nm}. For the m-th mode we get

$$\tilde{\phi}_m(z) = \sum_n A_n C_{nm} e^{-j\kappa_m z} + B_n C_{nm} e^{+j\kappa_m z} \tag{4.11}$$

Equation (4.11) is the modal representation that considers the fields in terms of modes propagating in the z-direction, each m-th term in the summation stands for an individual mode with amplitudes A_n and B_n that need to be found. If we insert equation (4.11) into equation (4.5) we get modal expansion of electric field in Region II that can be derived as

$$E_y(x,z) = \sum_m \sum_n C_{nm} \left(A_n e^{-j\kappa_m z} + B_n e^{+j\kappa_m z}\right) e^{jk_{xm}x} \tag{4.12}$$

where A_n and B_n are unknown field magnitudes of forward and backward propagating waves respectively. C_{nm} is the m-th component of the n-th eigenvector.

Accordingly, incident, reflected and transmitted waves are represented with plane-wave expansion for the region I and III where $E_y(x,z)$ can be written as follows:

$$E_y^I(x,z) = e^{j(k_{xm}x + k_{zm}z)} \sum_{m=-\infty}^{+\infty} R_m e^{j(k_{xm}x - k_{zm}z)} \tag{4.13}$$

and

$$E_y^{III}(x,z) = \sum_{m=-\infty}^{+\infty} T_m e^{j(k_{xm}x+k_{zm}z)} \tag{4.14}$$

where R_m and T_m are the normalized complex field amplitudes of the m-th reflected wave and transmitted wave respectively and

$$k_{zm} = \begin{cases} k_0\sqrt{n_H^2 - \left(\frac{k_{xm}}{k_0}\right)^2} & ,k_0 n_H > k_{xm} \\ & \qquad\qquad H = I,II \\ -jk_0\sqrt{\left(\frac{k_{xm}}{k_0}\right)^2 - n_H^2} & ,k_{xm} > k_0 n_H \end{cases} \tag{4.15}$$

The transmitted and reflected field amplitudes R_m and T_m are determined by satisfying the tangential electric and magnetic field boundary conditions at the surfaces. Components of scattering matrix of the UC is hence determined by identifying the all unknown constants.

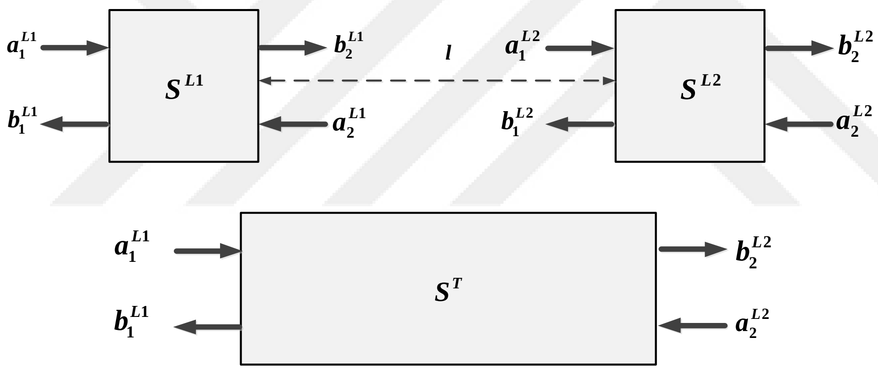

Figure 4.3 : Generalized scattering matrix cascading process of layers.

In the concept of GSM the UC is considered as a two-port network consisting N modes in which scattering parameters are derived by related normalized wave amplitudes at input/output ports which is represented as

$$\begin{bmatrix} \mathbf{b_1} \\ \mathbf{b_2} \end{bmatrix} = \begin{bmatrix} \mathbf{S_{11}} & \mathbf{S_{12}} \\ \mathbf{S_{21}} & \mathbf{S_{22}} \end{bmatrix} \begin{bmatrix} \mathbf{a_1} \\ \mathbf{a_2} \end{bmatrix} \tag{4.16}$$

which is divided into N by N submatrices. Satisfying the Floquet condition for the unit cell, modal amplitudes can be written in the form of

$$\mathbf{b_2} = \lambda \mathbf{a_1} \quad , \quad \mathbf{a_2} = \lambda \mathbf{b_1} \tag{4.17}$$

where λ represents the complex constant. Substituting equation (4.17) into (4.16), we can get the eigenvalue relation of the periodic system

$$\begin{bmatrix} \mathbf{I} & -\mathbf{S_{11}} \\ \mathbf{0} & -\mathbf{S_{12}} \end{bmatrix} \begin{bmatrix} \mathbf{b_1} \\ \mathbf{a_1} \end{bmatrix} + \lambda \begin{bmatrix} -\mathbf{S_{12}} & \mathbf{0} \\ -\mathbf{S_{22}} & \mathbf{I} \end{bmatrix} \begin{bmatrix} \mathbf{b_1} \\ \mathbf{a_1} \end{bmatrix} = \mathbf{0} \tag{4.18}$$

where $\mathbf{I}$ is the unitary matrix. Accordingly, each stack is connected together using GSM approach as shown in in Figure 4.3, matrix representation of the procedure is given below

$$\begin{bmatrix} \mathbf{b_1}^{L1} \\ \mathbf{b_2}^{L2} \end{bmatrix} = \begin{bmatrix} \mathbf{S_{11}}^{T} & \mathbf{S_{12}}^{T} \\ \mathbf{S_{21}}^{T} & \mathbf{S_{22}}^{T} \end{bmatrix} \begin{bmatrix} \mathbf{a_1}^{L1} \\ \mathbf{a_2}^{L2} \end{bmatrix} \tag{4.19}$$

where

$$\mathbf{S_{11}}^{T} = \mathbf{S_{11}}^{L1} + \mathbf{S_{12}}^{L1}\mathbf{S_{11}}^{L2}\left(\mathbf{I} - \mathbf{S_{22}}^{L1}\mathbf{S_{11}}^{L2}\right)^{-1}\mathbf{S_{21}}^{L1} \tag{4.20a}$$

$$\mathbf{S_{12}}^{T} = \mathbf{S_{12}}^{L1} + \left(\mathbf{I} - \mathbf{S_{11}}^{L2}\mathbf{S_{22}}^{L1}\right)^{-1}\mathbf{S_{12}}^{L2} \tag{4.20b}$$

$$\mathbf{S_{21}}^{T} = \mathbf{S_{21}}^{L2}\left(\mathbf{I} - \mathbf{S_{22}}^{L1}\mathbf{S_{11}}^{L2}\right)^{-1}\mathbf{S_{21}}^{L1} \tag{4.20c}$$

$$\mathbf{S_{22}}^{T} = \mathbf{S_{22}}^{L2} + \mathbf{S_{21}}^{L2}\mathbf{S_{22}}^{L1}\left(\mathbf{I} - \mathbf{S_{11}}^{L2}\mathbf{S_{22}}^{L1}\right)^{-1}\mathbf{S_{12}}^{L2} \tag{4.20d}$$

As it is well-known, transfer matrix method (TMM) is not stable because of transfer matrices including positive and negative arguments in the results of exponential functions. However, generalized scattering matrix method does not have stability issue because of consisting only negative arguments in exponential functions [74]. Therefore, GSM method is used in our paper and applied to our problem rigorously. Nevertheless, this technique is costly in terms of computational performance due to calculation of matrix inversions in every step of algorithm. Thus, it doesn't show any advantage in comparison to existing conventional methods which employed to compute the dispersion relations as it needs to solve eigen-equation in (4.18) yet. Following deduced formulation can be used based on the s-parameters of the UC, such as

$$\cos(K\Lambda) = \frac{1 - S_{11}^2 + S_{21}^2}{2S_{21}} \tag{4.21}$$

The $\cos(K\Lambda)$ term defines the photonic bands as follows: In the region where $|\cos(K\Lambda)| < 1$, $\cos(K\Lambda)$ has real value where structure supports at least one propagating Floquet mode.

In the region where $|\cos(K\Lambda)| > 1$, $\cos(K\Lambda)$ includes real and imaginary parts where photonic structure allows non-propagating evanescent Floquet modes, namely photonic bandgaps (PBG). The frequencies which render $|\cos(K\Lambda)| = 1$ defines the band-edges separating the two regions.

$$\lambda_{1,2} = e^{\pm j\theta}, \qquad \theta = K\Lambda \quad \varepsilon 0, \pi \tag{4.22}$$

The solution of (4.18) matching to λ values in (4.22) is referred to as a Floquet mode. If periodic structure allows at least one propagating Floquet mode in a certain frequency region it is called passband. The appearance of complex modes can be clarified by the existence of cutoff transitions at $(K\Lambda = \theta) \neq (0, \pm\pi)$ in the dispersion curve. The values where the band edges of dispersion relation (4.21) mitigates to $S_{11} \pm S_{21} = \pm 1$ and imaginary part of the $S_{11} \pm S_{21}$ vanishes at band-edge wavelengths which are found at zero transitions of the functions X_+ and X_- , defined as

$$X_{\pm} = Im\{S_{11} \pm S_{21}\} \tag{4.23}$$

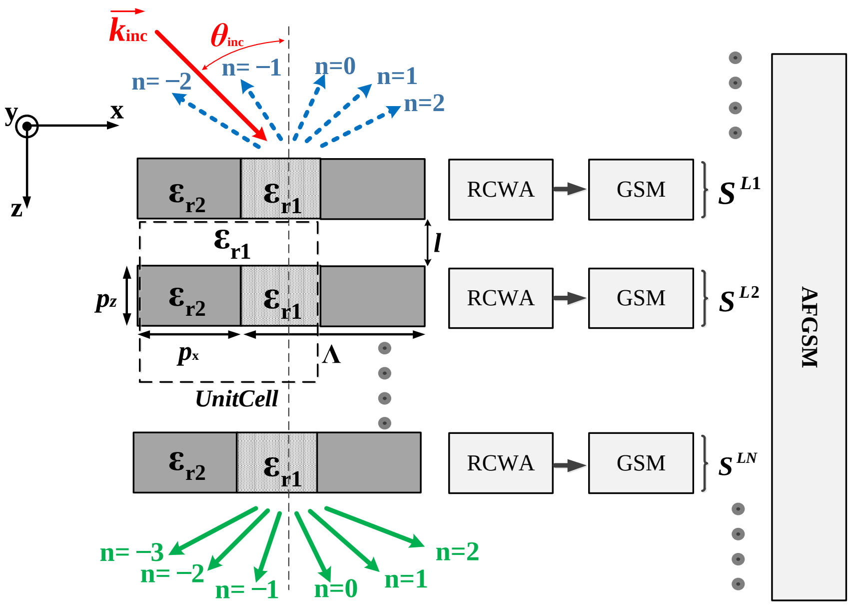

Figure 4.4 : Utilization of proposed technique for a cascaded 2D photonic crystal.

The method that governed by zero passings of related functions $(X_{\pm} = 0)$ precisely match the roots of (4.23), namely AFGSM allows to determine the PBGs of the

PC structure accurately. Primary subblock RCWA which is used to calculate UC scattering parameters including higher order modes, considers the dielectric functions of rectangular gratings as an expansion of Fourier series with space variables. Reflected and transmitted waves in each layer are used to calculate complex amplitudes and intensities for individual diffraction orders. Ones that correspond to reflected orders are denoted by dashed blue arrows whereas transmitted orders are denoted by solid green arrows having a series of $n = 0, \pm 1, \pm 2,...$ orders illustrated in Figure 4.4. As referred to detailed formulations given in [69] and [113], solutions of differential equations which are stated in the form of linear algebraic matrix formulation that represents the parameters of the UC.

This study provides a novel approach to identifying PBGs using auxiliary functions $(X_{\pm})$ that it does not need an eigenvalue solution when finite structures considered. The proposed algorithm effectively returns precise estimations for the calculation of bandedge frequencies governed by Floquet modes just by performing a straightforward root-determination algorithm in AFGSM. Thus, implemented technique smoothly yields to examine arbitrary form of PBG structures comprised of dielectric columns or air columns in background media in an enhanced and simple approach.

In the following part, we introduce our findings related to dispersion curves of the 2D PC structure comprised of circular and rectangular dielectric columns with varying dielectric constant while analyzing the dispersion curve effects of the changing electrical and dimensional parameters in an infinitely arrayed PC.

4.3 Numerical Results

In this section, we have assessed the computational performance and potential of proposed method. Furthermore, obtained results are compared with available data in the literature. Accuracy of numerical execution when physical and geometrical parameters varied are examined.
Below list of symbols used throughout this research is itemized:

"R" denotes radius of circular cross section dielectric rods,
"FR" denotes the filling ratio (duty cycle) given as the ratio of the p_x and Λ,
"N" denotes number of diffraction orders,

"D" denotes the discretization number of rectangular cross-section gratings to approximate circular,
"NC" denotes number of cascaded stack layers for a finite periodic PC,
"DLN" denotes the position of the defect layer in the UC.

In order to examine the proposed technique, PCs consisting of columns with various shapes, such as rectangular and circular (or cylindrical) cross sections and different lattice forms including rectangular and triangular are considered. The acronyms used in Figure 4.5 addresses the type of geometry used in numerical evaluations i.e. first letter designates the cross-section type of rod, e.g., rectangular or cylindrical, and second letter stands for the lattice type of array formation.

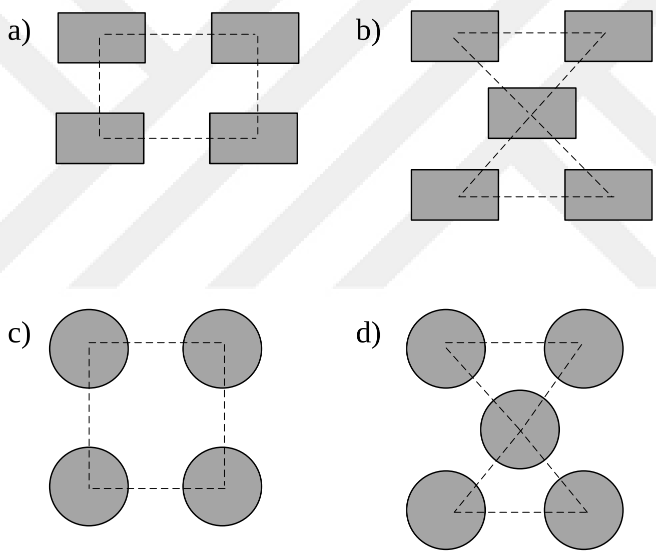

Figure 4.5 : a) RR-PC: rectangular cross section, rectangular lattice b) RT-PC: rectangular cross section, triangular lattice c) CR-PC: circular cross section, rectangular lattice d) CT-PC: circular cross section, triangular lattice.

4.3.1 Validation of method

This section presents the comparison of results we remarked within the studies with that of existing among research papers. First of all, RCWA subblock routine results are verified for a quasi-periodic geometry, subsequently, generalized scattering matrix approach is employed to obtain 2D unit cell scattering parameters. For the comparison purposes transmittance and reflectance plots are depicted in the same figure both for our approach and HFSS outputs as well as the data gathered from reports available

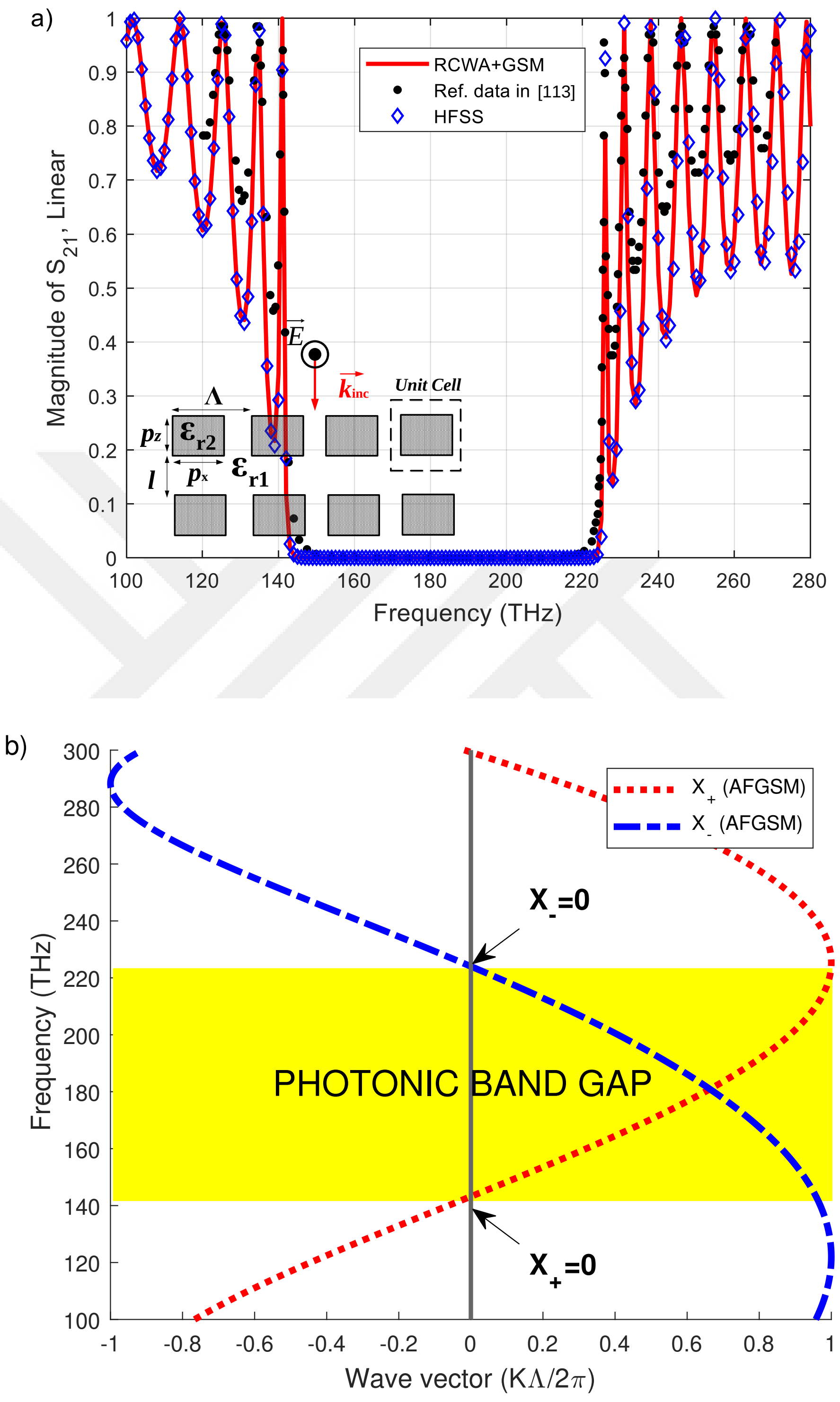

Figure 4.6 : a) Transmittance frequency response of *RR-PC* configuration (solid line) compared with results reported in Dansas and Paraire, 1998 (dots) and the results obtained with HFSS (diamonds) b) Dispersion diagram showing the variation of auxiliary functions ($X_{\pm}$) versus frequency. Normally incident plane wave is excited with TE-polarization and the parameters, $n_1 = 1, n_2 = 2.85, N = 11, FR = 0.35, p_x = p_z = 212nm, l = 194nm, \Lambda = 600nm, NC = 11$.

Table 4.1 : Comparison of band-edge frequencies for different number of layers.

Layer Numbers	Method	Band-edge frequencies (THz)	Computation time*
NC=11	RCWA+GSM	$149 < f < 220$	2.737
NC=20	RCWA+GSM	$144 < f < 223$	3.346
NC=25	RCWA+GSM	$143 < f < 223$	3.496
NC=∞	AFGSM	$143 < f < 224$	0.027

*simulation time in seconds

in the literature. This spectral response of magnitude is shown in the LHS of the figures. Concurrently, on the RHS of each figure zero transitions of AFGSM's auxiliary functions (X_+) are illustrated in dispersion diagrams in order to compare the bandedges with that of described aforementioned above. As it's clearly seen in the Figure 4.6(a) that combined approach (RCWA+GSM) outputs are consistent with with ones gathered by utilizing the AFGSM method shown in Figure 4.6(b). Considered geometry is *RR-PC* with the parameters; $n_1 = 1, n_2 = 2.85, N = 11, FR = 0.35, p_x = p_z = 212nm, l = 194nm, \Lambda = 600nm, NC = 11$ which a TE polarized plane wave is incident on the structure from air medium. Bandedge transitions given in Figure 4.6(b) reveals that a PBG exists between 143 THz and 224 THz and tuned at 183.5 THz center frequency. In Figure 4.6(a), it is proven that the results are amenable with the results reported in [113]. In order to explore the effect of varying NC values in computation time and precision on bandedge values are listed in the Table 4.1 for several NC values incorporated to computation durations for RR-PC structure given in Figure 4.6(a). It can be seen that given in Table 4.1, as the NC is increased, PBG edge frequencies approach to that of infinite periodic case while minimum values for the NC is defined as '25'.

In Figure 4.7(a) to attest our sub routine (RCWA+GSM) we implemented the data of experiment available in [114] and also results obtained with HFSS. In a similar fashion, a PBG is resides between 23.1 GHz and 38.1 GHz and it is respresented in Figure 4.7 (b) which the values received via utilizing the AFGSM method. The configuration parameters given in [114] are $n_1 = 1, n_2 = 3.1, N = 19, FR = 0.5, D = 20, R = 0.75, p_x = p_z = 1.5mm, l = 0.75mm, \Lambda = 3mm, NC = 18$ in which impinging wave is normally and TE polarized.

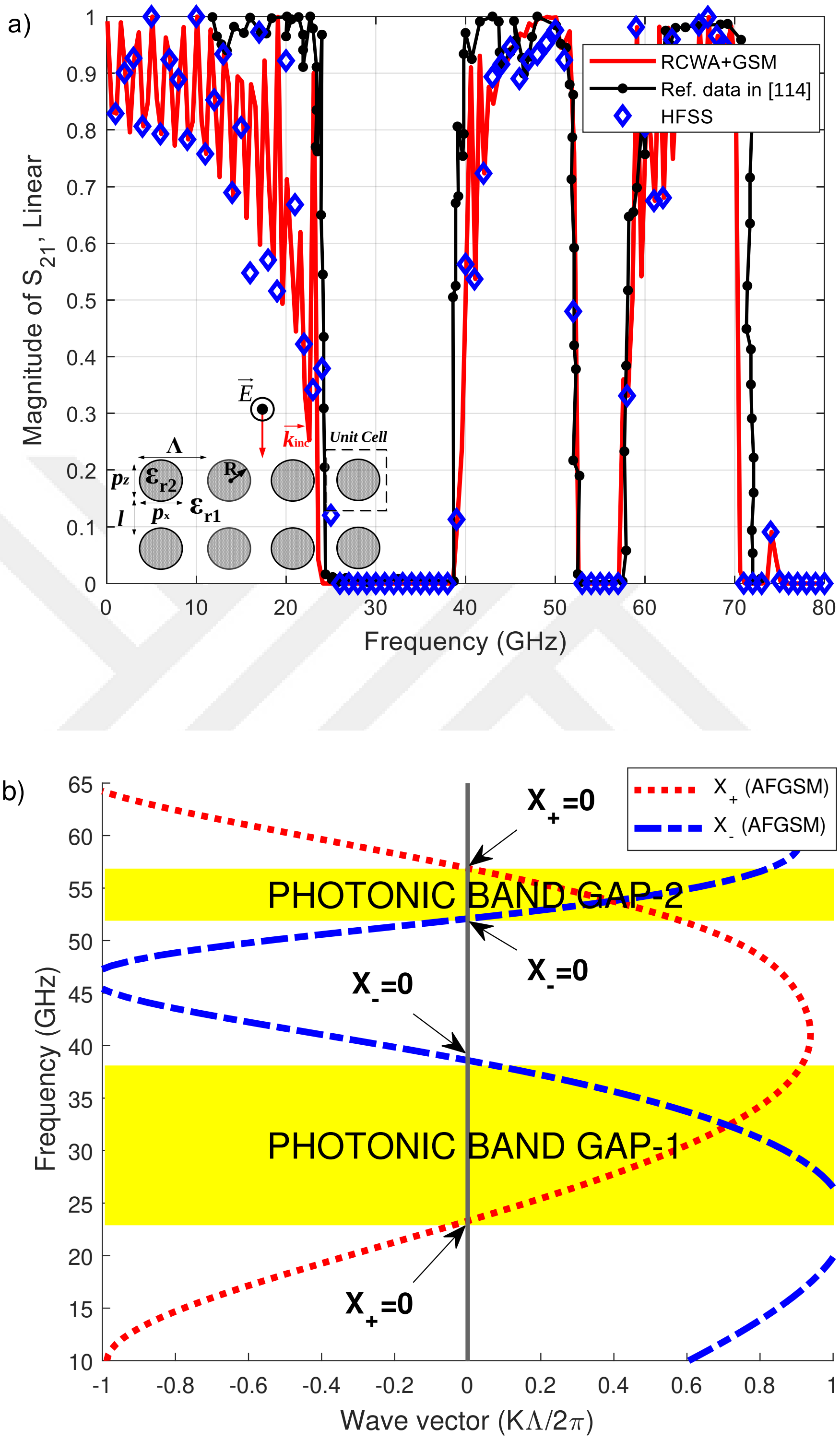

Figure 4.7 : a) Transmittance frequency response of *CR-PC* configuration (solid line) compared with results reported in Lourtioz et al., 2005 (dots) and the results obtained with HFSS (diamonds) b) Dispersion diagram showing the variation of auxiliary functions ($X_{\pm}$) versus frequency. Normally incident plane wave is excited with TE-polarization and the parameters, $n_1 = 1, n_2 = 3.1, N = 19, FR = 0.5, D = 20, R = 0.75, p_x = p_z = 1.5mm, l = 0.75mm, \Lambda = 3mm, NC = 18$.

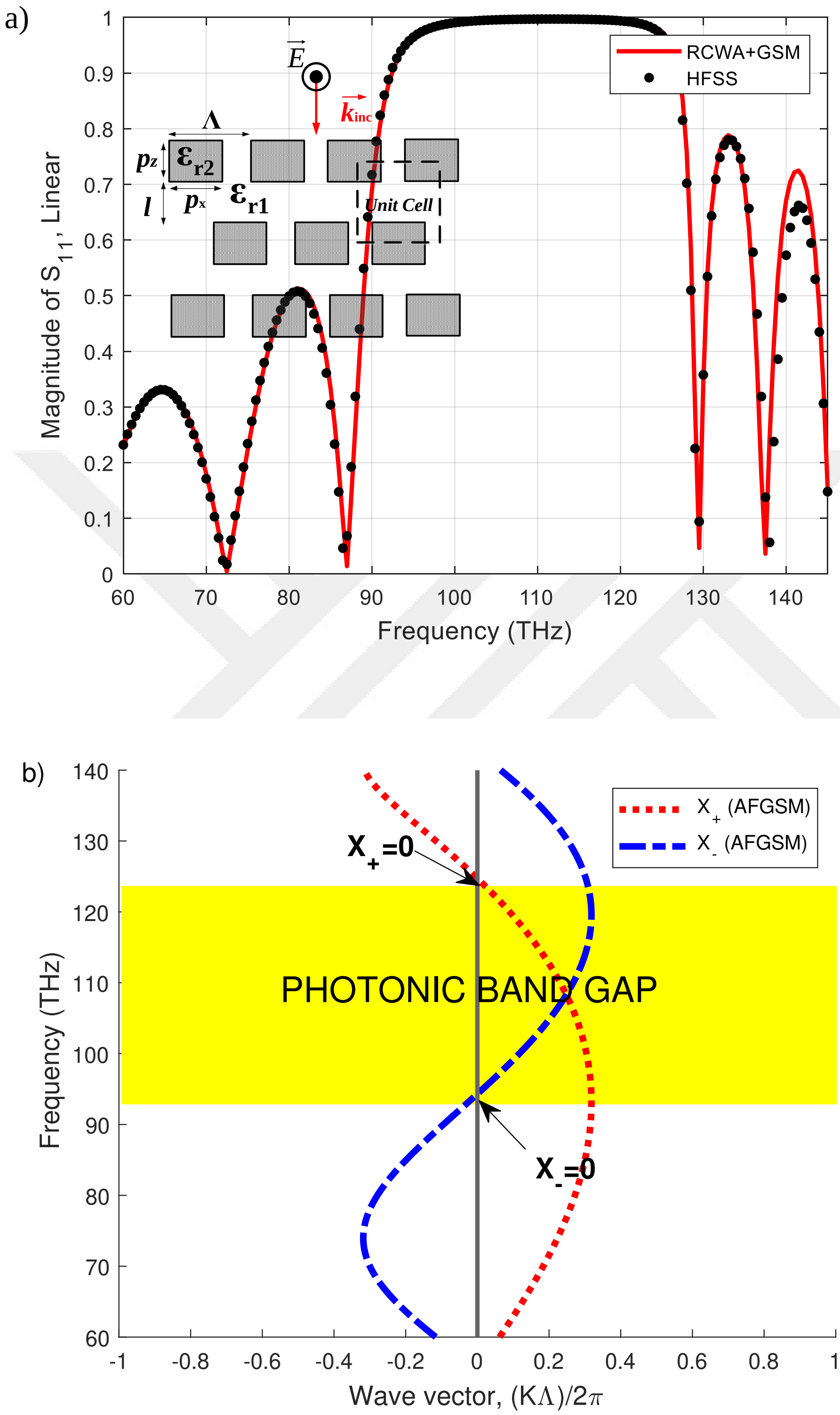

Figure 4.8 : a) Reflectance frequency response of *RT-PC* configuration (see the inset) as a function of frequency is shown (solid line) for comparison with results obtained with HFSS (dots) b) Dispersion diagram showing the variation of auxiliary functions ($X_{\pm}$) versus frequency. Normally incident plane wave is excited with TE-polarization and the parameters, $n_1 = 1, n_2 = 2, N = 3, FR = 0.33, p_x = p_z = 542.5nm, l = 272nm, \Lambda = 1627nm, NC = 3$.

Triangular grid pattern is also investigated and simulation results are given in comparison among the data retrieved through HFSS simulations . In this case, a lateral shift in the x-direction between two adjacent layers is applied. Identical approach used for comparison with combined routine (RCWA+GSM) given in Figures 4.6 and 4.7. Subsequently, AFGSM is applied to attest the dispersion characteristics of the equivalent structures. Figure 4.8(a) depicts the outcomes of sub-routine compared with HFSS results for the *RT-PC* shaped structure. From the Figure 4.8(b) one can see that there is a PBG existing between the 94 THz and 124.5 THz with a central frequency of 109.3 THz. Likewise, we have noticed perfect agreement between the results of HFSS, RCWA+GSM and AFGSM method for the *CT-PC* setup. In conclusion, we have implemented our sub-block routine to several different structure conformations to compare with the values found in literature and those of received from HFSS simulations. Due to practical constraints, accurate determination of PBGs in finite periodic structure needs adequate amount of cascaded stacks. However as the number of layers are increased computational performance mitigates. Instead of that alternatively calculating the scattering parameters and employing the AFGSM accordingly allows to determine bandedge values corresponding to total geometry by maintaining considerable benefit in computation time. That is to say, in finding the band-edge frequencies with particular precision the use of AFGSM mitigates the computing time by a factor of more than 10 when compared to the traditional method which based on solving the eigenvalue equation using a more finer frequency mesh [76]. After executing comprehensive simulation experiments it is found that, in the frequency region wherein the PC supports a single propagating Floquet wave, AFGSM estimates PBG frequencies with an improved accuracy more than 0.1% which constitute another vital finding of proposed method (Numerical computations are obtained on a modest PC which has Intel i7 @2.60 GHz Processor and 12 GB RAM). Table 4.2 displays a more explanatory information while comparing the calculation techniques in terms of computational performance governed in this study. Quantity of mesh size used in simulations ran over HFSS is 2254 for *RR-PC*, 19036 for *CR-PC* and 1834 for *RT-PC* respectively. PBG computation duration is less than 30 milliseconds via AFGSM method as seen from Table 4.1 when the GSM of UC is computed. Most striking computational performance is seen on a value difference (by a factor of 10^3) for *RR-PC* structure which including eleven stacked unit cell. In conclusion, some key

Table 4.2 : Simulation time comparison.

Structure Configuration	HFSS*	RCWA*	RCWA+GSM*	AFGSM*
RR-PC (Figure 6)	2344	2.26	3.02	0.026
CR-PC (Figure 7)	502	50.56	51.09	0.012
RT-PC (Figure 8)	177	0.65	1.47	0.025

*simulation time in seconds

supremacies of defined technique when using in computational experiments and related observations are remarked by attesting with the results available in the literature.

4.3.2 Effect of variations of physical and electrical parameters

In this part, we investigated the PBG frequencies along with the varying parameters such as filling ratio, wave polarization and angle of incidence. Contour figures are also presented for either TE and TM polarizations which can be useful in design studies.

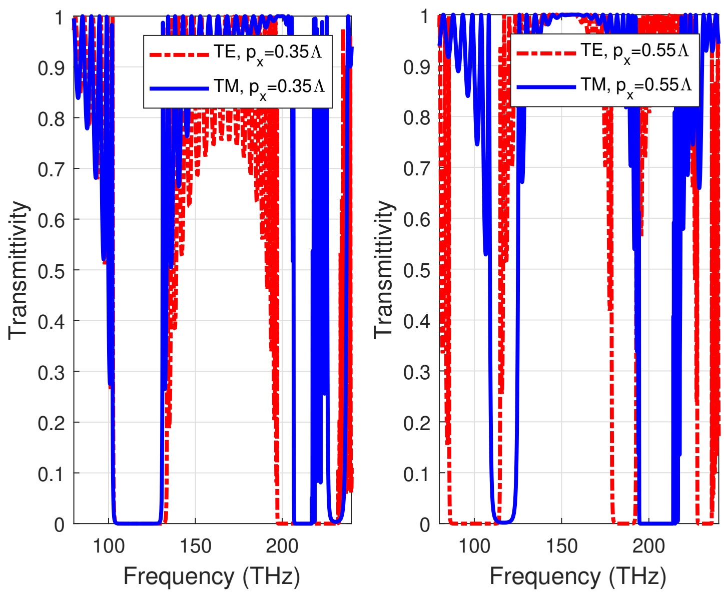

Figure 4.9 : Transmittance frequency response of *RR-PC* configuration (same as in Figure 4.2) as a function of frequency is shown for different values of $p_x = p_z$. Plane wave is excited under normal incidence with the parameters, $n_1 = 1, n_2 = 2, N = 27, FR = 0.55, p_x = p_z = 380nm$ (left), $p_x = p_z = 597nm$ (right) $l = 244nm, \Lambda = 1085nm, NC = 20$. In both figures, TE polarized wave (dashed line) and TM polarized wave (solid line) results plotted.

Initially, the impact on the spectral position of PBG when changing the filling ratio is examined and displayed in Figure 4.9. It's shown in the figure that two PBGs come out in the particular range of frequency. The first TE PBG located on $f_c \approx 118.2$ THz for $p_x = 0.35\Lambda$ whereas the first TE PBG for $p_x = 0.55\Lambda$ configuration centered on $f_c \approx 100.2$ THz which states an 18 THz shift towards the lower frequency region. Nevertheless, nearly no shift is noticed in the first PBG appearance of TM polarization when filling ratio is altered whereas PBG of which shows a heavy mitigation in size oppositely. For the second PBG a similar behavior can be observed, but shifting of center frequencies doubled this time, i.e., the TE PBG is shifted 29 THz to lower frequency region. The second photonic bandgap of $p_x = 0.35\Lambda$ configuration has a particular interest as it stimulates the widest stop band i.e., 35 THz which is 16.4% of central frequency $f_c \approx 214.9$ THz.

Additional valuable aspect found on the Figure 4.9 is the complete PBG which is defined as the overlap of stopbands that comes out in case of both TE and TM polarizations leading an intersection in frequency region [1]. For the Figure 4.9 two complete bandgaps centered on $f_c \approx 116.7$ THz and $f_c \approx 207.2$ THz respectively. The first complete bandgap is 26 THz and 12.7% of f_c which is the widest one and independent of polarization.

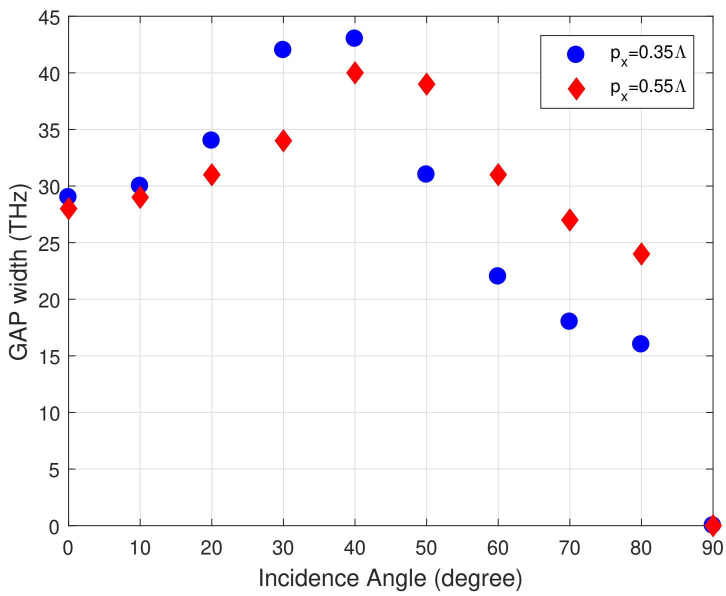

Figure 4.10 : Photonic bandgap size in (THz) as a function of the incidence angle for the same geometrical and physical parameters of Figure 4.9 normally incident TE-polarized wave. (dots: $p_x = p_z = 0.35\Lambda$, diamonds: $p_x = p_z = 0.55\Lambda$.

It should be noticed that, the bandgap features of the device is not only affected by a variation in duty cycle but also depends on the angle of incidence. Hence, the results shown in Figure 4.10 illustrate the impact of varying angle of incidence on the first

PBG edges for the same structure of Figure 4.9 in TE polarization. Also in the figure peak value of gap width for both configuration, appears in 40^0 incidence angle, i.e., 43 THz for $p_x = 0.35\Lambda$ and 40 THz for $p_x = 0.55\Lambda$ respectively. Afterwards that as the value rises, size of PBG likely to drop sharply through the smaller values, i.e., such as 16 THz at 80^0 for $p_x = 0.35\Lambda$ configuration.

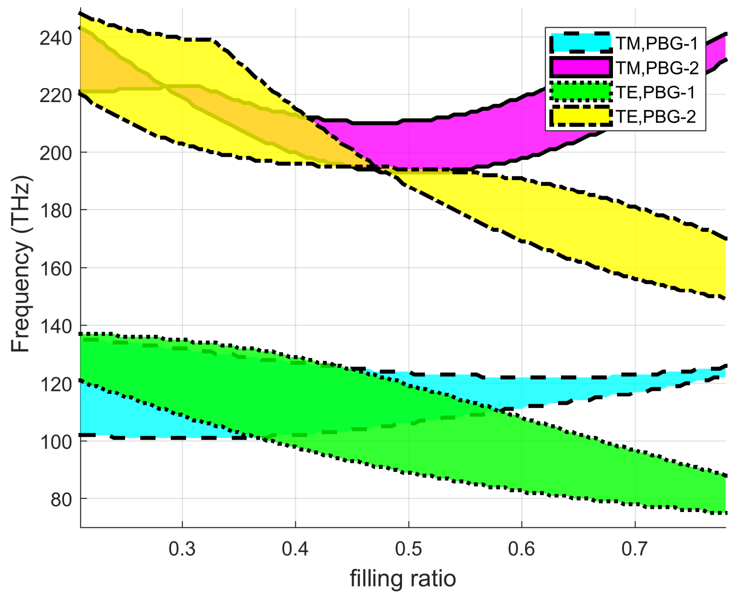

Figure 4.11 : Contour diagram in frequency spectrum as a function of filling ratio for the same structure as in Figure 4.9. First and second photonic bandgaps of both polarizations TE and TM is shown (dashed line: TM, PBG-1, solid line: TM, PBG-2, dotted line: TE, PBG-1 and dashed-dot line: TE, PBG-2).

Contour diagrams (sometimes called GAP maps) can be employed to a wide range of problems including the PC based component design. It is particularly important when design framework is structured to govern the variation and identification of the physical dimensions in order to maintain desired PBG specifications such as the minimum reflectance or peak transmission in a certain frequency range. Figure 4.11 depicts PBG results for changing filling ratio as a function of frequency spectrum for the same structure setup as given in Figure 4.10. As it can be seen in Figure 4.11, it is obvious that largest complete bandgap exist between the filling ratio values of 0.35 and 0.4, i.e., Δf = 27 THz bandgap size centered at FR=0.37. To be more precise, in case of inverse problem with an objective of designing a 2D PC with a stop-band between the 101 THz and 128 THz, and assuming the parameters $n_1 = 1, n_2 = 2, \Lambda = 1085$ nm, $NC = 20$ are given. It can be readily determined that the FR=0.37 value maintains the largest PBG in case of dual-polarization. However, generation of the contour plots requires significant computation resources because of the sweep process of the frequency mesh for each value of filling ratio concurrently. Enhanced performance of the AFGSM method allows to generate PBG maps faster than conventional methods as of computation time by about two orders of magnitude.

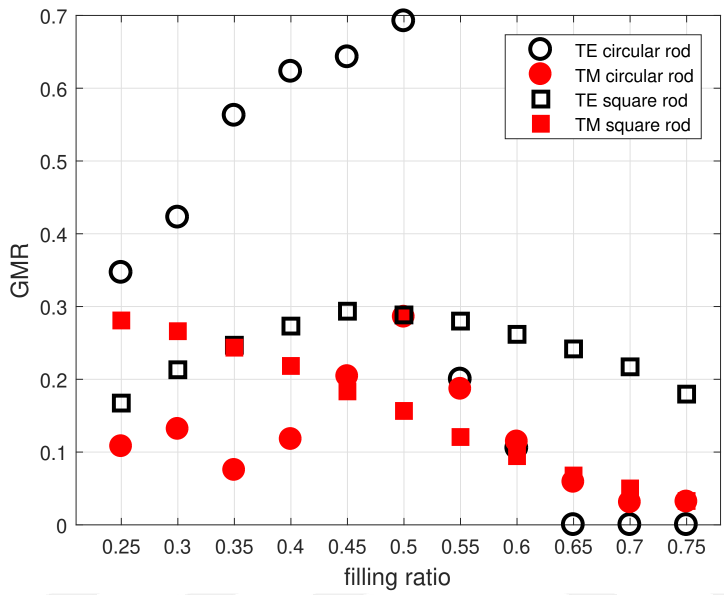

Figure 4.12 : Gap-width to midgap ratio as a function of the filling ratio for circular and square cross-section columns both for TE (open circles and open squares) and TM polarization (filled circles and filled squares).

Gap-midgap ratio (GMR) is another essential characterization of PBG which denotes the gap size in percentage. GMR is described as the $\Delta f/f_c$ where Δf is the width of bandgap in terms of frequency and f_c is the center frequency of PBG [1]. Figure 4.12 displays the variation of PBG characteristics by means of GMR against the duty cycle for circular and square column configurations. Figure 4.12 provides the highest GMR values as much as 0.7 centered on FR=0.5 for TE-polarized wave in case of circular type of cross-section. The results shown in Figure 4.12 can also be used to develop design approaches similar to ones in previous figures.

Table 4.3 compares the GMR values and center frequencies for varying structure configurations with corresponding filling ratios. As remarked in the table, *RT-PC* configuration provides the highest GMR value, i.e., 0.279 and second highest GMR value can be obtained with *CT-PC* type structure with a value of 0.268. Another important notice of Table 4.3 is the spectral location of PBG center frequencies which

Table 4.3 : Comparison of GMR for different structure configurations.

Structure Configuration	f_c^*	GMR	FR**
RT-PC	109.3	0.279	0.34
RR-PC	119.5	0.234	0.34
CT-PC	112	0.268	0.34
CR-PC	121	0.214	0.34

*in THz units, **filling ratio (duty cycle).

is shifted towards the higher frequency region in *CR-PC* structure configuration. For circular columns, peak value of discretized filling ratio is indicated.

4.3.3 Convergence and discretization of proposed approach

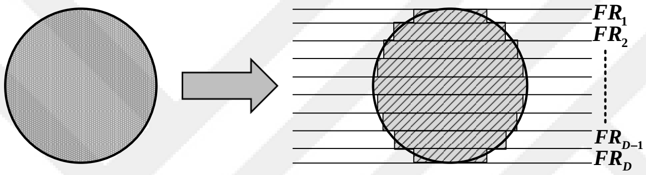

Figure 4.13 : Rectangular discretization of circular cross section.

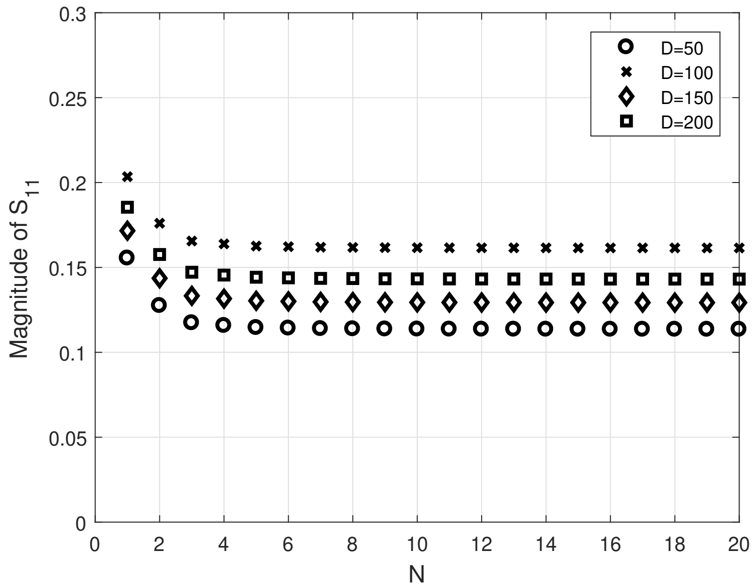

Figure 4.14 : Convergence performance of proposed method in case of increasing diffracted orders (N) for the same configuration parameters of Figure 4.8 when different values of discretization parameter considered: D=50 (circles), D=100 (crosses), D=150 (diamonds), D=200 (squares).

When arbitrary cross-section structures different than rectangular are considered mesh should be discretized properly. In Figure 4.13 a circular shaped column unit cell is discretized by splitting into rectangular forms having different duty cycles distributed in a range between FR_1 to FR_D where D denotes the number of discretized rectangular sections. Convergence performance of the proposed method is given in in Figure 4.14 for varying diffracted orders N with respect to different values of discretization parameter D for the same configuration as in Figure 4.8. It is obvious that, the proposed technique's convergency performance is rapid remarkably for each D value stably.

4.3.4 Introducing periodic defect

As noticed in introduction part, defect inclusion in periodic structures can be existent either because of fabrication faults or manmade for a particular objective such as missing columns of some layers, ensuring different shaped rods in a specified row or by occurrence of misaligned layers. On the basis of aim of designing numerous practical applications of PC structures with line or point defects can be examined comprehensively using proposed method. The response in case of the structure including defect (refractive index of defect layer located in the center is 2.89) compared with that of without defect, results illustrated in Figure 4.15. As shown in Figure 4.15 (see the inset) inserting a line defect in the middle of a PC yields a sharp transmission peak which is spectrally located on f_c = 254.3 THz and maintains a 100 GHz 3-dB width of the peak. According to findings given in this subsection, defect applied periodic structures could be examining in a quick and precise manner. Moreover, narrow-band or frequency selective filters can be easily designed and simulated with our approach accurately.

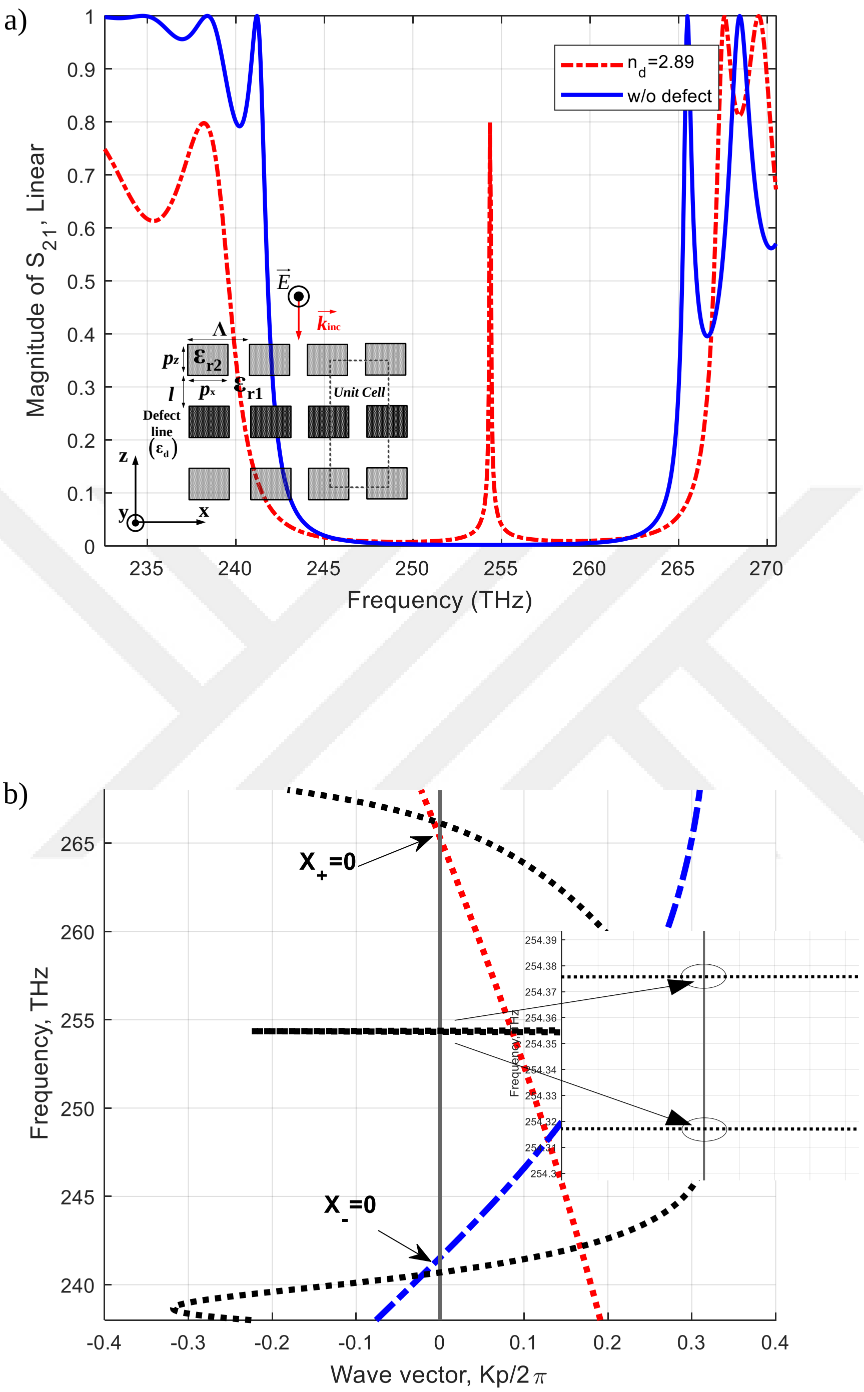

Figure 4.15 : a) Magnitude response of transmission spectrum of structure in the RR-PC configuration with (see the inset) and w/o defect. Plane wave is excited under normal incidence with TE-polarization with the parameters $n_1 = 1$, $n_2 = 3.69$, $N = 15$, $FR = 0.38$, $p_x = p_z = 232nm$, $l = 183nm$, $\Lambda = 600nm$, $NC = 21$. (solid line: structure without a defect configuration, dashed line: structure with a central defect configuration, $n_2 = 2.89$) b) Dispersion diagram showing the variation of auxiliary functions ($X_{\pm}$) as a function of frequency. Inset shows the transmission band response of AFGSM.

4.4 Conclusion

So far, we proposed a uniquely developed approach to investigate the PBG characteristics of 2D PC structures comprised of dielectric columns with various cross-sections and grid types. This study offers comprehensive numerical examples to support proposed originally developed idea that the allowed Floquet modes in an infinite periodic system provides the bandedge frequency information of the finite structure while maintaining the full-wave modal analysis. Additionally, the novelty of the technique resides on the independence of requirement to an eigenvalue solution for each layer in case of examining the finite structure. Thus, it allows to estimate the bandedge frequencies of the entire structure accurately. We experienced broad variety of simulation experiments including rectangular and circular shaped columns built on rectangular and triangular grid patterns. For each specific case, dispersion characteristics explored with our approach resulting transmittivity and reflectivity responses for a finite number of periodic layers compared in terms of PBG existence. Besides the numerical computations executed for verification purposes, existing experimental and theoretical data provided in the literature are compared with proposed method and a good agreement observed between them. Furthermore, some useful diagrams, e.g., Gap-Midgap-Ratio, PBG maps, are illustrated in case of varying the angle of incidence, physical and geometrical parameters for both TE and TM polarizations. The effect of introducing the defect in 2D PC is examined related results are presented.

In order to assess the frequency dependence of a band structure designed upon a particular UC and to find their suitable parameters for a desired application, our unique method can be utilized in a constant and efficient manner without a dependency on the number of layers. Particularly when designing practical applications proposed method maintains a framework to pattern the PBG characteristics in a quick and accurate way. It should be remarked that, proposed combined method including RCWA and AFGSM methods for 2D PCs is bounded with the limitations of RCWA method. The reported aspects might have key deductions for developing arbitrarily shaped 2D PC applications which we leave as a future work.

5. ENHANCED TRANSMITTING AND BLOCKING FILTER DESIGN APPROACH FOR LASER SCANNING APPLICATIONS BASED ON COMBINING GSM AND AFGSM METHODS [3]

5.1 Introduction

Photonic crystals (PC) comprised of dielectric materials have been widely used in many applications such as gratings, mirrors, filters [115–117], coupler and splitters, bends, etc. [118, 119], owing to their low power loss and high reflection at optical frequencies. Optical filters have also been employed in laser scanning microscopy applications to isolate the desired emitted light from tissue while blocking unwanted light [120, 121]. Photonic bandgap characteristics in which PCs exhibit transmission and reflection properties within a specified wavelength range can be constructed with proper design of multilayered dielectrics [122].

A variety of methods were proposed to determine bandgap characteristics of PCs, namely Plane Wave Expansion Method (PWE), Finite Difference Time Domain (FDTD) method, and Finite Element Method (FEM). While FDTD and FEM methods require fine meshing of the examined structure with a full-wave electromagnetic analysis, in PWE method the bandgaps are determined by solving an eigenvalue equation on a fine frequency mesh. In an effort to develop a computationally effective routine to examine bandgap characteristics which eliminates the need of solving an eigenvalue equation, we recently proposed the Auxiliary Functions of Generalized Scattering Matrix (AFGSM) method [60]. Here, we summarize our comprehensive filter design strategy via AFGSM and showcase its efficacy on a number of filters employed in laser scanning microscopy applications.

[3] This chapter is based on the paper submitted to AEU-International Journal of Electronics and Communications

5.2 Theory and Modeling

We base our filter designs, whose details are given in the numerical examples section, on the geometry illustrated in Figure 5.1, comprising a defective periodic dielectric stack (whose transmittance characteristics are achieved using GSM) sandwiched in between periodic dielectric stacks (whose transmittance characteristics are achieved using AFGSM). For any given filter, we start our design efforts with a multilayered periodic $\mathbf{(HL)^N}$ design to set the initial stop band (indeed acting as a mirror), where "**H**" and "**L**" represents high and low refractive index dielectric layers, respectively, and "**N**" is the number of periods used in the design. In order to introduce the transmission band, we introduce a defect in the middle of the initial design through breaking its periodicity to achieve $\mathbf{(HL)^{N/2}L(HL)^{N/2}}$, such that the number of total layer numbers in the initial design is conserved (**0.5N** value is ceiled, in case **N** is odd). The new $\mathbf{(HL)^{N/2}L(HL)^{N/2}}$ filter is called a Fabry-Perot resonator (FPR). General structure of FPR is based on inserting a quarter-wave layer **L** between the two groups of reflecting structures $\mathbf{(HL)^N}$. FPR provides narrow band transmission characteristics at the design wavelength λ_0.

Finally, AFGSM is utilized to extend the stop-bands on either side of the transmission band through a rapid sweep of material properties and thicknesses, while preserving the peak transmission. The extended stop-band is provided through two additional stop-band filters for left and right sides of the spectrum. The details of the overall design algorithm could be summarized with the following steps:

1. Material pairs, as well as thicknesses are selected to ensure that transmission band with desired full-width at half maximum (FWHM) value for stage-1 filter (Figure 5.1a,c). Note that the peak transmission value limited to satisfy a predetermined value (>90%). Table 5.1 summarizes a list of the considered dielectric materials. Note that there are surely more material options available, who can be deposited with precision using sputtering (magnetron, RF, DC) or evaporation techniques.

2. AFGSM is employed in designing additional periodic filter structures for an extended stop-band (Figure 5.1a,b). The bandgap values are limited to satisfy the given

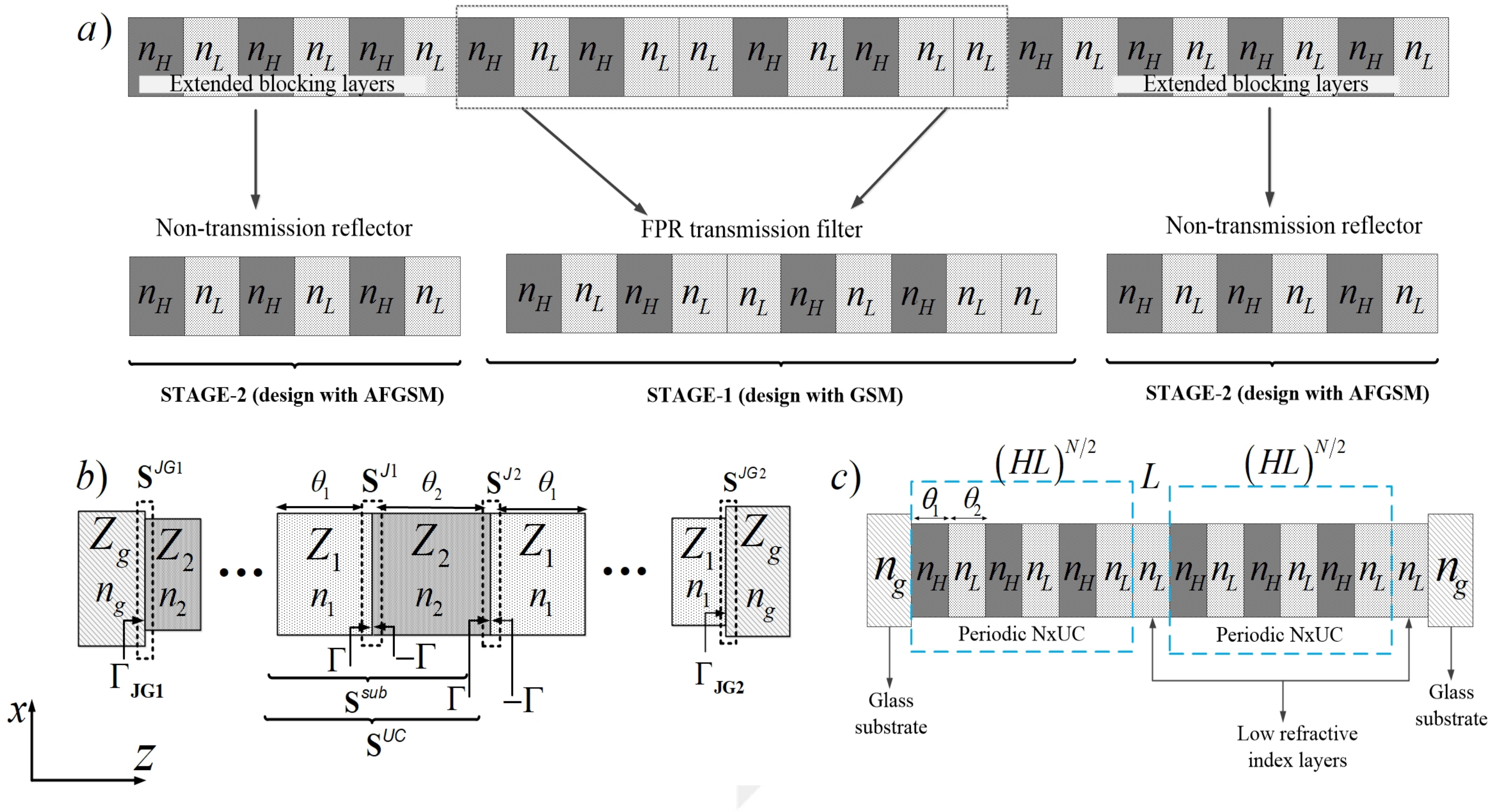

Figure 5.1 : General filter design concept: a) Two filter stages exist where a defective multi-layer stack (stage-1) is sandwiched in between two periodic stacks (stage-2). b) İllustration of layer impedance and reflection coefficients for stage 2 whose solution is achieved with AFGSM c) Details of degenerated (stage-1).

Table 5.1 : List of optical coating materials, and their refractive index at design wavelength ($\lambda = \lambda_0$).

Type (L vs. H)	Material	Symbol	Refractive Index	Reference
L $(n < 2)$	Cryolite	$\mathrm{Na_2AlF_2}$	1.35	[123]
	Magnesium Fluoride	MgF_2	1.38	[123]
	Calcium Fluoride	CaF_2	1.42	[124]
	Silicon Dioxide	SiO_2	1.46	[123]
	Sodium Chloride	$NaCl$	1.53	[125]
	Lead Difluoride	PbF_2	1.73	[123]
H $(n \geq 2)$	Hafnium Oxide	HfO_2	2.05	[126]
	Tantalum Oxide	$\mathrm{Ta_2O_5}$	2.10	[127]
	Zirconium Dioxide	ZrO_2	2.25	[128]
	Titanium Dioxide	TiO_2	2.35	[129]
	Tellurium	Te	4.6	[123]

constraint around the center frequency (f_c) such that the overall stop band becomes: $f_c \pm \Delta f$, where $2\Delta f$ is the frequency extent of the stop-band.

3. GSM method is utilized to cascade the defected intermediate filter with the periodic multilayered dielectric structures to calculate the overall filter characteristics. Once again the transmission value is limited to satisfy a predetermined value of >90% for the periodic filters (stage 2) as well.

In Figure 5.1 $n_1(= n_L)$ denotes the low refractive index material, $n_2(= n_H)$ denotes the high refractive index material. The scheme of the 3-stage algorithm illustrated in Figure 5.1a. In the first two steps of the algorithm desired filter characteristics including the stopband and passband windows are obtained. Accordingly, fine-tuning step is executed which varies for different filter designs, whose details will be shared in the upcoming sections.

5.2.1 Generalized scattering matrix approach and AFGSM method

Here, we summarize the well-known Generalized Scattering Matrix Approach. Propagation characteristics of periodic multilayered structures can be specified using the generalized scattering matrix (GSM) method. Since the GSM technique takes into account propagating and non-propagating modes of periodic structure together with all interactions between the layers, reflection and transmission properties of each layer can be represented by corresponding generalized scattering matrices [60]. In the following formulations, scattering parameters of each layer is formulated and then scattering matrix for the overall structure is obtained by appropriate matrix calculations.

Characteristic impedance of glass, low and high refractive index materials are denoted by Z_g, Z_1 and Z_2 respectively. For reference planes RP_1 and RP_2, Γ_{JGi}, i=1,2 junction reflection coefficients become as Γ_{JG1} and Γ_{JG2} which equal to $\Gamma_{JG1} = \frac{Z_2 - Z_g}{Z_2 + Z_g}$ and $\Gamma_{JG2} = \frac{Z_g - Z_1}{Z_g + Z_1}$. The corresponding characteristic impedance values are expressed as $Z_1 = \frac{\omega\mu}{k_1^z}$, $Z_2 = \frac{\omega\mu}{k_2^z}$ and $Z_g = \frac{\omega\mu_0}{k_0 n_g}$ where μ and μ_0 are the magnetic permeability of the medium and free space respectively.

Junction scattering matrices for reference planes at glass boundaries are expressed as

$$\mathbf{S^{JGi}} = \begin{bmatrix} S_{11}^{JGi} & S_{12}^{JGi} \\ S_{21}^{JGi} & S_{22}^{JGi} \end{bmatrix} \tag{5.1}$$

where

$$\begin{gathered} S_{11}^{JGi} = \Gamma_{JGi}, S_{12}^{JGi} = \sqrt{1 - \Gamma_{JGi}^2}, \\ S_{21}^{JGi} = \sqrt{1 - \Gamma_{JGi}^2}, S_{22}^{JGi} = -\Gamma_{JGi}, \text{ and i=1,2} \end{gathered} \tag{5.2}$$

Scattering matrix of subcell is determined by equation (5.3)

$$\mathbf{S^{sub}} = \begin{bmatrix} e^{-j\Theta_1} & 0 \\ 0 & e^{-j\Theta_2} \end{bmatrix} [\mathbf{S^{J1}}] \begin{bmatrix} e^{-j\Theta_1} & 0 \\ 0 & e^{-j\Theta_2} \end{bmatrix} \tag{5.3}$$

where

$$\begin{gathered} S_{11}^{sub} = S_{11}^{Ji} e^{-j2\Theta_1}, S_{12}^{sub} = S_{12}^{Ji} e^{-j(\Theta_1 + \Theta_2)}, \\ S_{21}^{sub} = S_{21}^{Ji} e^{-j(\Theta_1 + \Theta_2)}, S_{22}^{sub} = S_{22}^{Ji} e^{-j2\Theta_2} \end{gathered} \tag{5.4}$$

and

$$S_{11}^{J1} = \Gamma_{J1}, S_{12}^{J1} = \sqrt{1-\Gamma_{J1}^2},$$
$$S_{21}^{J1} = \sqrt{1-\Gamma_{J1}^2}, S_{22}^{J1} = -\Gamma_{J1} \tag{5.5}$$

$$S_{11}^{J2} = \Gamma_{J2}, S_{12}^{J2} = \sqrt{1-\Gamma_{J2}^2}, S_{21}^{J2} = \sqrt{1-\Gamma_{J2}^2}, S_{22}^{J2} = -\Gamma_{J2} \tag{5.6}$$

Finally s-matrix of unit cell is represented as given in equation (5.7)

$$\mathbf{S^{UC}} = \begin{bmatrix} S_{11}^{sub} & S_{12}^{sub} \\ S_{21}^{sub} & S_{22}^{sub} \end{bmatrix} \tag{5.7}$$

where Θ_1 and Θ_2 are the optical thicknesses of high and low refractive index regions (n_1 and n_2 respectively) as shown in Figure 5.1b and denoted by

$$\Theta_1 = k_1{}^z p_1, \Theta_2 = k_2{}^z p_2 \tag{5.8}$$

In equation (5.8), the term $k_i{}^z$ (i=*1,2*) denotes the z component of the wave vector of propagating modes, p_1 and p_2 ($p = p_1 + p_2$, period) denote the thicknesses of the corresponding dielectric regions respectively.

Following the s-matrix determination for a unit cell given in the equation (5.7), auxiliary functions can be used as an alternative technique to calculate bandgaps of periodic structure. This alternative method mentioned in [60] is referred to as Auxiliary Functions of Generalized Scattering Matrix (AFGSM) which neither requires imposing the Floquet condition (periodicity) nor solving the eigenvalue equation to compute band edges. Simply, regarding to fact that given in equation (5.9); zero transitions (or roots) of auxiliary functions ($X_\pm = 0$) coincide exactly with photonic band boundaries containing the certain frequency values of allowed and forbidden band-edges of the structure. Therefore, AFGSM method yields accurate estimates for the stopband/passband transition frequencies located within the single Floquet mode region only by calculating the roots of functions in equation (5.9).

$$X_\pm = Im\{S_{11} \pm S_{21}\} \tag{5.9}$$

With the initial design parameters, the blocking bands on either side of the central wavelength is relatively small. In order to increase the blocking range of the filter on both sides, proper material parameters must be selected to ensure a broad blocking range. On the other hand, the choice of material parameters can effectively block out of band transmission of incident radiation but they can also decrease the peak transmission value in the pass-band adversely. Therefore, to make sure that all unwanted laser noise is eliminated and a consistent peak transmission value maintained, precisely identification of parameters is very crucial. Utilizing the AFGSM method provides a considerable advantage in terms of computation time not only for bandgap determination but also for parameter scanning.

5.3 Filter Design Strategy for Laser Scanning Microscopy

Sub-cellular resolution imaging of biological specimens or tissue samples with laser scanning microscopy techniques such as confocal (reflectance and fluorescence), multi-photon and harmonic-generation microscopy [120, 121] has been a powerful tool in their assessment. For all aforementioned scanning microscopes, multiple optical filters are utilized to transmit the signal while block unwanted light for improved imaging performance. Here we focus on four different filters that are readily utilized in laser scanning microscopy, as illustrated in Figure 5.2. Next we apply our hybrid filter design strategy to meet the design requirements of these filters and compare our filters with those commercially available. Figure 5.2 shows all optical components involved in a i) reflectance confocal microscope, ii) fluorescence confocal microscope, and a iii) two-photon microscope (with both fluorescence and harmonic generation detection channels. Furthermore, Table 5.2 summarizes the types of filters used in different laser scanning microscopy techniques. A confocal reflectance laser-scanning microscope captures the laser light that is being scanned on the tissue. Thus the most critical filter is the laser-line filter that allows for capturing the light reflecting off the tissue, while blocking other wavelengths that may be available within the room in which experiments are being conducted. On the contrary, in a confocal fluorescence microscope, fluorescence signal from tagged or auto-fluorescing molecules are captured. The detected wavelength is lower in energy, and higher in wavelength, necessitating a laser-blocking (notch) filter to eliminate any spurious reflection of the laser light while isolating the fluorescent light.

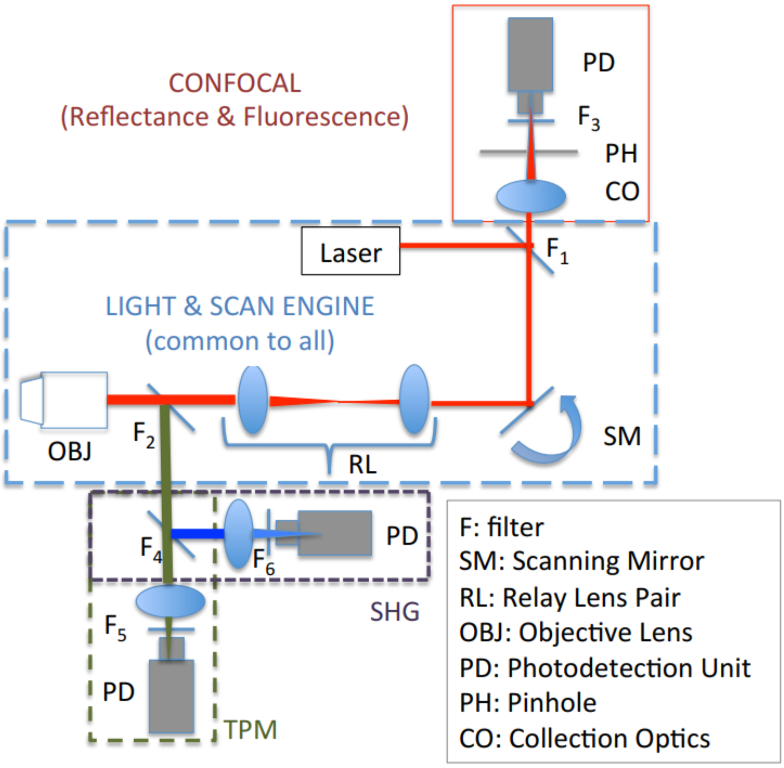

Figure 5.2 : Laser scanning microscopy architecture, comprising a light and scan engine unit that is common to all imaging modalities.

Thus a confocal fluorescence microscope is a slightly modified version of the confocal reflectance microscope, such that the beam splitter is replaced with a dichroic filter (also called as a dichroic beam splitter, which reflects laser light and transmits fluorescent light) and the laser line filter is replaced with a laser-notch filter. On the contrary, a multi-photon scanning microscope does not require the laser light to be de-scanned (the emitted light to hit the scanner once again on the return path). Thus, the first filter (F1) is not employed (could be replaced by a simple mirror). The emitted light is captured right after being collected with the objective lens with a dichroic filter. After reflecting of the dichroic mirror, the returning light may once

Table 5.2 : List of optical filters used in laser scanning microscopes.

	F1	F2	F3	F4	F5	F6
Confocal (reflectance)	Beam splitter	-	Laser line	-	-	-
Confocal (fluorescence)	Dichroic	-	Laser notch	-	-	-
Multiphoton (two-photon + SHG)	Mirror	Dichroic	-	Dichroic	Laser notch	Harmonic line

again be divided into two-photon (or any higher multi-photon modality) path that requires another dichroic filter, and a second (or higher) harmonic generation (SHG) path, which necessitates a band-pass filter.

In both reflectance confocal and multiphoton laser scanning microscopes, near-Infrared (NIR) Laser sources are typically utilized, owing to their superior tissue penetration depth (see ref: [130]). On the other hand, a lower wavelength source is employed in fluorescence confocal imaging to excite auto fluorescing proteins.
Without loss of generality, in the upcoming section, we summarize our effort in designing:

1. Laser line (narrow-band pass) filter (F1) @ λ = 800 nm for reflectance confocal microscopy, for oblique incidence.

2. Narrow band filter (F6) @ λ = 400 nm (laser source @ λ = 800 nm) for SHG microscopy, for oblique incidence.

3. Dichroic filter (F1,2,4) @ λ_{center} = 380 - 420 nm range, where $\lambda < \lambda_{center}$ is reflected, and $\lambda > \lambda_{center}$ is transmitted, for 45^0 incidence. This configuration is useful for 3 different filters illustrated in Figure 5.2.

    (a) It could be utilized as F1 in fluorescent confocal microscopy for a laser source of λ = 405 nm (or similar), to excite blue fluorescent protein types.

    (b) It could be utilized as F4 in multiphoton microscopy, to distinguish between SHG signal (λ = 400 nm), and two-photon emitted signal (400 nm $< \lambda <$ 600 nm), once again to excite blue fluorescent protein types (laser source @ λ = 800 nm).

    (c) It could be utilized as F2 in multiphoton microscopy, to reflect the captured light after the objective (laser source @ λ = 800 nm). This would indeed require the reflection and transmission band to interchange, i.e. range, where $\lambda > \lambda_{center}$ should be reflected now. Note that this filter would require quiet similar design steps to 3-a, and 3-b, respectively.

4. A band stop filter working at laser wavelength of: λ = 800 nm, to block any residue from the detector. Once again this filter would be useful as:

- A laser blocker for fluorescent confocal microscopy
- A laser blocker for SHG signal, and
- A laser blocker for two-photon microscopy.

Below, we give further details of the design strategy of all four-filter types that is based on the scheme illustrated in Figure 5.1.

5.3.1 Laser line filter @ λ = 800 nm

Laser line filter is designed for use in reflectance confocal laser scanning microscope, to only detect reflected laser light from the specimen while blocking other wavelengths. Assuming an NIR laser source at λ = 800 nm, the specification of an off-the-shelf laser line filter and the designed filter are shared in Table 5.3. In accordance with the design algorithm provided in *theory and modeling* section, we first design a preliminary and perfectly periodic version of stage-1 filter to provide a stop-band whose center matches the center transmission wavelength as $\mathbf{(HL)^7}$ and then introduce the low-index defect to define narrow-transmission region (Figure 5.3a), such that the initial periodic design $\mathbf{(HL)^3L(HL)^3}$. Then, stage 2 filters are designed with AFGSM to extend the stop-band toward lower and higher wavelengths, as illustrated in Figure 5.3a,b. Finally, the overall filter characteristic is illustrated in Figure 5.3c.

5.3.2 Harmonic line filter @ λ = 400 nm

The harmonic line filter is designed for use in SHG laser scanning microscope, to isolate the SHG light from tissues (such as collagen tissue) while blocking other wavelengths, once again assuming an NIR laser source at λ = 400 nm. The design is near identical to the laser line filter, but with different material selection and layer thicknesses. The stage-1, stage-2, and overall filter characteristics are illustrated in Figure 5.4a,b and Figure 5.4c, while the details are shared in Table 5.3, and Table 5.4.

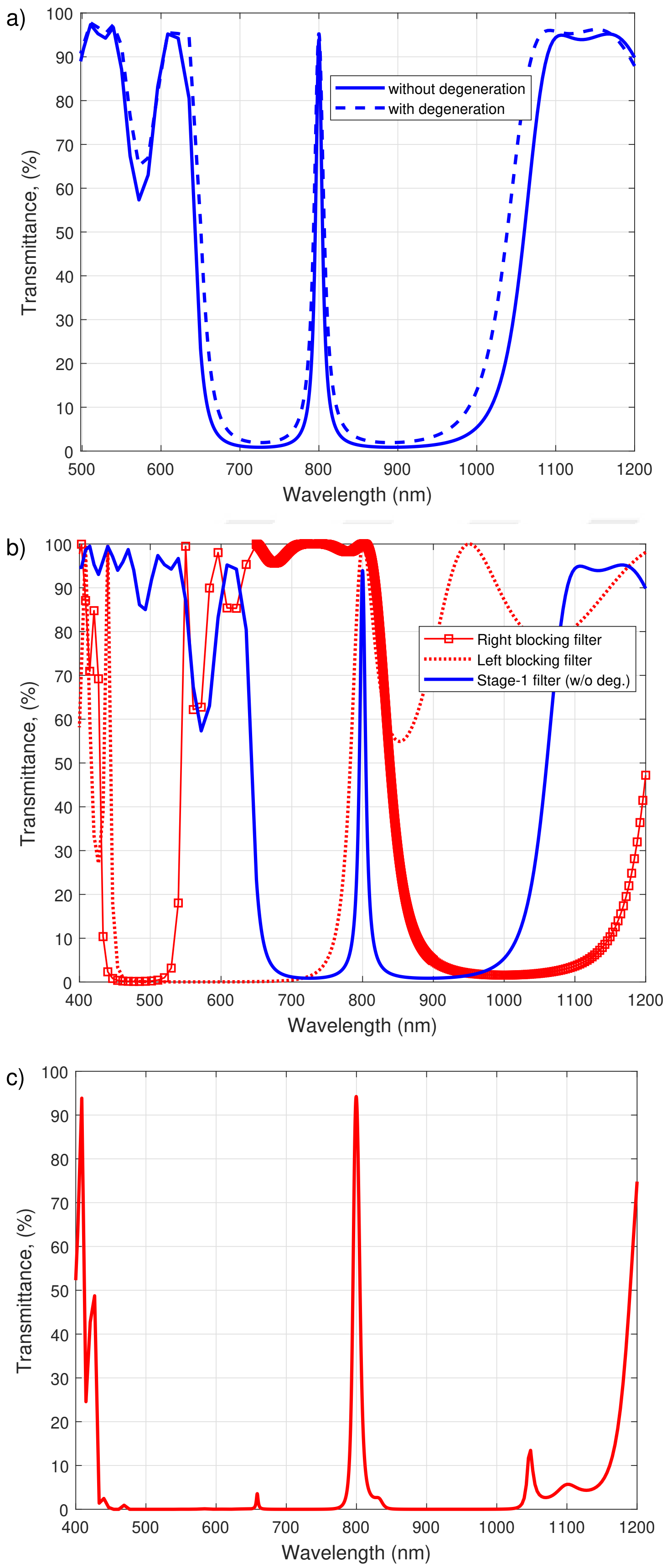

Figure 5.3 : Laser line filter; a) stage 1 filter characteristics with and without degeneration b) stage 2 filter characteristics, showing left (dashed red line) and right (squared solid line) blocking filter behavior, c) overall laser line filter characteristics.

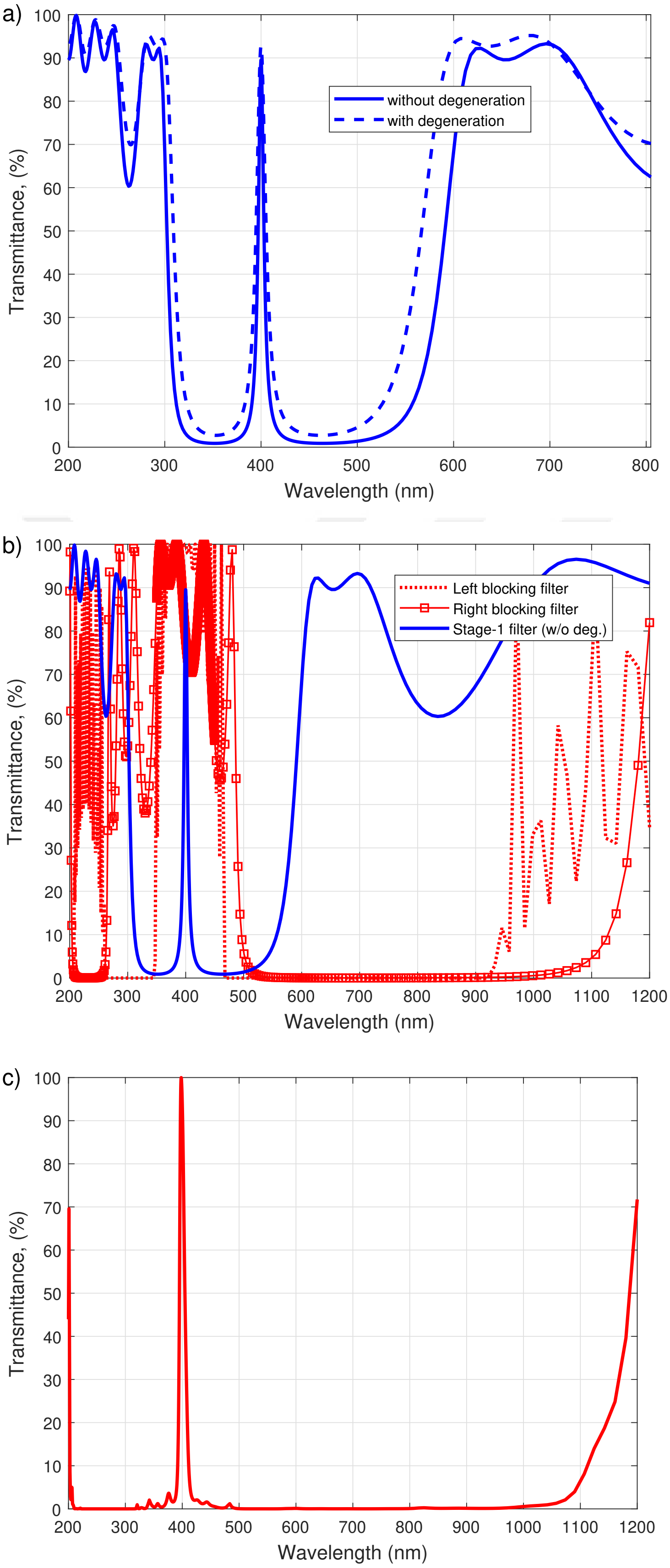

Figure 5.4 : Harmonic line filter; a) stage 1 filter characteristics with and without degeneration b) stage 2 filter characteristics, showing left (dashed red line) and right (squared solid line) blocking filter behavior, c) overall harmonic line filter characteristics.

Table 5.3 : Comparison of off-the shelf filters vs. designed.

	Laser Line[a]		Harmonic Line[b]		Dichroic		Notch	
	Designed	**RF1**[1]	**Designed**	**RF2**[2]	**Designed**	**RF3**[3]	**Designed**	**RF4**[4]
Center Wavelength (nm)	799.7	800 ± 2	399.9	400 ± 2	383.2	383.5	811.2	800 ± 2
Reflection Region (nm)	454 - 1018	200 - 1200	262 - 886	200 - 1200	360.4 - 406.8	360 - 407	NA	NA
Transmission Region (nm)	NA	NA	NA	NA	422 - 575	425 - 575	600 - 789.6 837.4 - 1100	610 - 778 838 - 1060
Peak Transmission (%)	94.23	≥ 85	90.05	≥ 85	94.8	≥ 90	90	≥ 90
FWHM (nm)	10.7	10 ± 2	7.3	8 - 10	NA	NA	32.4	34

[a] $\lambda_0 = 800$ nm.
[b] $\lambda_0 = 400$ nm.
[1] Reference Filter (RF1) : edmundoptics, part no:19773
[2] Reference Filter (RF2) : edmundoptics, part no:19730
[3] Reference Filter (RF3) : thorlabs, part no:MD416
[4] Reference Filter (RF4) : thorlabs, part no:NF808-34

In Table 5.3, transmission region and reflection region bands are determined by applying stage-1 and stage-2 of the proposed algorithm, respectively. Transmission region, peak transmission and FWHM values of designed filters in Table 5.3 perfectly agree with the reference filters which are commercially available. In Table 5.3, Magnitude square of scattering parameter (S_{21}) corresponds to transmittance of the designed filter ($|S_{21}|^2$). Furthermore, reflection region of corresponding frequency band is determined by satisfying $|S_{11}|^2 < 10^{(-4)}$ condition.

5.3.3 Dichroic filter

As detailed previously, the dichroic filter is designed for use in fluorescent confocal microscopy or multiphoton microscopy, to re-direct the emitted light from the tissue to the detector [131]. Assuming a source wavelength of λ = 800 nm, both setups require a filter having @ $\lambda_{center} \approx$ 380-420 nm range, where $\lambda < \lambda_{center}$ is reflected, and $\lambda > \lambda_{center}$ is transmitted, at 45^0 incidence. In accordance with our design scheme, we first determine the layer materials and thicknesses. For the dichroic filter, only utilizing a stage-1 design having **(0.5H L 0.5H)^{15}** form is sufficient, while using a slightly altered version having form **(0.5HL(HL)^{13}0.5H)** refines the ripple effects in the overall transmission behavior as illustrated in Figure 5.5. Therefore, basic stack of **(0.5H L 0.5H)^{15}** is modified by adding a periodic reflection block in the form of **(HL)^{13}**. In addition to that modification, entire building block designed to be coated with MgF_2 as incident medium and with *glass* as a substrate to ensure the supression of unwanted ripples.

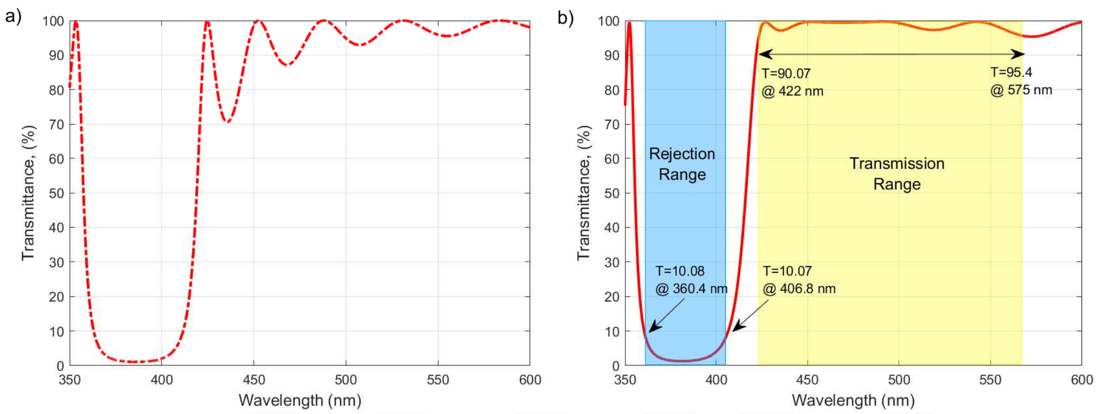

Figure 5.5 : Dichroic filter characteristics a) AFGSM results b) improved results after refinement.

5.3.4 Notch filter

This filter is to be employed in all of the aforementioned laser scanning imaging modalities apart from the reflectance confocal imaging, to block the laser light [132] (Here we assume a laser wavelength of λ = 800 nm).

In order to construct notch filter shape we first need to identify the properties of desired rejection zone which depends on the ratio of the refractive indices and thickness of the high and low index layers. Proposed method accelerates the identification of stop-band parameters which will primitively ensure narrow band reflection region. Therefore, we first employed AFGSM method to determine most proper refractive index values of materials, required number of layers and corresponding FWHM in the reflectance window for the desired filter characteristics. As a next step we calculate the layer thicknesses with a gradual thickness change in high index to low index by getting thinner from center of the stack towards the ends. Such refinement is ensured by applying a Gaussian shaped modulation formulated with well-known apodization functions which are used to calculate optical thicknesses of each layer;

$$T_H = ae^{-[n-\frac{N}{2}]^2/2C^2} \tag{5.10}$$

$$T_L = 2 - T_H(n) \tag{5.11}$$

where T_H and T_L indicates the quarter-wave optical thickness of n-th layer. N is the total number of layers in the structure and a is the apodization ratio used in functions. C is related to the FWHM of the Gaussian function by

$$C = \frac{FWHM}{[2\sqrt{2ln(2)}]} \tag{5.12}$$

Using the presented method desired notch (minus) filter characteristics are achieved utilizing that high-reflectivity around the center wavelength (λ_0) of the narrow rejection band while showing high-transmission elsewhere. Moreover, we demonstrated that, ripples in the transmission region can be suppressed considerably along with increasing the steepness in band edges. In this example, we consider the notch filter design with the performance that should satisfy high transmittance ($\geq 90\%$) in the pass-band wavelength ranges of 610 - 778 nm and 838 - 1060 nm, and high reflectivity centered at 808 $\pm$ 2 nm with a FWHM value of 34 nm under normal incidence (see Figure 5.6).

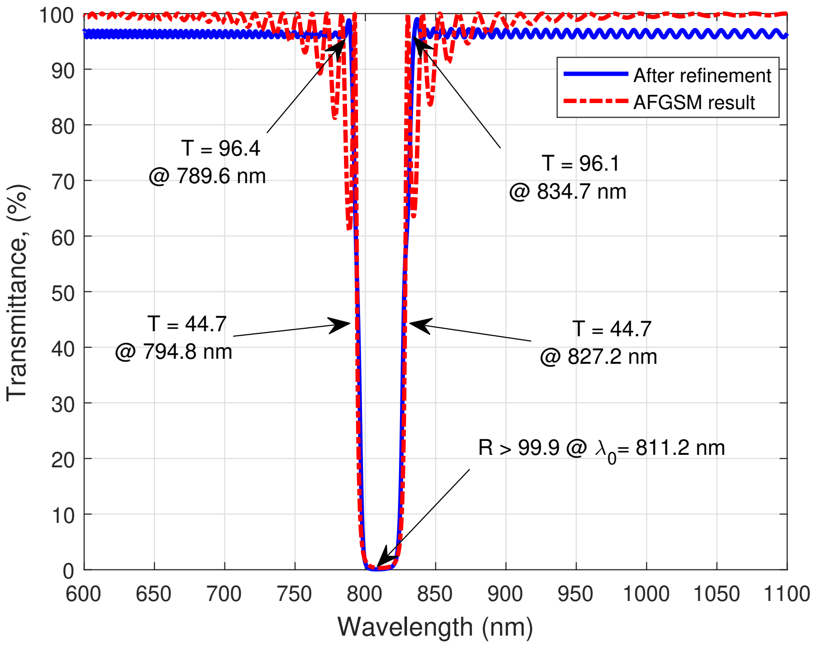

Figure 5.6 : Transmittance of the designed notch filter. Dashed line represents the response of AFGSM method and solid line shows the final proposed filter response after refinement with modulation functions.

Table 5.4 : Design summary of the presented filters.

Filter Type	Building Block Stack	p_1, p_2 (nm)	n_1, n_2	Number of Layers	Total Thickness
Filter 1 800 nm BPF	Left blocking = $(HL)^6$	45.4, 42.4	4.6, 1.4	17	2.74 μm
	Central FPR = $(HL)^3L(HL)^3$	85.1, 140.8	2.35, 1.42		
	Right blocking = $(HL)^4$	23.2, 157.6	4.6, 2.35		
Filter 2 400 nm BPF	Left blocking = $(HL)^6$	29.6, 45.6	2.35, 1.35	15	1.42 μm
	Central FPR = $(HL)^2L(HL)^2$	21.7, 42.5	4.6, 2.35		
	Right blocking = $(HL)^4$	36, 132	4.6, 1.35		
Filter 3 45^0 Dichroic	Incidence medium = MgF_2	-	1.38	18	1.55 μm
	Central block = $0.5HL(HL)^{13}0.5H$	50.8, 60.2	2.05, 1.73		
	Substrate = glass	-	1.52		
Filter 4 800 nm Notch	Incidence medium = glass	-	1.52	147	58.6 μm
	Modulated block = $(HL)^{145}$	T_H, T_L*	2.25, 1.47		
	Substrate = air	-	1		

* T_H, T_L are calculated as given in equation (5.10) and (5.11)

5.4 Conclusion

We present hybrid filter structures towards use in numerous laser scanning microscopy modalities, comprising a combination of periodic and degenerated multilayered dielectric structures. The proposed approach utilizing both GSM and AFGSM for the design of stage-1 and stage-2 parts of the overall filter structure provides significant flexibility in setting the desired transmission band while offering widened stop-bands. The flexibility and robustness comes from the computational advantages that AFGSM brings owing to obtaining bandgap edge frequencies without solving an eigenvalue equation. The designed filters are comparable in performance to the off-the-shelf filter counterparts. As a future work, we are planning to design sophisticated filters using our algorithm, which can replace multiple filters to simplify and reduce the number of components in laser scanning microscopy.

6. CONCLUSIONS

In this thesis, wave propagation characteristics in periodic structures have been studied. Particularly, in the framework of the thesis, alternative techniques have been developed to extend the bandgap analysis to various two-dimensional photonic bandgap structures (2D PBGs). Since the considered periodic structure is composed of the infinite succession of a unit cell, methods are based on the primarily exploring the scattering matrix of the unit cell in order to specify the PBG edges spectrally. Indeed, designing a new device is time consuming and expensive, numerical techniques are very crucial to characterize electromagnetic behavior of the existing devices. However, these techniques are restricted by the complexity of structures. Therefore, the main objective of this thesis is to provide an alternative method to overcome the limitations of numerical and heuristic approaches. First chapter of the thesis starts with a basic introduction of the scope and a summarized literature survey.

The second chapter of the thesis is concerned with the general formulation of the transmission line theory and conventional ABCD matrix approaches. Fundamental steps of the rigorous coupled wave analysis (RCWA) method, which is used as a preliminary computational routine to find out the s-parameters of a grating unit cell, introduced. Instead of conventional technique which requires solution of eigenvalue equation, we proved that dispersion diagram of the Floquet modes supported by the infinite periodic system provides the allowed and forbidden frequency band information of the finite structure which provides the full-wave modal analysis of a periodic structure. Here, a novel approach based on auxiliary functions of generalized scattering matrix (AFGSM) method is introduced to estimate the band-edge frequencies of the global structure properly provides bandedge frequencies of ideal structure. The proposed technique yields accurate estimates for the stop-band/pass-band transition frequencies located within the single Floquet mode region just by executing a simple root-finding algorithm. In final part of the chapter some numerical results of design applications are presented including four-channel photonic crystal based optical filter and omnidirectional reflector with extended stopband region.

The third part of the thesis present a hybrid method that is a combination of effective-medium theory (EMT) and AFGSM is an original technique proposed to literature. Presented alternative method yields accurate estimations of bandedge frequencies through solely varying the dimensional and physical factors of considered geometry. The approach applies EMT to deduce two-dimensional structure to one-dimensional (1D) multilayered equivalence to overcome the dimensional complexness of the problem. Accordingly, PBG edges of the equivalent 1D structure is specified by using the auxiliary functions of generalized scattering matrix (AFGSM) method. Formulated mixed process is implemented to square and circular formed rectangular grid PCs in order to explore bandgaps. Since method reduces the problem complexity of 2D geometry, it provides a faster analysis opportunity for design purposes. The remarks might create a significant contribution to the area of photonic bandgap investigation techniques.

In the fourth chapter of the thesis, we then have extended the findings to full-wave electromagnetic wave analysis of 2D PC structures constituted by arrays of dielectric rods with arbitrary cross-sections. In this study, 2D PBG (photonic bandgap) structure is considered as a stack of 1D gratings which diffraction properties are exploited by rigorous coupled wave analysis (RCWA) method. Considered 2D PCs are constituted by varying configurations such as rectangular and circular cross-sections of dielectric rods and arbitrary lattice types. Electromagnetic properties of such structures are analyzed in terms of photonic bandgpas located on reflectance spectrum as a function of filling ratio, incidence angle and frequency. Results are presented in a comparison with that of traditional ones reported in the literature as well as available experimental data. Moreover obtained results have been successfully validated with commercial electromagnetic simulator which uses finite element method on the frequency domain.

In the fifth and last part of the thesis, we presented an algorithm to design filter structures that can be used in numerous laser scanning microscopy applications including laser-line filter, notch filter and dichroic filter. The proposed algorithm consists of two main stages that GSM and AFGSM approaches applied respectively. Developed algorithm successfully provides significant flexibility in setting the desired transmission band while offering widened stop-bands. The designed filters are comparable in performance to the commercially available filter counterparts. A number of new applications can be developed using the solution technique implemented in Chapter 5. While this thesis provides novel theoretical contributions, many interesting and important problems are yet to be studied. The work presented in this thesis concentrates on lossless dielectric 2D PBG structures. However, in most of the real-world applications available materials involves metallic or lossy dielectrics. Therefore an alternative topic could be built upon the analysis of hybrid structures comprised of metallic and dielectric materials. We hope that the open problems presented herein stimulate the further research on wave propagation analysis and design approaches on photonic bandpag structures, both on the theoretical side as well as in the practical applications.

REFERENCES

[1] **Joannopoulos, J.D.**, **Johnson, S.G.**, **Winn, J.N. and Meade, R.D.** (2011). *Photonic crystals: molding the flow of light*, Princeton University Press.

[2] **Prather, D.W.**, **Shi, S.**, **Sharkawy, A.**, **Murakowski, J. and Schneider, G.** (2009). *Photonic crystals: Theory, Aplications and Fabrication*, Wiley Online Library.

[3] **Chigrin, D.N. and Torres, C.S.** (2001). Periodic thin-film interference filters as one-dimensional photonic crystals, *Optics and Spectroscopy*, *91*(3), 484–489.

[4] **Akahane, Y.**, **Mochizuki, M.**, **Asano, T.**, **Tanaka, Y. and Noda, S.** (2003). Design of a channel drop filter by using a donor-type cavity with high-quality factor in a two-dimensional photonic crystal slab, *Applied Physics Letters*, *82*(9), 1341–1343.

[5] **Qiu, M. and Jaskorzynska, B.** (2003). Design of a channel drop filter in a two-dimensional triangular photonic crystal, *Applied Physics Letters*, *83*(6), 1074–1076.

[6] **Wang, Z. and Fan, S.** (2003). Compact all-pass filters in photonic crystals as the building block for high-capacity optical delay lines, *Physical Review E*, *68*(6), 066616.

[7] **Wang, C.**, **Zhong, X.L. and Li, Z.Y.** (2012). Linear and passive silicon optical isolator, *Scientific reports*, *2*, 674.

[8] **Oh, S.S. and Choi, C.G.** (2009). Photonic-crystal-slab-type guided mode resonance filters in infrared range, *IEEE Photonics Technology Letters*, *21*(5), 316–318.

[9] **Akahane, Y.**, **Asano, T.**, **Song, B.S. and Noda, S.** (2003). High-Q photonic nanocavity in a two-dimensional photonic crystal, *Nature*, *425*(6961), 944–947.

[10] **Happ, T.**, **Markard, A.**, **Kamp, M.**, **Gentner, J.L. and Forchel, A.** (2001). InP-based short cavity lasers with 2D photonic crystal mirror, *Electronics Letters*, *37*(7), 428–429.

[11] **Morita, Y.**, **Tsuji, Y. and Hirayama, K.** (2008). Proposal for a compact resonant-coupling-type polarization splitter based on photonic crystal waveguide with absolute photonic bandgap, *IEEE photonics technology letters*, *20*(2), 93–95.

[12] **Wu, Y.D.**, **Huang, M.L. and Shih, T.T.** (2007). Optical interleavers based on two-dimensional photonic crystals, *Applied optics*, *46*(29), 7212–7217.

[13] **Pottier, P.**, **Gnan, M. and Richard, M.** (2007). Efficient coupling into slow-light photonic crystal channel guides using photonic crystal tapers, *Optics Express*, *15*(11), 6569–6575.

[14] **Kim, S.**, **Park, I. and Lim, H.** (2005). Proposal for ideal 3-dB splitters–combiners in photonic crystals, *Optics letters*, *30*(3), 257–259.

[15] **Chutinan, A.**, **Okano, M. and Noda, S.** (2002). Wider bandwidth with high transmission through waveguide bends in two-dimensional photonic crystal slabs, *Applied physics letters*, *80*(10), 1698–1700.

[16] **Wang, Y.**, **Zhang, D.**, **Xu, S.**, **Ouyang, Z. and Li, J.** (2016). Low-loss Y-junction two-dimensional magneto-photonic crystals circulator using a ferrite cylinder, *Optics Communications*, *369*, 1–6.

[17] **Wang, Y.**, **Zhang, D.**, **Xu, S.**, **Xu, B.**, **Dong, Z. and Huang, T.** (2017). Experimental evidence of photonic crystal waveguides with wide bandwidth in two-dimensional Al 2 O 3 rods array, *Chinese Optics Letters*, *15*(6), 062301.

[18] **Aly, A.H. and Mohamed, D.** (2015). BSCCO/SrTiO 3 one dimensional superconducting photonic crystal for many applications, *Journal of Superconductivity and Novel Magnetism*, *28*(6), 1699–1703.

[19] **El-Naggar, S.A.**, **Elsayed, H.A. and Aly, A.H.** (2014). Maximization of photonic bandgaps in two-dimensional superconductor photonic crystals, *Journal of Superconductivity and Novel Magnetism*, *27*(7), 1615–1621.

[20] **Wu, C.J.**, **Liao, J.J. and Chang, T.W.** (2010). Tunable multilayer Fabry-Perot resonator using electro-optical defect layer, *Journal of Electromagnetic Waves and Applications*, *24*(4), 531–542.

[21] **Meng, Q.B.**, **Fu, C.H.**, **Hayami, S.**, **Gu, Z.Z.**, **Sato, O. and Fujishima, A.** (2001). Effects of external electric field upon the photonic band structure in synthetic opal infiltrated with liquid crystal, *Journal of Applied Physics*, *89*(10), 5794–5796.

[22] **Aly, A.H.**, **El-Naggar, S.A. and Elsayed, H.A.** (2015). Tunability of two dimensional n-doped semiconductor photonic crystals based on the Faraday effect, *Optics express*, *23*(11), 15038–15046.

[23] **Yeh, P.**, **Yariv, A. and Hong, C.S.** (1977). Electromagnetic propagation in periodic stratified media. I. General theory, *JOSA*, *67*(4), 423–438.

[24] **Sakoda, K.** (2004). *Optical properties of photonic crystals*, volume 80, Springer Science & Business Media.

[25] **Johnson, S.G. and Joannopoulos, J.D.** (2001). Block-iterative frequency-domain methods for Maxwell's equations in a planewave basis, *Optics express*, *8*(3), 173–190.

[26] **Plihal, M. and Maradudin, A.** (1991). Photonic band structure of two-dimensional systems: The triangular lattice, *Physical Review B*, *44*(16), 8565.

[27] **Sözüer, H.S.**, **Haus, J. and Inguva, R.** (1992). Photonic bands: Convergence problems with the plane-wave method, *Physical Review B*, *45*(24), 13962.

[28] **Sukhoivanov, I.A. and Guryev, I.V.** (2009). *Photonic crystals: physics and practical modeling*, volume152, Springer.

[29] **Pendry, J.** (1994). Photonic band structures, *Journal of Modern Optics*, *41*(2), 209–229.

[30] **Sigalas, M.**, **Chan, C.**, **Ho, K. and Soukoulis, C.** (1995). Metallic photonic band-gap materials, *Physical Review B*, *52*(16), 11744.

[31] **Yee, K.** (1966). Numerical solution of initial boundary value problems involving Maxwell's equations in isotropic media, *IEEE Transactions on antennas and propagation*, *14*(3), 302–307.

[32] **Taflove, A. and Hagness, S.C.** (2005). *Computational electrodynamics: the finite-difference time-domain method*, Artech house.

[33] **Pelosi, G.**, **Cocchi, A. and Monorchio, A.** (2000). A hybrid FEM-based procedure for the scattering from photonic crystals illuminated by a Gaussian beam, *IEEE Transactions on Antennas and Propagation*, *48*(6), 973–980.

[34] **Saitoh, K. and Koshiba, M.** (2002). Full-vectorial imaginary-distance beam propagation method based on a finite element scheme: application to photonic crystal fibers, *IEEE Journal of Quantum Electronics*, *38*(7), 927–933.

[35] **Jin, J.M.** (2015). *The finite element method in electromagnetics*, John Wiley & Sons.

[36] **Winn, J.N.**, **Fink, Y.**, **Fan, S. and Joannopoulos, J.** (1998). Omnidirectional reflection from a one-dimensional photonic crystal, *Optics letters*, *23*(20), 1573–1575.

[37] **Fink, Y.**, **Winn, J.N.**, **Fan, S.**, **Chen, C.**, **Michel, J.**, **Joannopoulos, J.D. and Thomas, E.L.** (1998). A dielectric omnidirectional reflector, *Science*, *282*(5394), 1679–1682.

[38] **Fowles, G.R.** (1989). *Introduction to modern optics*, Courier Corporation.

[39] **Awasthi, S.K.**, **Malaviya, U.**, **Ojha, S.P.**, **Mishra, N.K. and Singh, B.** (2008). Design of a tunable polarizer using a one–dimensional nano sized photonic bandgap structure, *Progress In Electromagnetics Research*, *5*, 133–152.

[40] **Hsu, H.T.**, **Chang, T.W.**, **Yang, T.J.**, **Chu, B.H. and Wu, C.J.** (2010). Analysis of wave properties in photonic crystal narrowband filters with left-handed defect, *Journal of Electromagnetic Waves and Applications*, *24*(16), 2285–2298.

[41] **Dai, X.**, **Xiang, Y. and Wen, S.** (2011). Broad omnidirectional reflector in the one-dimensional ternary photonic crystals containing superconductor, *Progress In Electromagnetics Research*, *120*, 17–34.

[42] **Xu, Z.**, **Wang, J.**, **He, Q.**, **Cao, L.**, **Su, P. and Jin, G.** (2005). Optical filter based on contra-directional waveguide coupling in a 2D photonic crystal with square lattice of dielectric rods, *Optics express*, *13*(15), 5608–5613.

[43] **Hecht, E. and Zajac, A.** (1974). Optics addison-wesley, *Reading, Mass*, *19872*, 350–351.

[44] **Meade, R.D.**, **Brommer, K.D.**, **Rappe, A.M. and Joannopoulos, J.** (1992). Existence of a photonic band gap in two dimensions, *Applied Physics Letters*, *61*(4), 495–497.

[45] **Villeneuve, P.R. and Piche, M.** (1992). Photonic band gaps in two-dimensional square and hexagonal lattices, *Physical Review B*, *46*(8), 4969.

[46] **Villeneuve, P.R. and Piché, M.** (1992). Photonic band gaps in two-dimensional square lattices: Square and circular rods, *Physical Review B*, *46*(8), 4973.

[47] **Dyogtyev, A.**, **Sukhoivanov, I. and De La Rue, R.** (2010). Photonic band-gap maps for different two dimensionally periodic photonic crystal structures, *Journal of Applied Physics*, *107*(1), 013108.

[48] **Kee, C.S.**, **Kim, J.E. and Park, H.Y.** (1997). Absolute photonic band gap in a two-dimensional square lattice of square dielectric rods in air, *Physical Review E*, *56*(6), R6291.

[49] **Haas, T.**, **Hesse, A. and Doll, T.** (2006). Omnidirectional two-dimensional photonic crystal band gap structures, *Physical Review B*, *73*(4), 045130.

[50] **Hwang, R.B. and Pu, T.C.** (2007). Omnidirectional stop band by using composite two-dimensionally artificial crystal, *Microwave and Optical Technology Letters*, *49*(8), 1914–1917.

[51] **Chen, B.**, **Tang, T.**, **Liu, C. and Chen, H.** (2010). Study on optical waveguides based on omnidirectional reflection of two-dimensional photonic crystals, *JOSA B*, *27*(5), 972–974.

[52] **Chen, B.**, **Li, S.**, **Tang, T.**, **Liu, C.**, **Chen, H.**, **Li, Y.**, **Huang, L. and Liu, G.** (2011). Study on Omnidirectional Reflection Bands of Two-Dimensional Photonic Crystals and Optical Waveguides Based on This Effect, *Journal of Lightwave Technology*, *29*(13), 1975–1979.

[53] **Gazonas, G.A.**, **Weile, D.S.**, **Wildman, R. and Mohan, A.** (2006). Genetic algorithm optimization of phononic bandgap structures, *International journal of solids and structures*, *43*(18-19), 5851–5866.

[54] **Jiang, L.**, **Zheng, G.**, **Shi, L.**, **Yuan, J. and Li, X.** (2008). Broad omnidirectional reflectors design using genetic algorithm, *Optics Communications*, *281*(19), 4882–4888.

[55] **Sharma, A.**, **Dwivedi, V.K. and Singh, G.** (2008). THz rectangular patch microstrip antenna design using photonic crystal as substrate, *Progress in Electromagnetic Research Symposium, Cambridge, USA*, pp.161–165.

[56] **Liang, J. and Yang, H.D.** (2009). Microstrip patch antennas on tunable electromagnetic band-gap substrates, *IEEE transactions on antennas and propagation*, *57*(6), 1612–1617.

[57] **Banaei, H. A., R.A.** (2008). A novel proposal for passive all-optical demultiplexer for DWDM systems using 2-D photonic crystals, *Journal of Electromagnetic Waves and Applications*, *22*(4), 471–482.

[58] **Djavid, M., A.M.S.** (2012). Multi-channel drop filters using photonic crystal ring resonators, *Optik-International Journal for Light and Electron Optics*, *123*(2), 167–170.

[59] **Simsek, S., T.E.** (2007). Some properties of generalized scattering matrix representations for metallic waveguides with periodic dielectric loading, *IEEE Transactions on Microwave Theory and Techniques*, *55*(11), 2336–2344.

[60] **Erkan, O.**, **Akıncı, M.N. and Şimşek, S.** (2018). Bandgap analysis of 2D photonic crystals with Auxiliary Functions of Generalized Scattering Matrix (AFGSM) method, *AEU-International Journal of Electronics and Communications*, *95*, 287–296.

[61] **Gans, M.** (1965). A general proof of floquet's theorem (Correspondence), *IEEE transactions on microwave theory and techniques*, *13*(3), 384–385.

[62] **Pozar, D.M.** (2009). *Microwave engineering*, John Wiley & Sons.

[63] **Yablonovitch, E.** (1987). Inhibited spontaneous emission in solid-state physics and electronics, *Physical review letters*, *58*(20), 2059.

[64] **John, S.** (1987). Strong localization of photons in certain disordered dielectric superlattices, *Physical review letters*, *58*(23), 2486.

[65] **Akahane, Y.**, **Mochizuki, M.**, **Asano, T.**, **Tanaka, Y. and Noda, S.** (2003). Design of a channel drop filter by using a donor-type cavity with high-quality factor in a two-dimensional photonic crystal slab, *Applied Physics Letters*, *82*(9), 1341–1343.

[66] **Qiu, M. and Jaskorzynska, B.** (2003). Design of a channel drop filter in a two-dimensional triangular photonic crystal, *Applied Physics Letters*, *83*(6), 1074–1076.

[67] **El-Naggar, S.A.**, **Elsayed, H.A. and Aly, A.H.** (2014). Maximization of photonic bandgaps in two-dimensional superconductor photonic crystals, *Journal of Superconductivity and Novel Magnetism*, *27*(7), 1615–1621.

[68] **Meng, Q.B.**, **Fu, C.H.**, **Hayami, S.**, **Gu, Z.Z.**, **Sato, O. and Fujishima, A.** (2001). Effects of external electric field upon the photonic band structure in synthetic opal infiltrated with liquid crystal, *Journal of Applied Physics*, *89*(10), 5794–5796.

[69] **Okano, M. and Noda, S.** (2004). Analysis of multimode point-defect cavities in three-dimensional photonic crystals using group theory in frequency and time domains, *Physical Review B*, *70*(12), 125105.

[70] **Hsue, Y.C.**, **Freeman, A.J. and Gu, B.Y.** (2005). Extended plane-wave expansion method in three-dimensional anisotropic photonic crystals, *Physical Review B*, *72*(19), 195118.

[71] **Li, Z.Y. and Ho, K.M.** (2003). Application of structural symmetries in the plane-wave-based transfer-matrix method for three-dimensional photonic crystal waveguides, *Physical Review B*, *68*(24), 245117.

[72] **Astratov, V.**, **Whittaker, D.**, **Culshaw, I.**, **Stevenson, R.**, **Skolnick, M.**, **Krauss, T. and De La Rue, R.** (1999). Photonic band-structure effects in the reflectivity of periodically patterned waveguides, *Physical Review B*, *60*(24), R16255.

[73] **Massaro, A.**, **Errico, V.**, **Stomeo, T.**, **Cingolani, R.**, **Salhi, A.**, **Passaseo, A. and De Vittorio, M.** (2008). 3-d fem modeling and fabrication of circular photonic crystal microcavity, *Journal of Lightwave Technology*, *26*(16), 2960–2968.

[74] **Arndt, F.**, **Bornemann, J.**, **Vahldieck, R. and Grauerholz, D.** (1984). E-plane integrated circuit filters with improved stopband attenuation (Short Papers), *IEEE transactions on microwave theory and techniques*, *32*(10), 1391–1394.

[75] **Şimşek, S.**, **Topuz, E. and Niver, E.** (2012). A novel design method for electromagnetic bandgap based waveguide filters with periodic dielectric loading, *AEU-International Journal of Electronics and Communications*, *66*(3), 228–234.

[76] **Şimşek, S.** (2013). A novel method for designing one dimensional photonic crystals with given bandgap characteristics, *AEU-International Journal of Electronics and Communications*, *67*(10), 827–832.

[77] **Şimşek, S.** (2014). A fast and accurate design method for broad omnidirectional bandgaps of one dimensional photonic crystals, *AEU-International Journal of Electronics and Communications*, *68*(9), 865–868.

[78] **Lalanne, P.** (1996). Effective medium theory applied to photonic crystals composed of cubic or square cylinders, *Applied optics*, *35*(27), 5369–5380.

[79] **Lalanne, P. and Hugonin, J.P.** (1998). High-order effective-medium theory of subwavelength gratings in classical mounting: application to volume holograms, *JOSA A*, *15*(7), 1843–1851.

[80] **Bräuer, R. and Bryngdahl, O.** (1994). Design of antireflection gratings with approximate and rigorous methods, *Applied optics*, *33*(34), 7875–7882.

[81] **Born, M. and Wolf, E.** (1999). Principles of Optics, Cambridge University Press, *New York*, 704.

[82] **Lidorikis, E.**, **Egusa, S. and Joannopoulos, J.** (2007). Effective medium properties and photonic crystal superstructures of metallic nanoparticle arrays, *Journal of Applied Physics*, *101*(5), 054304.

[83] **Robertson, W.**, **Arjavalingam, G.**, **Meade, R.**, **Brommer, K.**, **Rappe, A.M. and Joannopoulos, J.** (1992). Measurement of photonic band structure in a two-dimensional periodic dielectric array, *Physical review letters*, *68*(13), 2023.

[84] **Frezza, F.**, **Pajewski, L. and Schettini, G.** (2003). Characterization and design of two-dimensional electromagnetic band-gap structures by use of a full-wave method for diffraction gratings, *IEEE Transactions on Microwave Theory and Techniques*, *51*(3), 941–951.

[85] **Śmigaj, W. and Gralak, B.** (2008). Validity of the effective-medium approximation of photonic crystals, *Physical Review B*, *77*(23), 235445.

[86] **Wu, Y.**, **Lai, Y. and Zhang, Z.Q.** (2012). *Effective Medium Theories and Symmetry Properties of Elastic Metamaterials*, InTech.

[87] **Geng, T.**, **Zhuang, S.**, **Gao, J. and Yang, X.** (2015). Nonlocal effective medium approximation for metallic nanorod metamaterials, *Physical Review B*, *91*(24), 245128.

[88] **Petersen, R.**, **Pedersen, T.G.**, **Gjerding, M.N. and Thygesen, K.S.** (2016). Limitations of effective medium theory in multilayer graphite/hBN heterostructures, *Physical Review B*, *94*(3), 035128.

[89] **Yasumoto, K.** (2005). *Electromagnetic theory and applications for photonic crystals*, CRC press.

[90] **Bettotti, P.** (2015). *Nanodevices for Photonics and Electronics: Advances and Applications*, CRC Press.

[91] **Gong, Q. and Hu, X.** (2014). *Photonic crystals: principles and applications*, Pan Stanford.

[92] **Datta, A.K. and Munshi, S.** (2016). *Information Photonics: Fundamentals, Technologies, and Applications*, CRC Press.

[93] **Hsu, H.T.**, **Lee, M.H.**, **Yang, T.J.**, **Wang, Y.C. and Wu, C.J.** (2011). A multichanneled filter in a photonic crystal containing coupled defects, *Progress In Electromagnetics Research*, *117*, 379–392.

[94] **Guven, K. and Ozbay, E.** (2005). Coupling and phase analysis of cavity structures in two-dimensional photonic crystals, *Physical Review B*, *71*(8), 085108.

[95] **Frezza, F.**, **Pajewski, L. and Schettini, G.** (2005). Numerical investigation on the filtering behavior of 2-D PBGs with multiple periodic defects, *IEEE transactions on nanotechnology*, *4*(6), 730–739.

[96] **Yanik, M.F.**, **Fan, S. and Soljačić, M.** (2003). High-contrast all-optical bistable switching in photonic crystal microcavities, *Applied Physics Letters*, *83*(14), 2739–2741.

[97] **Frezza, F.**, **Pajewski, L. and Schettini, G.** (2003). Periodic defects in 2D-PBG materials: full-wave analysis and design, *IEEE transactions on nanotechnology*, *2*(3), 126–134.

[98] **Saleh, A.A.** (1974). An Adjustable Quasi-Optical Bandpass Filter—Part I: Theory and Design Formulas, *IEEE Transactions on Microwave Theory and Techniques*, *22*(7), 728–734.

[99] **Coccioli, R.**, **Yang, F.R.**, **Ma, K.P. and Itoh, T.** (1999). Aperture-coupled patch antenna on UC-PBG substrate, *IEEE Transactions on microwave theory and techniques*, *47*(11), 2123–2130.

[100] **Wang, X.**, **Zhang, M. and Wang, S.J.** (2011). Practicability analysis and application of PBG structures on cylindrical conformal microstrip antenna and array, *Progress In Electromagnetics Research*, *115*, 495–507.

[101] **Netti, M.**, **Harris, A.**, **Baumberg, J.**, **Whittaker, D.**, **Charlton, M.**, **Zoorob, M. and Parker, G.** (2001). Optical trirefringence in photonic crystal waveguides, *Physical review letters*, *86*(8), 1526.

[102] **Kopp, V.I.**, **Genack, A.Z. and Zhang, Z.Q.** (2001). Large coherence area thin-film photonic stop-band lasers, *Physical review letters*, *86*(9), 1753.

[103] **Jiang, W. and Chen, R.T.** (2003). Multichannel optical add-drop processes in symmetrical waveguide-resonator systems, *Physical review letters*, *91*(21), 213901.

[104] **Mazurenko, D.A.**, **Kerst, R.**, **Dijkhuis, J.**, **Akimov, A.**, **Golubev, V.**, **Kurdyukov, D.**, **Pevtsov, A. and Sel'Kin, A.** (2003). Ultrafast optical switching in three-dimensional photonic crystals, *Physical review letters*, *91*(21), 213903.

[105] **Elsheakh, D.M.N.**, **Elsadek, H.A.**, **Abdallah, E.A.**, **El-Hennawy, H.M.S. and Iskander, M.F.** (2011). Ultra-wide bandwidth microstrip monopole antenna by using electromagnetic band-gap structures, *Progress In Electromagnetics Research*, *23*, 109–118.

[106] **Zhang, Y. and Li, B.** (2007). Ultracompact waveguide bends with simple topology in two-dimensional photonic crystal slabs for optical communication wavelengths, *Optics letters*, *32*(7), 787–789.

[107] **Yang, H.Y.** (1996). Finite difference analysis of 2-D photonic crystals, *IEEE transactions on microwave theory and techniques*, *44*(12), 2688–2695.

[108] **Yasumoto, K. and Yoshitomi, K.** (1999). Efficient calculation of lattice sums for free-space periodic Green's function, *IEEE Transactions on Antennas and Propagation*, *47*(6), 1050–1055.

[109] **Li, Z.Y. and Lin, L.L.** (2003). Photonic band structures solved by a plane-wave-based transfer-matrix method, *Physical Review E*, *67*(4), 046607.

[110] **Coves, Á.**, **Marini, S.**, **Gimeno, B. and Boria, V.** (2012). Full-wave analysis of periodic dielectric frequency-selective surfaces under plane wave excitation, *IEEE Transactions on Antennas and Propagation*, *60*(6), 2760–2769.

[111] **Erkan, O.**, **Akıncı, M.N. and Şimşek, S.** (2018). A fast hybrid method for the bandgap analysis of 2D photonic crystals based on EMT and AFGSM methods, *AEU-International Journal of Electronics and Communications*, *87*, 107–112.

[112] **Moharam, M.**, **Grann, E.B.**, **Pommet, D.A. and Gaylord, T.** (1995). Formulation for stable and efficient implementation of the rigorous coupled-wave analysis of binary gratings, *JOSA a*, *12*(5), 1068–1076.

[113] **Dansas, P. and Paraire, N.** (1998). Fast modeling of photonic bandgap structures by use of a diffraction-grating approach, *JOSA A*, *15*(6), 1586–1598.

[114] **Lourtioz, J.M.**, **Benisty, H.**, **Berger, V.**, **Gérard, J.M.**, **Maystre, D. and Tchelnokov, A.** (2005). Three-Dimensional Structures in Optics, *Photonic Crystals: Towards Nanoscale Photonic Devices*, 339–358.

[115] **Fan, S.**, **Villeneuve, P.R.**, **Joannopoulos, J.D. and Haus, H.A.** (1998). Channel drop filters in photonic crystals, *Optics express*, *3*(1), 4–11.

[116] **Costa, R.**, **Melloni, A. and Martinelli, M.** (2003). Bandpass resonant filters in photonic-crystal waveguides, *IEEE Photonics Technology Letters*, *15*(3), 401–403.

[117] **Zhang, T.**, **Sun, J.**, **Yang, Y. and Li, Z.** (2018). Photonic crystal filter based on defect mode and waveguide mode symmetry matching, *Optics Communications*, *428*, 53–56.

[118] **Kim, S.**, **Cai, J.**, **Jiang, J. and Nordin, G.P.** (2004). New ring resonator configuration using hybrid photonic crystal and conventional waveguide structures, *Optics express*, *12*(11), 2356–2364.

[119] **Butt, H.**, **Dai, Q.**, **Wilkinson, T.D. and Amaratunga, G.A.** (2011). Photonic crystals & metamaterial filters based on 2D arrays of silicon nanopillars, *Progress In Electromagnetics Research*, *113*, 179–194.

[120] **Denk, W.**, **Strickler, J.H. and Webb, W.W.** (1990). Two-photon laser scanning fluorescence microscopy, *Science*, *248*(4951), 73–76.

[121] **Nie, S.**, **Chiu, D.T. and Zare, R.N.** (1994). Probing individual molecules with confocal fluorescence microscopy, *Science*, *266*(5187), 1018–1021.

[122] **Iqbal, Y. and Faryad, M.** (2017). Photonic band structures of one dimensional multilayered dielectric-magnetic photonic crystals, *Photonics and Nanostructures-Fundamentals and Applications*, *24*, 63–68.

[123] **Orfanidis, S.J.** (2002). Electromagnetic waves and antennas.

[124] **Alpert, N.L.**, **Keiser, W.E. and Szymanski, H.A.** (2012). *IR: Theory and practice of infrared spectroscopy*, Springer Science & Business Media.

[125] **D. Shannon, R.**, **Shannon, R.C.**, **Medenbach, O. and Fischer, R.X.** (2002). Refractive index and dispersion of fluorides and oxides, *Journal of physical and chemical reference data*, *31*(4), 931–970.

[126] **Martínez, F.**, **Toledano-Luque, M.**, **Gandía, J.**, **Cárabe, J.**, **Bohne, W.**, **Röhrich, J.**, **Strub, E. and Mártil, I.** (2007). Optical properties and structure of HfO2 thin films grown by high pressure reactive sputtering, *Journal of Physics D: Applied Physics*, *40*(17), 5256.

[127] **Çetinörgü, E.**, **Baloukas, B.**, **Zabeida, O.**, **Klemberg-Sapieha, J.E. and Martinu, L.** (2009). Mechanical and thermoelastic characteristics of optical thin films deposited by dual ion beam sputtering, *Applied optics*, *48*(23), 4536–4544.

[128] **Hojabri, A. and Pourmohammad, S.** (2016). Optical Properties of Nano-Crystalline Zirconia Thin Films Prepared at Different Post-Oxidation Annealing Times, *Acta Physica Polonica A*, *129*(4), 647–649.

[129] **Thaidun, M.**, **Rao, B.V.**, **Reddy, L.R.M. and Chalapathi, G.V.** (2013). Structural, dielectric and optical properties of sputtered TiO 2 nano-films, *IOSR J Appl Phys*, *4*, 49–53.

[130] **Vogel, A. and Venugopalan, V.** (2003). Mechanisms of pulsed laser ablation of biological tissues, *Chemical reviews*, *103*(2), 577–644.

[131] **Yu, K.**, **Zhou, X.y.**, **Wang, J.q.**, **Xu, J.j. and Yin, J.j.** (2014). A non-polarization short-wave-pass thin film edge filter, *Optoelectronics Letters*, *10*(4), 247–249.

[132] **Lyngnes, O. and Kraus, J.** (2014). Design of optical notch filters using apodized thickness modulation, *Applied optics*, *53*(4), A21–A26.

CURRICULUM VITAE

Name Surname: Onur Erkan

E-Mail: erkanonu@itu.edu.tr

EDUCATION:

- **B.Sc.:** 2007, Yıldız Technical University, Electrical and Electronics Engineering Faculty, Electrical Engineering Department
- **M.Sc.:** 2013, Doğuş University, Engineering Faculty, Electronics and Communication Engineering Department

PUBLICATIONS, PRESENTATIONS AND PATENTS ON THE THESIS:

- **Erkan, O.**, Akıncı, M. N., Şimşek, S., (2018). A fast hybrid method for the bandgap analysis of 2D photonic crystals based on EMT and AFGSM methods. *AEU-International Journal of Electronics and Communications*, 87, 107-112.
- **Erkan, O.**, Akıncı, M. N., Şimşek, S., (2018). Bandgap analysis of 2D photonic crystals with Auxiliary Functions of Generalized Scattering Matrix (AFGSM) method. *AEU-International Journal of Electronics and Communications*, 95, 287-296.
- **Erkan, O.**, Şimşek, S., (2017, November). Transmission and stopband characteristics of one-dimensional photonic crystals. *10th International Conference on Electrical and Electronics Engineering*, (ELECO), (pp. 977-981), IEEE.
- **Erkan, O.**, Şimşek, S., (2018, November). Design of Photonic Crystal Based Multi-Channel Optical Filter Using AFGSM Method. *Conference on Electric-Electronics and Biomedical Engineering*, (ELECO)
- **Erkan, O.**, Şimşek, S., (2019). Investigation of Omnidirectional Bandgaps in Photonic Crystals. *Journal of Engineering Sciences and Design*, (Accepted, May 20, 2019)
- **Erkan, O.**, Şimşek, S., (2019). Fast Characterization and Modeling of Arbitrary Cross Section 2D Photonic Bandgap Structures Using AFGSM Method. *Progress in Electromagnetics Research Symposium*, (PIERS 2019)